UNIVERSITY OF CALIFORNIA

Los Angeles

Evolution of Snow-Affected Water Resources in a Warming Climate: Mechanisms, Feedback, and Future

A dissertation submitted in partial satisfaction of the requirements for the degree Doctor of Philosophy in Geography

by

Zhaoxin Ban

2023

ABSTRACT OF THE DISSERTATION

Evolution of Snow-Affected Water Resources in a Warming Climate:
Mechanisms, Feedback, and Future

by

Zhaoxin Ban

Doctor of Philosophy in Geography
University of California, Los Angeles, 2023
Professor Dennis P. Lettenmaier, Chair

Over 26% of the world's land area and ~8% of its population depend on snowmelt as the primary water source. A typical example is the western U.S. (WUS), where snowmelt has been the center of streamflow research for the past two decades. Under climate warming, snow's contribution to streamflow will decrease, increasing the uncertainty of streamflow fluctuations and challenging streamflow forecasting and management that are based on traditional snow-based methods. Addressing these challenges requires a deep understanding of the linkages among warming, snowmelt, and other runoff-generating processes and how they affect future streamflow. In my dissertation, I take the WUS as an example, using hydrologic modeling and in-situ data to explore the following questions: 1. How does seasonal warming affect annual streamflow in different watersheds, and why? 2. What composes runoff during water-scarce seasons, and how

does the composition change under warming? 3. What mechanism dominates annual runoff decline under warming in snow-affected areas, and how do its dynamics affect the evolution of runoff? In 1, I found and explained an asymmetrical pattern that controls annual streamflow response to seasonal warming, which indicates the cooler, inland region streamflow is more sensitive to warm season warming, whereas warmer, coastal region streamflow is more sensitive to cool season warming. I found this asymmetry is explained by the bell-shape variation of evapotranspiration-temperature sensitivity as a function of increasing temperature, filling a long-lasting gap in the sub-annual linkages between water and climate in WUS. In 2, I developed a custom-period water source partition algorithm that uses a handful of output variables from land surface models to quantify the fractional contribution of custom-period rainfall to custom-period streamflow. Using this algorithm, I detected an increasing contribution of seasonal rainfall to summer streamflow under warming, which shed light on the evolution of a new dynamic for summer streamflow generation in the water-short WUS. In 3, I explored the ongoing runoff decline under warming across major WUS snow-covered regions and explored the linkage between the evolving trend dynamics with changing snow. In three major snow-covered basins, I discovered a smaller warming-sensitivity of runoff under a warmer climate with fixed precipitation, which could break the long-lasting static mechanism paradigm that governs hydrologic dynamics and a more rigorous assessment of future streamflow. In summary, the dissertation provides important contributions to understanding ongoing and future runoff evolution in WUS snow-affected regions under a warmer future.

The dissertation of Zhaoxin Ban is approved.

Yongkang Xue

Yongwei Sheng

Alton Park Williams

Steven A. Margulis

Daniel R. Cayan

Bradley Udall

Dennis P. Lettenmaier, Committee Chair

University of California, Los Angeles

2023

DEDICATION

I dedicate my dissertation to my family and many friends. A special feeling of gratitude to my loving parents and grandparents, Zhenyu Wang, Bin Ban, Yaoqing Ban, and Yuzhi Wu, whose words of encouragement and push for tenacity ring in my ears. My aunt, uncles, sisters, and brothers have never left my side and always helped me while I was studying abroad.

I also dedicate this dissertation to my husband, Zhe Jia. He is always with me from the ups and downs. He has given me much support, guidance, and love, making me a better person.

I dedicate this dissertation and thank my special friends Q. Su and H. Ye for being there throughout the entire doctoral program. Both of you have been my best cheerleaders.

Table of Contents

LIST OF FIGURES

LIST OF TABLES

ACKNOWLEDGEMENTS

I want to express my gratitude to my advisor, Prof. Dennis Lettenmaier, for his unwavering guidance, support, and motivation during my time at UCLA. His invaluable instructions have equipped me with profound insights and knowledge. Throughout my journey of exploring scientific problems under his guidance, I have been strongly impressed by Prof. Dennis Lettenmaier's subtle thinking approach and clever methods countless times. His mentorship has enabled me to cultivate my critical, systematic, and independent thinking abilities, which hold great importance in scientific exploration, engineering practice, and life. His unwavering stamina, enduring confidence in facing challenges, and his pursuit of truth have deeply influenced me. With endless patience, he tirelessly assisted me in refining my papers, transforming them from initially awkward English into the best graduate student papers in our department. He taught me how to express my scientific ideas effectively and meticulously. In summary, Dennis not only guided me scientifically but also played a significant role in shaping me as a better individual. He instilled in me a sense of serenity and confidence when confronting difficulties and challenges. I am incredibly fortunate to have been a student of Dennis; he is not only my scientific mentor but also a guiding light in my life.

I acknowledge my dissertation committee members: Prof. Yongkang Xue, Yongwei Sheng, Park Williams, Steve Margulis, Dan Cayan, and Brad Udall, for their help and support throughout my postgraduate studies. I hold fond memories of Prof. Xue's enlightening lectures on land surface processes, as the knowledge gained played a pivotal role in my following dissertation research. I thank Prof. Sheng for the helpful discussions at the Palm Court and during EOS. These conversations served as a wellspring of inspiration, providing me with great insights. I want to thank Park for his inspiring talks and helpful answers to many of my questions, which teach me

many things, such as experiment design and statistical methods, effective communication of scientific papers to the general public, delivering impactful presentations, and navigating the paths of academic career development. I sincerely thank Steve for his excellent course on data assimilation and hydrometeorology. The valuable knowledge I acquired from these courses greatly contributed to my doctoral thesis. I am also grateful for his unwavering patience in addressing my questions, providing me with clarity and understanding. Each class was filled with genuine care for students, leaving me with cherished memories of his warm smile and enthusiastic lectures. I sincerely thank Dan for his support and helpful discussions throughout my studies, greatly benefiting my Master's thesis and Ph.D. dissertation. I want to extend my heartfelt gratitude to Brad for his invaluable help, from inspiring papers to essential datasets that played a vital role in my dissertation.

I have also learned a lot from other faculty members in our department. I want to thank Eric Sheppard for his enlightening class in my first graduate year, which let me know that there are potentially other paths of science discovery and engineering besides the current one, urging me to remain open-minded and proactive in contemplating interdisciplinary scientific research and the creation of novel branches of science. I want to thank Kyle Cavanaugh for his paper writing class, which taught me what kind of good scientific articles and stories are and how to write them. I want to thank Greg Okin for his drone class that taught me how to collaborate to start a project from scratch and for his support and encouragement throughout my graduate years. Outside my department, I would also like to thank Prof. William W-G Yeh, Rong Fu, and Mekonnen Gebremichael in CE&E, and Rong Fu, Gang Chen, Jacob Bortnik, and Karen McKinnon for their fantastic courses and the many enjoyable moments discussing together.

Throughout my graduate studies, I am grateful for the help provided by Tapash Das, Chris Milly, David Pierce, Bart Nijssen, Richard Vogel, Sankar Arumugam, and Chandramauli Awasthi. Their support and help have been invaluable to my academic journey.

I want to thank every one of my group members. I am grateful that I could join the land surface group at UCLA with instruction from Mu Xiao (now at Scripps Institute of Oceanography, UCSD). I also want to thank Qian Cao (now at SIO-UCSD), Solomon Vimal (now at Geothara), Abinash Bhattachan (now at Cal State East Bay), and Ali Mehran (now at the University of North Georgia) for their guidance and help during the first several years of my Ph.D. studies.

I would also like to thank my other labmates, friends, and roommates, Lu Su, Dongyue Li, Xiaoyu Ma, Jessica Fayne, Huilin Huang, Ye Liu, Sarfaraz Alam, Liyin He, Chen Xin, Yiwen Fang, Kimberly Wang, Emilie Tarouilly, Ting Yuan, Yiqun Han, Yan Chen, Ningning Zhao, Yazhen Luo, and Jessica Cobian. Each of you is so unique. Thank you for your encouragement, help, and the many hours of proofreading and many more happy hours together.

I also thank our department staff for their help, especially Kasi McMurray and Brian Won. Finally, I especially owe great thanks to my mother, Zhenyu Wang; my father, Bin Ban; my grandfather Yaoqing Ban; and my grandmother Yuzhi Wu, who brought me up, as well as the rest family members. My mother shows me the strength of being optimistic, strong, independent, and enterprising. My father teaches me the value of caution, calmness, curiosity, and self-esteem. My grandpa taught me foresight, endurance, balance, and hard work, and my grandmother showed me the pursuit of perfection, perseverance, creativity, and passion. They are the most amazing and kindhearted people in my world. Without their continuous encouragement and unconditional support, I would not be who I am today.

CURRICULUM VITAE

EDUCATION

M.A. Geography, University of California, Los Angeles, 2019
B.S. Geographical Sciences, Nanjing University, 2017

PROFESSIONAL EXPERIENCES

Graduate Research Assistant: University of California, Los Angeles 2017-current

SELECTED PUBLICATIONS

Ban, Z. & Lettenmaier, D. P. (2023). Less Warming-Induced Runoff Decline in a Warmer Future, in preparation.

Ban, Z., C. Xin, Y. Fang, X. Ma, D. Li, and D. P. Lettenmaier (2023b), Snowmelt-radiation feedback impact on Western U.S. streamflow, *Geophysical Research Letters*, under review.

Ban, Z., Li, D., & Lettenmaier, D. P. (2023). The increasing role of seasonal rainfall in western US summer streamflow. *Geophysical Research Letters*, 50(9), e2023GL102892.

Ban, Z., & Lettenmaier, D. P. (2022). Asymmetry of Western US river basin sensitivity to seasonally varying climate warming. *Water Resources Research*, 58(2), e2021WR030367.

Ban, Z., Das, T., Cayan, D., Xiao, M., Lettenmaier, D. P. (2020). Understanding the asymmetry of annual streamflow responses to seasonal warming in the Western United States. *Water Resources Research*, 56(12), e2020WR027158.

Huang, H., Fischella, M. R., Liu, Y., **Ban, Z.**, Fayne, J. V., Li, D., ... Lettenmaier, D. P. (2022). Changes in mechanisms and characteristics of western US floods over the last sixty years. *Geophysical Research Letters*, 49(3), e2021GL097022.

Xu, S., McVicar, T. R., Li, L., Yu, Z., Jiang, P., Zhang, Y., **Ban, Z.**, Xing, W. Dong, N., Zhang, H., & Zhang, M. (2022). Globally assessing the hysteresis between sub-diurnal actual evaporation and vapor pressure deficit at the ecosystem scale: Patterns and mechanisms. *Agricultural and Forest Meteorology*, 323, 109085.

Alam, S., Gebremichael, M., **Ban, Z.**, Scanlon, B. R., Senay, G., Lettenmaier, D. P. (2021). Post-Drought Groundwater Storage Recovery in California's Central Valley. *Water Resources Research*, 57(10), e2021WR030352.

SELECTED PRESENTATIONS

Ban, Z. Asymmetry of Western U.S. river basin sensitivity to seasonally varying climate warming, Hydro90, China (online), May 29, 2021 (invited talk).

Ban, Z. Understanding the asymmetry of annual streamflow responses to seasonal warming in the Western U.S. CESM Workshop, June 16, 2021 (talk).

Ban, Z., Cayan, D., and Lettenmaier, D. P., Sensitivity of Western US river basins to seasonally varying climate warming. AGU Fall Meeting, December 10, 2020 (talk).

Ban, Z., Vimal, S., Bhattachan, A., Cucchi, K., Hoover, C., Skaff, N., Remais, J. and Lettenmaier, D. P., Assessing inundation in the Central Valley, CA and its implications for West Nile Virus transmission using remote sensing and hydrological modeling. AGU Fall Meeting, December 12, 2018 (talk).

Lettenmaier, D. and **Ban, Z.** Milly and Dunne's 2020 Science paper and implications for hydrology climate sensitivities across the West? Chris Milly Retirement Symposium, January 20, 2023. (talk).

Lettenmaier, D. and **Ban, Z.** The impact of declining Western U.S. snowpacks on annual river discharge in a warming climate. Southwest Extreme Precipitation Symposium, April 20, 2022 (talk).

Xin, C., Fang, Y., Li, D., Ma, X., **Ban, Z.**, Sun, H., Turnbull, S. J., and Lettenmaier, D. P. Quantifying the impact of declining snow on river discharge in a warming climate. AGU Fall Meeting, December 2020 (talk).

Ban, Z., Bhattachan, A., Vimal, S., Remais, J., Lettenmaier, D. P., and Irish, A. Predicting mosquito population with high-resolution inundation in California: implications forWest Nile Virus. AGU Fall Meeting, December 15, 2021 (poster).

Ban, Z., Das, T., Cayan, D., Xiao, M., Lettenmaier, D. P., Understanding the Role of Asymmetrical Warming on Streamflow Changes in the Western US Using a Multi-model Approach. AGU Fall Meeting, December 10, 2019 (poster).

Ban, Z., Das, T., Cayan, D., Xiao, M., Lettenmaier, D. P., Understanding the Role of Asymmetrical Warming on Streamflow Changes in the Western US Using a Multi-model Approach. AGU Fall Meeting, December 12, 2018 (poster).

Ban, Z., Yang, K., Pitcher, L. H., and Smith, L. C., Interannual variability of moulins on the Southwest Greenland Ice Sheet. AGU Fall Meeting, December 13, 2017 (poster).

SELECTED AWARDS

Dissertation Year Fellowship, $20000 + tuition, UCLA	2023
Best Student Paper Award, UCLA Department of Geography	2021, 2023
Graduate Student Fellowship, $5000, UCLA	2017
Outstanding graduates at Nanjing University	2017
Baosteel Scholarship at Nanjing University (only woman undergrad recipient, Top 0.35‰)	2016
CSST Award for Outstanding Research and Presentation (10 out of 98)	2016
UCLA-CSST Scholarship (only recipient in geography across China)	2016
Finalist Winner: Mathematical Contest in Modeling	2016
Duxia scholarship at NJU (Top 1‰ in University)	2015
National scholarship at NJU (Top 1% in University)	2014

OTHER CONTRIBUTIONS & ROLES

Reviewer for PLOS ONE, JAWRA, ESPR	2023-present
AGU Fall Meeting session chair.	Dec 2022
UCLA Director of COAA-SCC	2020 – present
American Geophysical Union member	2017 – present

Chapter 1 Introduction

In the western U.S. (WUS), seasonal snowpack is the dominant source of streamflow [*Li et al.*, 2017]. Precipitation accumulates as snow in winter and melts in spring, providing the source for late-spring to early-summer seasonal peak flows. Snowmelt also replenishes the groundwater that dominates early-summer to fall low flows [*Huntington and Niswonger*, 2012; *Li et al.*, 2017; *Smakhtin*, 2001]. Peak flows are critical for reservoir storage which provides agricultural and municipal water supply, hydroelectric power generation, and supports other uses like recreation, while summer and fall low flows are critical for ecosystem functioning (e.g., anadromous and migratory fish populations) and are correlated as well with tree mortality, insect outbreaks, and wildfire risk. Both peak flows and low flows, as well as annual streamflow volumes are critical for a region's socioeconomic security. Reliably predicting these flows is important for water systems that are intended to buffer against streamflow variations and provide a stable water supply.

Historically, WUS seasonal streamflow forecasts mostly have focused on late-spring to early-summer seasonal peak flows (e.g., Apr-Jul) and widely rely on snow water equivalent (SWE) as the most important predictor and the primary initial hydrologic condition (IHC). As the warmer climate reduces snowpacks, these traditional methods have become less reliable. For example, *Sturtevant and Harpold* [2019] showed that forecast errors from regression-based methods that use SWE and precipitation as predictors during below-average snow years (snow droughts) are biased high by roughly one-third compared with above-average snow years. *Livneh and Badger* [2020] applied 28 climate model projections and showed a decline in the ability of snow to predict seasonal drought under declining future snowpack for historically snowmelt-dominated areas of the WUS. They also showed that the decrease of Apr 1st SWE-based prediction skill could not be fully compensated by adding ancillary predictors such as Apr 1st soil moisture. This change in

SWE's reliability in forecasting late-spring to early-summer peak flow highlighted the need for better predictors and more adaptive forecast methods, which requires a dynamic understanding of the role of snowmelt and other runoff-generation mechanisms in (predicting) streamflow under a warming future.

Given this background, my dissertation focuses on three questions having to do with streamflow responses in WUS to a warmer, reduced-snow future:

1) How does seasonal warming affect annual streamflow in different watersheds, and why?

2) What composes runoff during water-scarce seasons, and how does the composition change under warming?

3) What mechanism dominates annual runoff decline under warming in snow-affected areas, and how do its dynamics affect the evolution of runoff?

I address these questions in three core chapters of this dissertation (Chapters 2-4). In **Chapter 2** I employ the Variable Infiltration Capacity (VIC) hydrological model [*Liang et al.*, 1994] and observations to explore and explain the annual streamflow responses to seasonal warming across the WUS. I find that annual streamflow is most sensitive to warm season warming in cool, inland basins, especially the northern Columbia River basin and most of the Upper Colorado River Basin, and most sensitive to cool season warming in warm, coastal basins. This bi-directional pattern is enhanced by vegetation coverage but weakened by long-term snowpack decline. In the coldest basins with short snow-free seasons, net radiation changes dominate the streamflow response asymmetry. For basins with cold-to-intermediate temperatures, vapor pressure deficit changes dominate. For the warmest basins, surface resistance changes (due to stomatal response to variations in aridity) dominate. This chapter was published in *Water Resources Research* [*Ban and Lettenmaier*, 2022].

In **Chapter 3** I developed a custom-period water source tracking algorithm and applied it to two widely used hydrological models to quantify the water source composition of summer streamflow and evaluate how the evolution of the composition under uniformly 1°C warming impacts summer streamflow predictability. Applying the snowmelt-rainfall tracking algorithm to two hydrological models, I show that cool-season rainfall provides an important volumetric contribution to summer streamflow for many WUS streams in the current climate, and this contribution will increase under climate warming, especially in years with warm snow droughts and abnormally dry summers. I also show that seasonal rainfall (warm-/cool-seasons) dominates the variability of summer streamflow across ~70% of WUS in areal extent. I show that an increasing warm-season rainfall contribution to summer streamflow (largely replacing snowmelt) results in reduced summer streamflow predictability. This chapter was published in *Geophysical Research Letters* [*Ban et al.*, 2023a].

In **Chapter 4**, I show that snow loss and subsequent annual runoff decline will become less sensitive to warming as the reference climate warms. My analysis is based on warming experiments with land surface models (LSMs) and analysis of LSM-coupled downscaled global climate model (GCM) ensembles, applied to three major WUS river basins. This work extends from an earlier paper [*Ban et al.*, 2023b] that discussed runoff sensitivity to annual warming and its association with snowmelt-radiation feedback across regions with different temperatures in the WUS. In Chapter 4, I find a decreasing sensitivity of snow loss to warming under a warmer reference temperature, which could decelerate streamflow decline and even reverse it (streamflow increase) with accompanied precipitation increase under near-linear warming. This chapter will be submitted to *Nature Climate Change*.

In conclusion, this dissertation shows that:

1) Considering as background that the projected warm season warming signal in climate models is stronger than cool season warming, river basins with annual streamflow that is more sensitive to warm season than cool season warming tend to be cooler, inland basins, whereas warmer, coastal basins are more sensitive to cool season than to warm season warming. I therefore argue that cooler, inland river basins will be more sensitive (in terms of annual streamflow change) to future warming than warmer, coastal basins.

2) Seasonal rainfall's contribution to summer streamflow will increase in a warmer climate across the WUS, and the increasing effect of warm-season rainfall will reduce the predictability of summer streamflow.

3) Annual runoff sensitivity to warming across the WUS (i.e., per degree C of warming) will weaken as temperatures warm and snowpacks decline as the strength of the snowmelt-radiation feedback weakens.

Taking 1) - 3) together, strongly snow-affected inland mountainous river basins are expected to have the strongest (negative) runoff response to warming in the future. If humans manage to control the rate of climate warming, I argue that the WUS will witness reduced (annual) streamflow declines and snow loss as the snowmelt-radiation feedback weakens. This may even lead to some increases in (annual) streamflow, probably starting from the warmer coastal regions of the WUS.

Future research on the impacts of warming on WUS streamflow could: 1) quantitatively analyze the dynamic impact of the snowmelt-radiation feedback on streamflow evolution; 2) investigate the mechanisms that lead to the evolving impact of the snowmelt-radiation feedback on the rate of annual streamflow declines (as discussed in Chapter 4 & 5); 3) investigate other runoff-climate response factors, such as the changing atmospheric opacity, which could impact

streamflow loss by affecting radiation and thus evapotranspiration; 4) conduct model- and observation-based analyses intended to understand the aggregate effect of vegetation dynamics and discrete events such as wildfires, droughts, and event-scale precipitation on streamflow changes in a warmer climate.

References

Ban, Z., and D. P. Lettenmaier (2022), Asymmetry of Western US river basin sensitivity to seasonally varying climate warming, *Water Resources Research*, *58*(2), e2021WR030367.

Ban, Z., D. Li, and D. P. Lettenmaier (2023a), The increasing role of seasonal rainfall in westem US summer streamflow, *Geophysical Research Letters*, *50*(9), e2023GL102892.

Ban, Z., C. Xin, Y. Fang, X. Ma, D. Li, and D. P. Lettenmaier (2023b), Snowmelt-radiation feedback impact on Western U.S. streamflow, *Geophysical Research Letters*.

Huntington, J. L., and R. G. Niswonger (2012), Role of surface-water and groundwater interactions on projected summertime streamflow in snow dominated regions: An integrated modeling approach, *Water Resources Research*, *48*(11).

Li, D., M. L. Wrzesien, M. Durand, J. Adam, and D. P. Lettenmaier (2017), How much runoff originates as snow in the western United States, and how will that change in the future?, *Geophysical Research Letters*, *44*(12), 6163-6172.

Liang, X., D. P. Lettenmaier, E. F. Wood, and S. J. Burges (1994), A simple hydrologically based model of land surface water and energy fluxes for general circulation models, *Journal of Geophysical Research: Atmospheres*, *99*(D7), 14415-14428.

Livneh, B., and A. M. Badger (2020), Drought less predictable under declining future snowpack, *Nature Climate Change*, *10*(5), 452-458.

Miller, M. P., D. D. Susong, C. L. Shope, V. M. Heilweil, and B. J. Stolp (2014), Continuous estimation of baseflow in snowmelt-dominated streams and rivers in the U pper C olorado R iver B asin: A chemical hydrograph separation approach, *Water Resources Research*, *50*(8), 6986-6999.

Smakhtin, V. U. (2001), Low flow hydrology: a review, *Journal of hydrology*, *240*(3-4), 147-186.

Sturtevant, J. T., and A. A. Harpold (2019), Forecasting the effects of snow drought on streamflow volumes in the western US, paper presented at Proc. 87th Annual Western Snow Conf.

Chapter 2 Asymmetry of Western U.S. River Basin Sensitivity to Seasonally Varying Climate Warming

(This chapter has been published in *Water Resources Research*: Ban, Z., & Lettenmaier, D. P. (2022). Asymmetry of Western U.S. River Basin Sensitivity to Seasonally Varying Climate Warming. Water Resources Research, 58(2), e2021WR030367.

Abstract: Future climate warming over the Western U.S. (WUS) is projected to be greater in summer than winter. Previous model-based studies of large river basins in the WUS showed much different annual streamflow responses to warming in warm vs. cool seasons. However, it remains unclear how are the annual streamflow relative responses to seasonal warming (asymmetry) and drivers of the response asymmetry vary across the entire WUS at the catchment-scale, and how the simulated results compare with observations. Here, we investigate the asymmetry of annual streamflow responses to warm vs. cool season warming at the HUC-8 level across the entire WUS using model simulations and observations. We also examine the asymmetries' relationship with land surface and hydroclimate characteristics, and the primary contributor to the response asymmetry for each HUC-8 basin. The HUC-8 level results reveal more complexity than do earlier analyses of much larger river basins. Over 25% of WUS area has annual streamflow increases in response to warming in at least one season (mostly cool season). Annual streamflow is most sensitive to warm season warming in cool, inland basins, especially the northern Columbia River basin and most of the Upper Colorado River Basin, and most sensitive to cool season warming in warm, coastal basins. This bi-directional pattern is enhanced by vegetation coverage but weakened by long-term snowpack decline. In coldest basins with short snow-free seasons, net radiation changes dominate the streamflow response asymmetry. For basins with cold-to-intermediate

temperatures, vapor pressure deficit changes dominate. For warmest basins, surface resistance changes dominate.

1 Introduction

More than 26% of the global land area and ~8% of the global population depend on snowmelt as their dominant water resource [*Qin et al.*, 2020]. Water availability in snowmelt-dominated regions may change as snow accumulations decline under climate warming, threatening the regions' economic, social, and ecological water uses [*Adam et al.*, 2009; *Barnett et al.*, 2005].

The winter accumulation and spring melting of snow play a major role in the seasonal water supply for the Western U.S. (WUS), which is typical of many snow-dominated regions globally. Over the past decades, warming in the WUS has caused notable changes in the seasonal timing of runoff [*Stewart et al.*, 2004], the fraction of runoff attributable to snowmelt [*Qin et al.*, 2020], and annual runoff decreases [*Forbes et al.*, 2018; *Milly and Dunne*, 2020]. Warming in the WUS is not evenly distributed on a sub-annual scale, with substantially larger warming in the warm season (Apr-Sep) than in the cool season (Oct-Mar) projected across most of the region [*Ban et al.*, 2020; *Das et al.*, 2011; *Rupp et al.*, 2017]. Different seasons' warming in the snowmelt dominated basins of the WUS will alter streamflow volumes quite differently. Cool season warming causes slower snow accumulation and earlier snowmelt, which may exacerbate dry-season water scarcity due to reduced storable snowmelt [*Li et al.*, 2017]. Warm season warming may cause larger peak flows that will strain reservoir capacities and may cause larger evaporative losses in summer [*Li et al.*, 2017]. Both season's warming may contribute to water scarcity, but their relative impact can substantially differ due to different seasonal warming magnitudes and seasonal sensitivities to warming [*Ban et al.*, 2020; *Vano et al.*, 2015]. To better predict streamflow responses to climate

warming and adapt to future water scarcity, understanding the streamflow sensitivity to seasonally varying climate warming is essential.

Only a few studies have examined the relative impact of differential seasonal warming on the streamflow sensitivity of WUS basins. *Das et al.* [2011] used the Variable Infiltration Capacity model (VIC) [*Liang et al.*, 1994] to simulate streamflow responses to seasonal warming for four regionally important river basins in the WUS. *Vano and Lettenmaier* [2014] and *Vano et al.* [2015] quantified the streamflow sensitivity to seasonal warming in the Colorado River basin (at basin-scale), and the Pacific Northwest (HUC-8 level). Notwithstanding this work and seasonal differences in projected future warming (Ban et al., 2020; Das et al., 2011; Hayhoe et al., 2004), questions remain as to the impacts of seasonally differential warming. These include the signature of streamflow responses to seasonal warming, which season's warming most strongly affects annual streamflow volumes, and the processes that dominate asymmetrical streamflow responses to seasonal warming. The answers to these questions have implications for the societal response to changing streamflow, especially in the water short WUS. To date, aside from Vano et al. (2015) (HUC-8 level over the Pacific Northwest) most studies that have addressed seasonal warming signatures on streamflow have been at the scale of large continental rivers (Das et al., 2011; Ban et al., 2020).

Our previous work [*Ban et al.*, 2020] studied streamflow responses to seasonal warming for four regionally important river basins in the WUS using four hydrological models. It defined streamflow response asymmetry (termed Pref_Q as explained in section 3.2) as the ratio of annual streamflow decreases under warm season warming to annual streamflow decreases for the same temperature increment in the cool season. Using this definition, Ban et al. (2020) concluded that river basins with two features have larger annual streamflow decreases for warm season warming

as contrasted with cool season warming. The first feature is relatively cool temperature. The other is a relatively large ratio of warm season to cool season Gross Incoming Water, defined as initial water storage in soil and snow in the season plus the season's precipitation [*Ban et al.*, 2020]. However, their analysis was based on relatively large basins (15,000 ~ 600,000 km^2 drainage areas), which suppresses spatial variability that might be apparent for smaller river basins. Moreover, the ability to explore the impact of other basin surface characteristics (apart from temperature and water availability) on the streamflow responses, and how the model simulations compared with observation-based streamflow responses was limited by the large size, and small number of the basins analyzed in that study.

Here we expand the study area to the entire WUS at the HUC-8 level. We also explore observation-based annual streamflow sensitivities in comparison with model-based estimates, and evaluate the relative role of net radiation as drivers of annual streamflow sensitivity to seasonal warming under different potential evapotranspiration frameworks (Priestley-Taylor and Penman-Monteith). Our aim in enlarging the number of basins relative to Ban et al. (2020) goes beyond simply extending our earlier analysis. Rather, the higher granularity (HUC-8) allows us to explore issues that *Ban et al.* [2020] and *Das et al.* [2011] were unable to test or explain, including statistically meaningful evaluation of similarity between simulated and observational streamflow response signals, and how those responses vary with basin characteristics and hydroclimatic factors. We also go beyond our earlier work in providing a new proxy for directly calculating the main contributor to the asymmetry of annual streamflow responses to warm and cool season warming (hereafter streamflow response asymmetry). Motivated by these goals, we address here three questions:

(1) How does the annual streamflow response asymmetry vary spatially across the WUS at the HUC-8 scale, and what controls the associated spatial patterns?

(2) How does the streamflow response asymmetry at HUC-8 scale vary with different land surface characteristics, such as vegetation coverage, root depth, runoff ratio, and seasonal snow coverage?

(3) What are the primary contributors to annual streamflow response asymmetry for each HUC-8 basin, and do they vary across the WUS?

To address these questions, we first examine the annual streamflow responses to seasonal warming across the 616 HUC-8 basins that comprise the WUS using VIC model simulations (section 4.1) and compare the simulated sensitivities with those estimated from observations (section 4.2). We then examine the variation of annual streamflow responses to seasonal warming with different hydroclimatic and land surface characteristics (sections 4.3 and 4.4). Finally, we attribute and quantify the contribution of different ET-related processes, such as warming-induced changes in net radiation, vapor pressure deficit, and surface resistance to streamflow response asymmetry across the 616 HUC-8 basins (section 4.5). We discuss the results in section 5.0 in light of a comparison between the streamflow response attribution using the Penman-Monteith framework as contrasted with the Priestley-Taylor framework in *Milly and Dunne* [2020], and end with conclusions in section 6.

2. Study area

Our study domain consists of the WUS and the Canadian part of the Columbia River Basin. Additionally, we added a buffer of one HUC-8 basin width east of the Continental Divide to examine whether this geographical divide also separates the characteristics of streamflow response to seasonal warming. The study area covers a wide range of hydroclimatic conditions and land

surface characteristics, with elevations ranging from below sea level (-71 m) to around 3700 m (Figure 1a). A total of 616 HUC-8 basins are included in the study area, with an average drainage area of about 4000 km^2. We took HUC-8 basin boundaries from the USGS National Hydrography Dataset (Simley and Carswell, 2009).

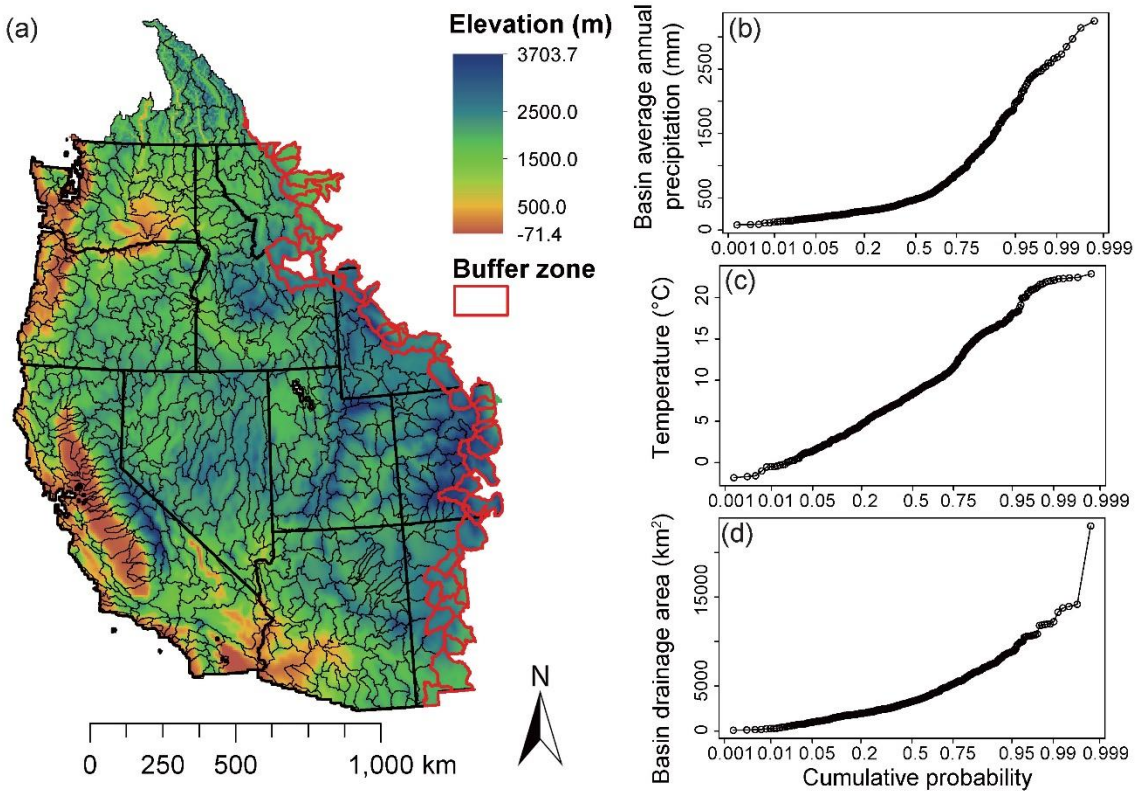

Chapter 2 Figure 1. 616 HUC-8 basins in our study area, which covers the WUS, the Canadian portion of the Columbia River Basin, and a set of buffer basins (red outlines) just east of the Continental Divide. (a) elevation (Gesch et al., 1999). (b) and (c): cumulative distribution functions (CDF) of long-term climatological basin-average annual precipitation (mm) and annual mean temperature (°C), averaged from water year 1951 to 2018 using the Livneh (L13) meteorological forcings (Livneh et al., 2013), and forcings extended to 2018 by Su (Su et al., 2021). (d) CDF of basin drainage areas.

3. Methods and data

3.1 Model and forcing data set

We conducted warming experiments using the VIC macroscale land-surface hydrology model [*Liang et al.*, 1994] version (4.1.2). The VIC model forcings and parameters are the same as in *Ban et al.* [2020]. The analysis period differs, though, with water years 1915-1950 used for spinup and water years 1951-2018 used for analysis. We chose the VIC model for our simulations because the VIC model results were closest to the multi-model mean simulated streamflow sensitivities to warming from four land surface models in Ban et al. (2020), and to observed hydrographs relative to the other models in our previous work [*Ban et al.*, 2020]. The new analysis period was selected to check the robustness of the conclusions in *Ban et al.* [2020] for different simulation periods and because the forcing data quality is generally higher after 1950.

3.2 Annual streamflow response asymmetry under seasonal warming

We first calculated the temperature sensitivity of annual streamflow and evapotranspiration to warm and cool season warming by comparing the baseline simulation with two seasonal warming simulations. We conducted the baseline simulation using historical L13 forcings, extended to 2018 by Su. We set up the two seasonal warming simulations by adding 1°C to both daily maximum and minimum temperatures in every day of a) the warm season only, and b) the cool season only. Perturbing both maximum and minimum temperature ensures that the downward shortwave radiation generated by the Mountain Microclimate Simulation Model (MTCLIM) embedded in VIC [*Bohn et al.*, 2013] is not changed. Downward and emitted longwave radiation from MTCLIM do change, as they are temperature-related. We isolated the warming impact on temperature sensitivity by keeping the precipitation unperturbed.

We calculated the temperature sensitivities of annual streamflow, annual evapotranspiration, and seasonal evapotranspiration as changes of their long-term averages (from water years 1951-2018) between a baseline and warmed scenarios, divided by the temperature increment (1°C). In all cases, temperature sensitivities are reported for each of the 616 HUC-8 basins. For pixels that are partially within a river basin, we counted the grid cell's values weighted by their fractional area in the basin.

We applied the same measure of response asymmetry to describe the relative responses of annual streamflow ($Pref_Q$) and evapotranspiration ($Pref_{ET}$) to seasonal warming, as was used in Ban et al. (2020) (Eqs. 1-2).

$$Pref_Q = \frac{\overline{Q_{a,w1d}} - \overline{Q_{a,b}}}{\overline{Q_{a,c1d}} - \overline{Q_{a,b}}} \quad \text{(Eq. 1)}$$

$$Pref_{ET} = \frac{\overline{ET_{a,w1d}} - \overline{ET_{a,b}}}{\overline{ET_{a,c1d}} - \overline{ET_{a,b}}} \quad \text{(Eq. 2)}$$

On the right-hand side of Eqs. 1-2, Q indicates streamflow, ET indicates evapotranspiration, the first subscript indicates the period of calculation (a: annual, w: warm season, and c: cool season), and the second subscript indicates the warming scenario (w1d: warm season 1°C warming, c1d: cool season 1°C warming, and b: baseline). Therefore, $Pref_Q$ ($Pref_{ET}$) is defined as the ratio of annual streamflow (annual evapotranspiration) changes in response to a constant warming magnitude (1°C) in warm season only to the same change in cool season only. A more positive $Pref_{ET}$ ($Pref_Q$) indicates a stronger "preference" for a basin to have stronger annual evapotranspiration (streamflow) response under warm vs. cool season warming. A negative $Pref_{ET}$ ($Pref_Q$) means that the annual evapotranspiration (streamflow) responses have opposite signs under the two seasonal warming. According to the long-term water balance, when the annual soil and snow storage change is negligible and precipitation is fixed, the annual streamflow reduction under

temperature warming equals the annual evapotranspiration increase. Under this water balance framework, Ban et al. (2020) made two critical assumptions: (a) $Pref_Q \approx Pref_{ET}$, and (b) the relative rank of $Pref_{ET}$ across basins is governed by the relative rank of the seasonal ET-T sensitivity ratios (ratios of warm season ET-T sensitivity to cool season ET-T sensitivity, see Eq. 3, the notation is the same as in Eqs. 1-2).

$$\mathrm{rank}(Pref_{ET}) = \mathrm{rank}\left(\frac{\overline{ET_{w,w1d}} - \overline{ET_{w,b}}}{\overline{ET_{c,c1d}} - \overline{ET_{c,b}}}\right) \quad \text{(Eq. 3)}$$

Ban et al. [2020] tested the above two assumptions for four major river basins in the WUS (the Columbia, the Upper Colorado River basin (hereafter UCRB), and the Northern Sierra and Southern Sierra basins). Here, we tested the two assumptions by comparing the $Pref_{ET}$, $Pref_Q$, and seasonal ET-T sensitivity ratios across all 616 HUC-8 basins.

3.3 Annual streamflow response asymmetry estimated from observations

We checked whether our model-based streamflow response asymmetry could be reproduced using observations of annual streamflow from two sources: (i) USGS GAGES Version 2 (GAGES II) reference database, which are identified as stations with minimum anthropogenic disturbances [*Falcone*, 2011], and (ii) USGS WaterWatch streamflow data [*Brakebill et al.*, 2011], which provides a relatively complete set of streamflow data at the HUC-8 level from water year 1951 to 2018. In the GAGESII database, we only chose the gages with more than 20 years that have more than ~11 months (335 days) record each year, resulting in 513 GAGESII stations. We also performed a screening of the WaterWatch records to remove the HUC-8 basins with USGS stations affected by large dams. Specifically, we identified large dams as having storage capacity greater than a quarter of the long-term average annual streamflow based on data from the Global Reservoir and Dam Database (GranD v1.3) [*Lehner et al.*, 2011]. This screening yielded 286 HUC-8 basins as having annual flows that are at most modestly affected by reservoir regulations.

For each selected GAGESII station's contributing area and each screened WaterWatch HUC-8 basin, we calculated the corresponding annual precipitation (P_a) and seasonal mean temperature (T_w and T_c) from VIC model outputs. We applied linear regression at each of the 513 GAGESII stations across years with more than 11 months record, and 286 screened WaterWatch HUC-8 basins across water year 1951 to 2018 using annual streamflow (Q_a) as the dependent variable, and P_a, T_w, and T_c as predictors (Eq. 4).

$$Q_a = S_w T_w + S_c T_c + S_p P_a \quad \text{(Eq. 4)}$$

In Eq. 4, S_w, S_c, and S_p are the regression coefficients. $Pref_Q$ thus is estimated as S_w/S_c. In section 4.2, we focus more on the $Pref_Q$ estimates for basins that have both statistically significant (p=0.1) S_w and S_c.

3.4 Relationships between annual streamflow response asymmetry and basin characteristics

We checked the variations of seasonal ET-T sensitivity (a proxy governing streamflow response asymmetry, tested in sections 3.2 and 4.1) with temperature and seasonal water availability at the HUC-8 basin level. We used simulated basin-average temperature and Gross Incoming Water, and basin-aggregated seasonal evapotranspiration across the 616 HUC-8 basins from the VIC control experiment outputs to carry out the check. In addition to the above two hydroclimate variables, we also incorporated seven basin land surface and hydroclimatic characteristics:

- Elevation: 1/16th degree, aggregated from the GTOPO30 Global 30 Arc Second (~1km) Elevation Dataset (Gesch et al., 1999).
- Runoff ratio, snow cover fraction, and annual mean snow water equivalent (SWE): VIC baseline simulation outputs in this paper.

- Vegetation density: product of the annual mean leaf area index (LAI) and the vegetation cover fraction for each vegetation type summed for each pixel, where LAI and vegetation cover fraction came from the VIC vegetation parameter file.
- Root depth: sum of root depth for each vegetation type weighted by the vegetation cover fraction for each pixel, where the root depth and vegetation cover fraction came from the VIC vegetation parameter file.
- Vegetation height: sum of vegetation height for each vegetation type weighted by the vegetation cover fraction for each pixel, where the vegetation height and vegetation cover fraction came from the NLDAS vegetation classification scheme (Hansen et al., 2000) and parameters (https://ldas.gsfc.nasa.gov/nldas/vegetation-parameters).

We classified the 616 HUC-8 basins based on the seven characteristics and examined how the asymmetries of seasonal ET-T sensitivity and annual streamflow response to seasonal warming vary with the seven characteristics above.

3.5 Detection of the processes dominating ET-T sensitivity

We considered five major processes that affect evapotranspiration change under temperature warming, as derived using a Penman-Monteith framework (e.g. *Ban et al.* [2020] and *Y Yang et al.* [2019]): (a) change of available radiation (R*, net radiation minus ground heat flux) due to processes like albedo change during snowmelt, (b) enhanced vapor-pressure deficit (e_s-e_a) associated with warming, (c) increased surface resistance (r_s) associated with elevated vapor pressure deficit, (d) reduced aerodynamic resistance (r_a) over warmer, less stable land surfaces, and (e) elevated slope of the saturated vapor pressure δ associated with warming. We estimated contributions of the five processes to seasonal ET-T sensitivity using a Penman-Monteith first-

order derivative expansion based on differences between the two season's warming scenarios and baseline, which is the same as in section 3.6 in *Ban et al.* [2020].

4. Results

4.1 Asymmetry of annual streamflow responses to seasonal warming

To check the similarity between the seasonal ET-T sensitivity ratio (see Eq. 3), $Pref_Q$, and $Pref_{ET}$ (see Eqs. 1-2), we plotted their spatial distributions (model-simulated) at the HUC-8 level (Figure 2a-c). The three proxies show highly consistent spatial patterns, as indicated by their pattern correlation values: $Pref_{ET}$ vs. $Pref_Q$: 0.995, $Pref_Q$ vs. dET_{rt}: 0.796, $Pref_{ET}$ vs. dET_{rt}: 0.795 (we calculated pattern correlations using samples within 5% and 95% percentile of the proxies to remove outliers). The consistent spatial patterns are similar to those in *Ban et al.* [2020] for larger basins (smaller panels in Figures 2a-2c, values in those smaller panels are consistent with the cumulative effect expected from the HUC-8 basins involved). Additionally, proxies for HUC-8 basins east of the Continental Divide act mostly like neighbors west of the divide, suggesting strong spatial continuity.

In general, among basins with positive Pref (hereafter referring to both $Pref_Q$ and $Pref_{ET}$) values, basins with larger responses to warm season warming (higher Pref values) are located within the northeast part of the study domain. Basins with smaller responses to warm season warming (lower Pref values) are located within the southwestern part of the study domain (Figures 2a-c). This southwest-northeast gradient in Pref values generally coincides with the direction of decreasing annual temperature and increasing warm vs. cool season Gross Incoming Water ratio (Figures 2d and 2e), which follows the conclusion in *Ban et al.* [2020].

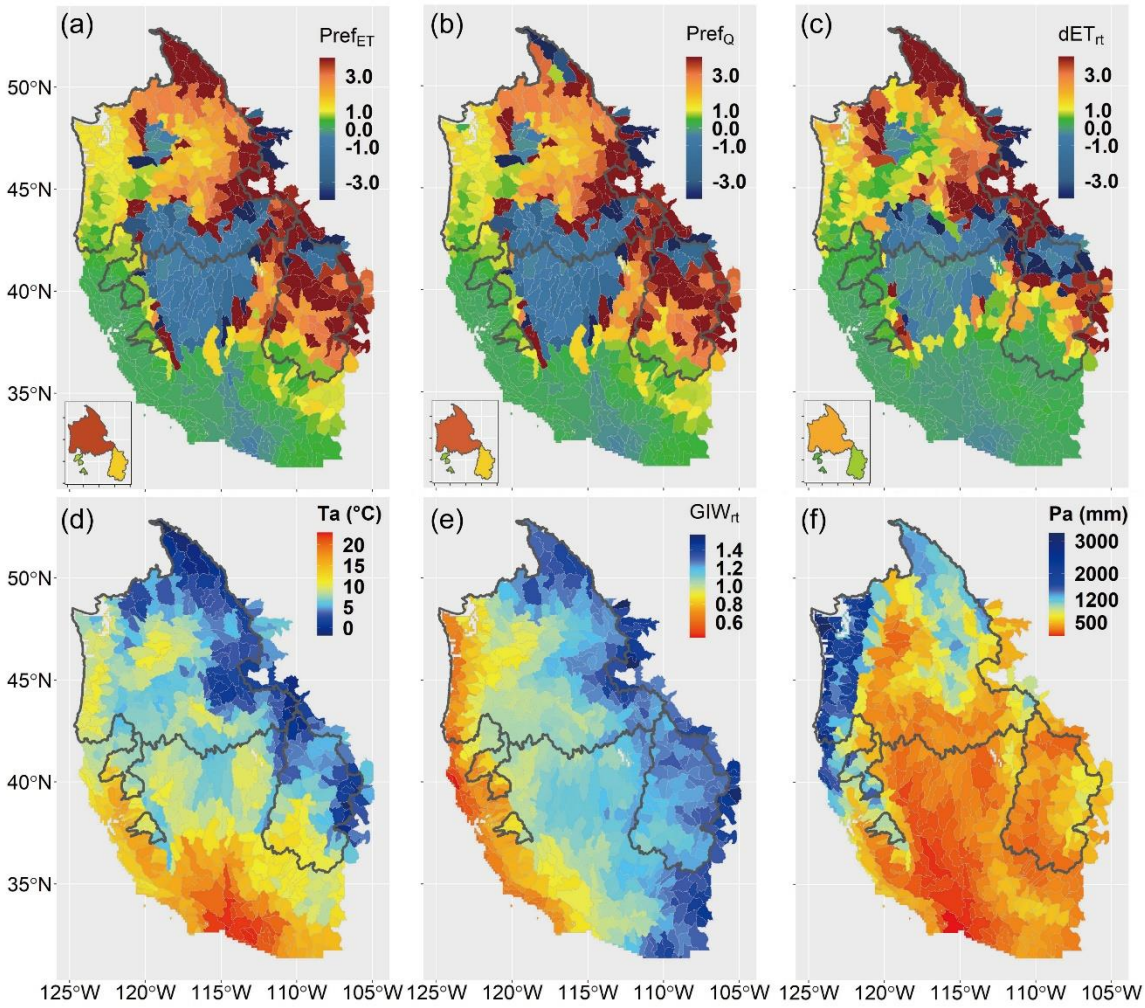

Chapter 2 Figure 2. Proxies of response asymmetry and related variables. (a) $Pref_Q$, (b) $Pref_{ET}$, and (c) seasonal ET-T sensitivity ratio (dET_{rt}) under 1°C warm and cool season warming from the VIC-4.1.2 model results for HUC-8 basins, averaged from the water year 1951 to 2018. The small panels illustrate the basin-average values from multi-model mean results in Ban et al. (2020). (d) basin average annual mean temperature, (e) GIW_{rt}: ratio of basin average warm season Gross Incoming Water (GIW) to basin average cool season GIW, (f) basin average annual precipitation. All values in (d) to (f) are based on climatologies from water year 1951 to 2018.

The HUC-8 level maps of the three proxies (Figures 2a-c) however reveal more complexity than do the larger basin maps, especially concerning negative Pref values. In *Ban et al.* [2020],

multi-model mean Pref values for all four basins were positive, but at the HUC-8 level, negative Pref values are present for some basins and usually are clustered. Negative $Pref_{ET}$ or $Pref_{Q}$ values are caused by annual evapotranspiration decrease or annual streamflow increase only under one of the two seasonal warming cases (mostly under cool season warming). No basin has annual evapotranspiration (streamflow) decreases (increases) under both warming scenarios. Therefore, the positive $Pref_{ET}$ and $Pref_{Q}$ values are only related to the annual evapotranspiration (streamflow) increase (decrease) under both warming scenarios. The Columbia Basin has the largest area with negative Pref values, which cluster in the southern part of the basin (mostly arid to semi-arid, and borders on the Great Basin). The UCRB has negative Pref values in the northeastern part, while the two California basins have no negative Pref values. To further explore the relationship between seasonal responses and the sign and magnitude of Pref, we classified the basins into snow-affected (basin long-term mean Apr 1st SWE >= 20mm) and non-snow-affected group (basin long-term mean Apr 1st SWE < 20mm). We divided each group into four subgroups according to different signs and magnitudes of Pref values (Figure 3):

A. *Snow-affected (SA) group.* 301 of 616 basins (48.86%) (the colored basins in the first row of Figure 3).

A1. *Pref positive and larger than 1.0*, colored in red in Figures 3a-3b. In such basins, annual evapotranspiration (streamflow) increases (decreases) are stronger under warm season warming than under cool season warming. 218 of the 301 snow-affected basins for $Pref_{ET}$ (72.4%) and 209 of 301 snow-affected basins for $Pref_{Q}$ (69.4%) had these characteristics. Most of them coincide with ET-T sensitivity ratios that are positive and larger than 1.0 (colored red in Figure 3c).

A2. *Pref positive and smaller than 1.0*, colored in brown in Figures 3a-3b. In such basins, annual evapotranspiration (streamflow) increases (decreases) are stronger under cool season

warming than under warm season warming. 61 of 301 snow-affected basins for $Pref_{ET}$ (20.3%) and 67 of 301 snow-affected basins for $Pref_{Q}$ (22.3%) had these characteristics. Most of them coincide with ET-T sensitivity ratios that are positive and smaller than 1.0 (colored brown in Figure 3c).

A3. *Pref negative and smaller than -1.0,* colored in dark blue in Figures 3a-3b. 19 of 301 snow-affected basins for $Pref_{ET}$ (6.3%), and 22 of 301 snow-affected basins for $Pref_{Q}$ (7.3%) had these characteristics. Most of them coincide with the ET-T sensitivity ratios that are more negative than -1.0 (colored dark blue in Figure 3c). The 19 negative $Pref_{ET}$ values are all caused by annual evapotranspiration decreases under cool season warming. Among these 19 basins, responses for 10 basins are contributed solely by cool season evapotranspiration decreases, responses for 5 basins are contributed solely by warm season evapotranspiration decrease, and responses for four basins are contributed by both warm and cool season evapotranspiration decreases (Figure S2a). Among the 22 negative $Pref_{Q}$ values, 19 are caused by cool season streamflow increases under cool season warming, and 3 are caused by warm season streamflow increases under warm season warming (Figure S2b). The latter three basins are in the northern part of the Columbia basin, at high elevation with short snow-free seasons and relatively lower vegetation density and shallower root depths than the surroundings (Figure S1). They have much later snowmelt season end dates than low elevation basins and have streamflow increases only in the warm season. The annual streamflow increase magnitudes in these three basins are relatively small (all less than 1%). These three basins do not have annual evapotranspiration decreases, suggesting that the slight annual streamflow increases at these three high elevation basins are associated with snowpack declines.

A4. *Pref negative and larger than -1.0,* colored light blue in Figures 3a-3b. 3 of 301 snow-affected basins (1.0%) for both $Pref_{ET}$ and $Pref_{Q}$ had these characteristics. Most of them coincide

with ET-T sensitivity ratios that are less negative than -1.0 (colored light blue in Figure 3c). The negative Pref values are caused by annual evapotranspiration decreases (annual streamflow increases) under cool season warming, which have a smaller magnitude than the opposite response under warm season warming. All the three annual evapotranspiration decreases (annual streamflow increases) are solely contributed by cool season evapotranspiration decreases (streamflow increases).

For conditions A3 and A4, excepting the three high elevation basins in the northern Columbia River Basin for which annual streamflow increases under warm season warming, all other basins with negative Pref values experienced annual evapotranspiration decreases (annual streamflow increases) under cool season warming. Spatially, these latter basins are mostly located within or at the boundary of the cold desert region (Ecoregion Level-II classification: https://www.epa.gov/eco-research/ecoregions-north-america) in or near the Great Basin, and the West-Central semi-arid prairies area in the northeastern buffer zone of the Columbia River Basin boundary (Figures 3a-3b). Such regions have moderate temperatures (Figure 2d), moderate elevations (Figure S1e), low precipitation (Figure 2f), low runoff ratios (Figure S1d), low vegetation coverage (Figures S1a-S1b), and low snow coverage (Figures S1f-S1g). For these basins, the warm season evapotranspiration decreases under cool season warming can be explained by the Dettinger hypothesis [*Dettinger et al.*, 2004]: under cool season warming, earlier snowmelt releases water exiting the basin before summer comes, which leaves less water available for evapotranspiration later in the year (i.e., warm season). Possible reasons for the small decreases (all <5%) of cool season evapotranspiration under cool season warming (colored in cyan in Figure S2a) are:

1) those basins are mostly water-limited, thus relatively insensitive to elevated evaporative demand under warming [*Condon et al.*, 2020].

2) warmer cool season temperature increases the chance for cool season snowpack to melt before sublimating, which enables a larger portion of snowmelt to become streamflow or to penetrate into deeper soil layers without being sublimated (Barnhart et al., 2016), which is the dominant cool season evapotranspiration process in these basins (Table S1).

3) those basins usually have thin and sparse snow coverage in the cool season. In this context, warming can cause temporally discontinuous snow coverage within the cool season, thus extending the cool season's water-limited period.

B. *Non-snow-affected (nonSA) group.* 315 of the 616 basins (51.1%) were in this group (the colored basins in the second row of Figure 3).

B1. *Positive Pref greater than 1.0* (colored red in Figures 3d-3e). Annual evapotranspiration increases (annual streamflow decreases) are stronger under warm season warming than under cool season warming in these basins, of which there are 60 for $Pref_{ET}$ (19.0%), and 59 for $Pref_{Q}$ (18.7%). Most of these basins have ET-T sensitivity ratios that are positive and larger than 1.0 (colored in red in Figure 3f).

B2. *Positive Pref, less than 1.0*, colored in brown in Figures 3d-3e. Annual evapotranspiration increases (annual streamflow decreases) are stronger under cool season warming than under warm season warming for these basins, of which there are 151 for $Pref_{ET}$ (47.9%) and 154 for $Pref_{Q}$ (48.9%). Most of them have ET-T sensitivity ratios that are positive and smaller than 1.0 (colored in brown in Figure 3f).

B3. *Negative Pref, more negative than -1.0*, colored in dark blue in Figures 3d-3e. 35 basins fall into this category for $Pref_{ET}$ (11.1%) and 36 for $Pref_{Q}$ (11.4%). Most of these basins coincide

with ET-T sensitivity ratios that are negative and smaller than -1.0 (colored in dark blue in Figure 3f). The negative $Pref_{ET}$ and $Pref_{Q}$ values are caused by annual evapotranspiration decreases and annual streamflow increases under cool season warming. For the 35 basins with annual evapotranspiration decreases, 25 are associated solely with cool season evapotranspiration decreases, seven are associated solely with warm season evapotranspiration decreases, and three have both cool season and warm season evapotranspiration decreases (Figure S2a). For the 36 basins with annual streamflow increases, 26 are contributed solely by cool season streamflow increases, and 10 have both warm and cool season streamflow increases (Figure S2b). All these basins are located within or near the boundary of cold desert areas. The decreasing warm season evapotranspiration under cool season warming is due to stronger soil moisture deficits in the beginning of the warm season following enhanced evapotranspiration during cool season warming. Possible reasons for the decreasing cool season evapotranspiration under cool season warming are the same as we discuss for A3 and A4 above.

B4. *Negative Pref, less negative than -1.0*, colored in light blue in Figures 3d and 3e. 69 of 315 non-snow-affected basins for $Pref_{ET}$ (21.9%) and 66 $Pref_{Q}$ (21.0%) had these characteristics. Most of them coincide with ET-T sensitivity ratios that are less negative than -1.0 (colored in light blue in Figure 3f). For the 69 basins that have negative $Pref_{ET}$, 27 basins are associated with warm season evapotranspiration decreases under warm season warming, 39 are associated with cool season evapotranspiration decreases under cool season warming, and three basins are associated with both warm and cool season evapotranspiration decreases under cool season warming. For the 66 basins with negative $Pref_{Q}$, 25 are dominated by cool season streamflow increases under warm season warming, and 41 are dominated by cool season streamflow increases under cool season warming. The 27 basins with warm season evapotranspiration decreases (which includes the 25

basins with cool season streamflow increases) under warm season warming fall into the warm desert Ecoregion Level-II classification (reddish color in Figures S2a and S2b) near the Mojave and Sonoran Deserts. The warm desert regions generally have low precipitation (Figure 2f), low vegetation coverage (Figures S1a and S1b), as well as low snow coverage (Figures S1f and S1g), low runoff ratios (Figure S1d), low elevation (Figure S1e) and higher temperatures (Figure 2d) as compared to the cold desert type. These basins are very arid and have limited streamflow, with maximum basin average annual streamflow less than 40 mm, relative increases of annual streamflow less than 1%. The warm season evapotranspiration decreases under warm season warming in these 27 basins are mostly due to elevated surface resistance associated with warmer temperatures, which is supported by the high surface temperature part (>20 °C) in Figure S3.

In general, the basins with negative Pref values (126 basins for $Pref_{ET}$ and 127 basins for $Pref_{Q}$) are in low elevation, arid regions with high temperatures and little snow coverage. These basins contribute slightly less than 9% of the total streamflow for all 616 HUC-8 basins in the WUS, according to the VIC simulation results. Although these basins have streamflow increases under certain warming scenarios, their streamflow increases tend to be small and far from enough to compensate for streamflow declines elsewhere across our WUS domain.

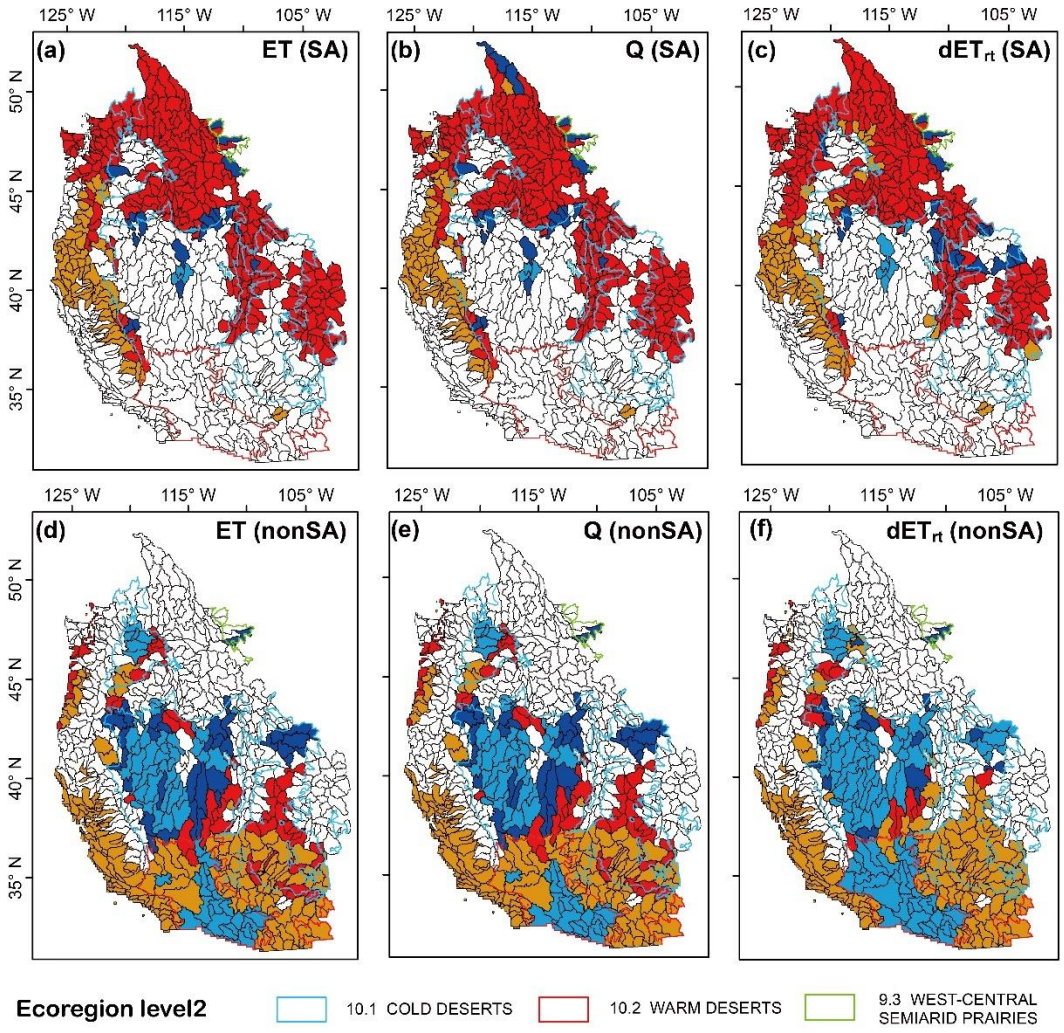

Prefs and dET$_{rt}$	SA (301 basins)	nonSA (315 basins)
More than 1	A1: Inland, high latitude/elevation basins ~71% of SA, .	B1: Inland, high latitude/elevation basins ~19% of nonSA.
(0,1)	A2: Coastal moist basins ~21% of SA.	B2: Coastal moist, or low-latitude, moderate warm basins. ~49% of nonSA.
Less than -1	A3: Cool and arid, or extremely cold, long snow season basins. ~7% of SA.	B3: Cool and arid basins. ~11% of nonSA.
[-1,0)	A4: Cool and arid basins. ~1% of SA.	B4: Cool and arid, or warm desert basins. ~21% of nonSA.

*Prefs and dET$_{rt}$: More than 1: warm season warming dominates, (0,1): cool season warming dominates, Negative: opposite changes under two seasonal warming.

Chapter 2 Figure 3. Map of 616 HUC-8 basins categorized based on snow-affected (SA: mean Apr 1st SWE>20mm) or non-snow affected (nonSA: mean Apr 1st SWE < 20mm) conditions;

signs of $Pref_{ET}$, $Pref_Q$, and ET-T sensitivity ratios (dET_{rt}), and their absolute values relative to 1.0 for the three indices (shown separately in subplots a-f).

4.2 Observation-based asymmetry of annual streamflow responses to seasonal warming

We compared all of the observation-based and VIC model-simulated $Pref_Q$ (Figures 4a and 4b) on a point-by-point basis and found that, despite differences between observation-based and simulated estimates, they share similar probability distributions, and are roughly similar in their variations with air temperature, especially the basins with statistically-significant temperature regression coefficients (S_w and S_c, at p=0.1 level) (Figures 4 and S4). Comparison of Figures 4a and 4b shows that $Pref_Q$ values estimated using WaterWatch have a better match with VIC-simulated ones than do the GAGESII (USGS Reference) gauges, probably because the WaterWatch basin areas (mean drainage area 3180 km^2) are larger than the GAGESII ones (mean drainage area 520 km^2). Both Figures 4a and 4b show decreasing $Pref_Q$ (both model- and observation-inferred) as temperature increases, despite the different spatial coverage between the two datasets (Figure S5). This decreasing trend echoes the pattern of lower $Pref_Q$ under warmer temperature found from multiple model simulations in *Ban et al.* [2020]. We also conducted two similar comparisons for S_w and S_c separately (Figures S6 and S7), and compared $Pref_Q$ spatially (Figure S5), which also show some hint of similarity. The above results provide some data support to the simulated patterns and interpretations of simulated asymmetry in the following sections.

A high fraction of temperature coefficients estimated from Eq. 4 are statistically insignificant (only 30 out of 513 gages, and 31 out of 286 basins are statistically significant at significance level=0.1). Nonetheless, the significant coefficient fractions (5.8% and 10.8%) are still much larger than that can be attributed to chance (0.1*0.1=0.01=1%). Considering all the

above, we argue that the similarity between model- and observation-inferred $Pref_Q$ distribution is not coincidental, which adds credibility to our model-based results.

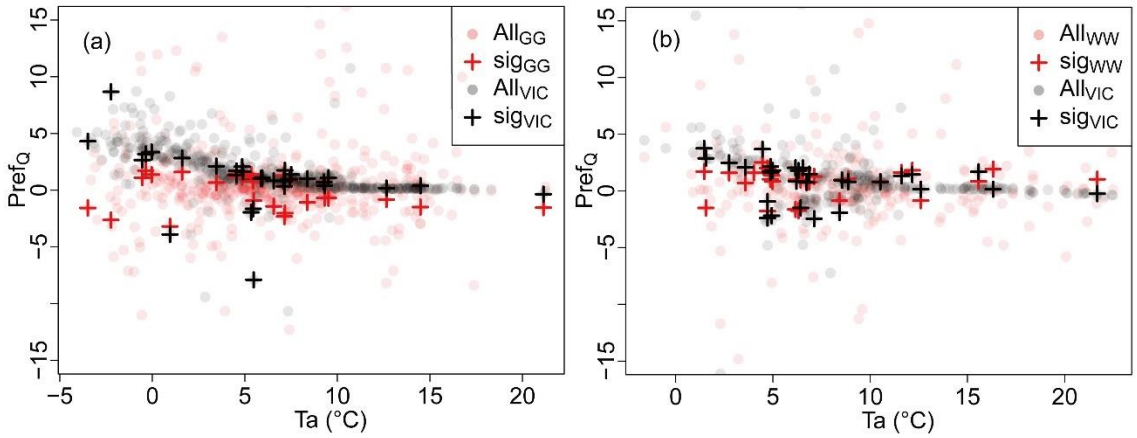

Chapter 2 Figure 4. Point-by-point comparisons between VIC-simulated and observation-based $Pref_Q$, for (a) GAGESII (GG) basins, and (b) WaterWatch (WW) HUC-8 basins. Crosses highlight the basins that have statistically significant (p=0.1) temperature regression coefficients in Eq.4, and other points show all basins' estimates.

4.3 ET-T sensitivity as a function of temperature and gross incoming water

In section 4.1, we confirmed the similarity between the seasonal ET-T sensitivity ratios and the Pref values. Here, we examine another conclusion in *Ban et al.* [2020] relative to the variation of ET-T sensitivity with temperature and Gross Incoming Water (see Section 1 for definition) at the HUC-8 level. Warm and cool season ET-T sensitivities from each of the 616 HUC-8 basins are plotted together as a function of seasonal surface temperature and LOWESS-smoothed into a red curve in Figure 5a. In Figure 5b, relationships between ET-T sensitivities and Gross Incoming Water are plotted as scatterplots separately for warm and cool season.

The increasing-to-decreasing pattern (above -5°C) of ET-T sensitivity as temperature increases (Figure 5a) and the positive relationship between ET-T sensitivity and Gross Incoming Water (Figure 5b) confirm the findings in *Ban et al.* [2020]: i) ET-T sensitivity increases (decreases)

with temperature in cool (warm) environments, so cooler basins have a higher ratio of warm to cool season ET-T sensitivity, thus higher Pref values; and ii) higher water availability favors higher ET-T sensitivity, so among basins with similar temperatures, a higher warm-to-cool-season Gross Incoming Water ratio favors a higher ET-T sensitivity ratio, thus higher Pref values. These relationships support the southwest-to-northeast increasing Pref values (Figures 2a-2b), west-to-east increasing Gross Incoming Water ratio (Figure 2e), and southwest-to-northeast decreasing annual mean temperature across the WUS (Figure 2d, which is a consequence of the both south-to-north increasing latitude and west-to-east increasing elevation), as identified in Section 4.1. We further separated the basins into snow-affected and non-snow-affected subgroups to evaluate the patterns (Figure S8) and found that the patterns in Figures 5a and 5b above are generally consistent in both subgroups.

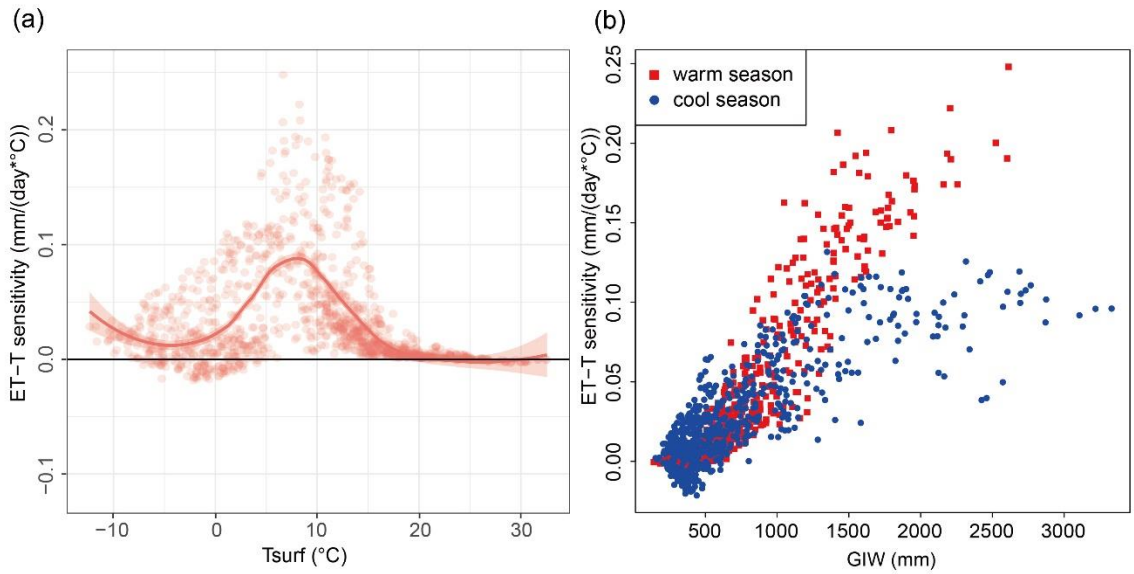

Chapter 2 Figure 5. (a) ET-T sensitivity as a function of seasonal surface temperature (Tsurf). The red curve is LOWESS-smoothed from the seasonal values from each of the 616 HUC-8 basins. Both warm and cool season values are plotted in panel a). The LOWESS-smooth span parameter is 0.5; shading denotes the confidence interval (level=0.95) for the possible locations of the

smoothed lines. The lower 1st and upper 99th percentiles of cool season temperature basins are excluded as outliers and are not plotted in this figure. (b) Relationship between ET-T sensitivity and Gross Incoming Water (GIW: initial water storage in soil and snow in the season plus the season's precipitation). Red (blue) points are for warm (cool) season. Each point denotes a basin's basin-average value.

4.4 Streamflow response asymmetry and ET-T sensitivity asymmetry across basin characteristics

Here we focus on the relationship among basin surface characteristics (other than temperature and water availability discussed above), the asymmetry of annual streamflow response to seasonal warming, and seasonal ET-T sensitivity asymmetry. We calculated seven basin characteristics for each of the 616 HUC-8 basins with VIC parameters and simulations (as described in section 3.4): vegetation height, vegetation density, root depth, runoff ratio, elevation, climatological annual mean snow water equivalent (SWE), and climatological annual mean snow cover fraction (see Figures S1a-g for maps). We also calculated the annual streamflow response asymmetry and ET-T sensitivity asymmetry for each of the 616 HUC-8 basins, in the form of SUB_Q and SUB_{ETS} (defined in Eqs. 5-6, notation is the same as in Eqs. 1-3, where Q indicates streamflow, and ETS is short for ET-T Sensitivity).

$$\mathrm{SUB}_Q = (\overline{Q_{a,b}} - \overline{Q_{a,w1d}}) - (\overline{Q_{a,b}} - \overline{Q_{a,c1d}}) \quad \text{(Eq. 5)}$$

$$\mathrm{SUB}_{ETS} = (\overline{ET_{w,w1d}} - \overline{ET_{w,b}}) - (\overline{ET_{c,c1d}} - \overline{ET_{c,b}}) \quad \text{(Eq. 6)}$$

By construct, a more positive value of SUB_Q or SUB_{ETS} means stronger annual streamflow (evapotranspiration) decreases (increases) under warm vs. cool season warming.

We plotted the 616 HUC-8 basins' SUB_Q and SUB_{ETS} (model-estimated) together with their (seven) basin characteristics and LOWESS-smoothed the results in Figures 6a-6g. To highlight the relationship among SUB_Q, SUB_{ETS} and basin surface characteristics apart from temperature

impacts, we parsed the 616 basins into three zones according to long-term annual mean air temperature (cool: < 4°C, moderate: 4~12°C, warm: >12°C). We also plotted scatterplots corresponding to Figures 6a-6g in Figures S9 and S10, with long-term average annual mean precipitation indicated by colors.

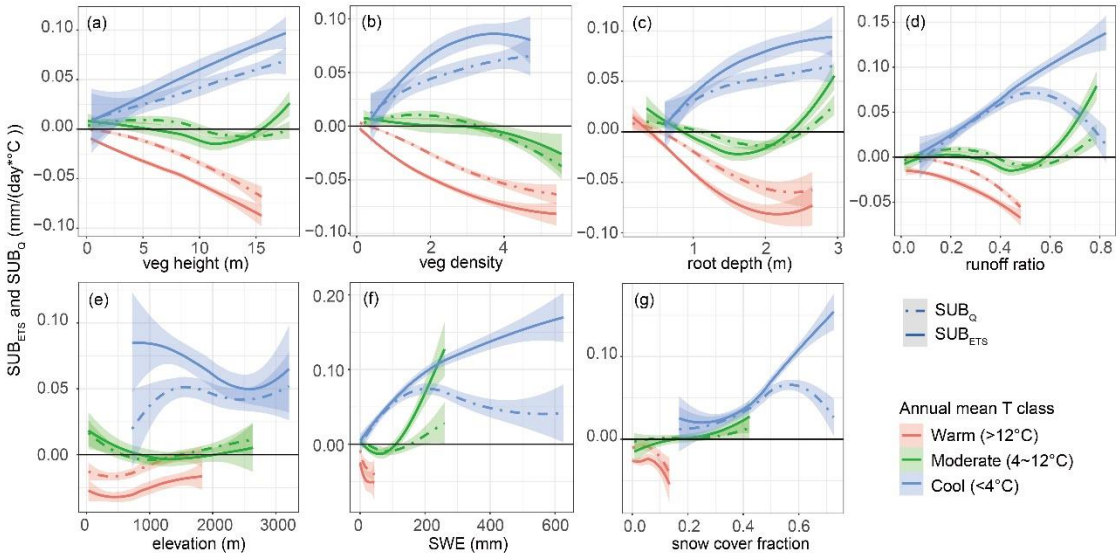

Chapter 2 Figure 6. Variation of asymmetry of seasonal ET-T sensitivity (SUB_{ETS}), and asymmetry of annual streamflow response to seasonal warming (SUBQ) with (a) vegetation height, (b) vegetation density, (c) root depth, (d) runoff ratio, (e) elevation, (f) climatological annual mean SWE, and (g) climatological annual mean snow cover fraction, in three different temperature zones divided according to long-term average annual mean air temperature (Cool: <4°C, Moderate: 4~12°C, and Warm: >12°C) across the HUC-8 basins. Each plot shows LOWESS-smoothed curves of scatterplots (points are not plotted for clarity) between the asymmetries and basin characteristics using values from each 616 HUC-8 basins. The LOWESS-smoothing span parameter is 1.0, shading is as in Figure 5a.

Figures 6a-c suggest that the increasing SUB_{ETS}, SUB_Q is associated with higher, denser, and deeper vegetation structure in cool zones, while in warm zones the relationship is reversed,

and in moderate regions the relationship lies between the two. This is understandable within the VIC model configuration: higher vegetation increases evaporation by increasing roughness length and aerodynamic resistance; denser vegetation increases transpiration by reducing canopy resistance; and deeper root increases transpiration by supporting more water extraction. Therefore, more vegetation enhances the asymmetry of annual evapotranspiration response to seasonal warming, leading to a stronger preference for warm season warming (i.e., more positive SUB_Q and SUB_{ETS} with increasing vegetation) in the cool zones, and contrastingly, a stronger preference for cool season warming (i.e., more negative SUB_Q and SUB_{ETS} with increasing vegetation) in the warm zones.

Figure 6d shows the variation of SUB_{ETS} and SUB_Q with runoff ratio. In cool zones, among basins with runoff ratio <0.5, a higher runoff ratio generally means more rapid spring snowmelt and cooler snowpack, which indicates less sensitive winter snowpack to cool season warming, and more snowmelt occurring in the warm season. This seasonal pattern of snowmelt leads to a stronger preference for evapotranspiration increase under warm season warming (i.e., more positive SUB_Q and SUB_{ETS}). For runoff ratio > 0.5, basins with deep snowpacks can experience non-negligible net snowpack decrease on a long-term scale, generating additional streamflow increases. In such basins, the additional streamflow increases more under warm season warming than under cool season warming, which reduces streamflow reduction from warm season warming by a larger degree than from cool season warming, thus reducing SUB_Q. This tendency is stronger in cooler basins with deeper snowpacks and higher runoff ratios, leading to decreasing preference for warm season warming (i.e., decreasing SUB_Q). In warm zones, higher runoff ratios correspond to higher precipitation, mostly in coastal regions (Figures 2d, 2f, S1d) and greater precipitation in winter vs.

summer (Figure 2e), leading to a stronger preference for cool season warming (i.e., more negative SUB_Q and SUB_{ETS}).

Figure 6e shows relationships among SUB_{ETS}, SUB_Q, and elevation. Across the three temperature zones, there is no significant increasing or decreasing pattern, indicating that elevation's impact on asymmetry mostly comes from its influence on temperature and precipitation (also see Figures S9-S10), excluding which the remaining impact is insignificant.

The curves in Figures 6f-6g share similar patterns. In cool zones, higher SWE and snow cover fraction favors lower temperature, more water available for evapotranspiration in the warm season, and less sensitive snowmelt (and thus evapotranspiration) to warming in the cool season, thus higher SUB_{ETS}. SUB_Q is smaller than SUB_{ETS} and started to decline for cool zones with SWE > ~200 mm and snow cover fraction > ~0.6, which is due to net snowpack decrease as discussed above. In moderate zones, SUB_{ETS} and SUB_Q generally increase with higher SWE and snow cover fractions, which relates to lower temperatures. In warm regions, the snow coverage and SWE are both very low, so the snow impact is not substantial (as shown in Figures S9t-u and S10t-u).

The similarity of curve shapes across Figures 6a-d and 6f-g can be explained by the spatial coincidence of the above basin characteristics. Regions with more abundant snowpack (higher SWE, snow cover fraction) usually support higher runoff ratio and vegetation growth (Figures S1a-d, S1f-g). Across Figures 6a-g, regions with high values of the asymmetry all tend to have lower temperatures. They especially tend towards moderate elevations-high latitude parts of the domain (the northern part of the Columbia River Basin in particular) and moderate latitude-high elevation regions (the northern and eastern parts of the UCRB) (Figures 2d and S1h).

Taken over Figures 6a to 6g, the SUB_{ETS} generally is lower than the SUB_Q in warm zones and at lower values of the seven basin characteristics for the other two temperature zones, which

corresponds with warmer, more arid regions. The SUB_{ETS} generally is higher than the SUB_Q when the values of the seven basin characteristics are higher, corresponding to cooler, more humid basins. The smaller SUB_{ETS} relative to the SUB_Q are due to the compensating effect of warm season evapotranspiration decreases under cool season warming, as discussed in *Ban et al.* [2020]. The larger SUB_{ETS} relative to the SUB_Q generally occur for basins with high snow cover fraction and high SWE, which leads to situations where the net snow storage decline can be non-negligible [*Mote et al.*, 2005; *Mote et al.*, 2018], as discussed above. In other words, long-term snow storage decline mitigates the general trend of stronger streamflow responses to warm season warming at cooler regions, at the price of reducing snowpack.

4.5 Processes dominating streamflow response asymmetry across temperatures

Figure 7a shows the five primary ET-T sensitivity-related processes' (see section 3.5 and Figure 7 captions) contributions to SUB_{ETS} (defined in Eq. 6) as a function of annual mean surface temperature. We calculated their contributions to SUB_{ETS} as their contributions to warm season ET-T sensitivity (using derivative expansion, described in section 3.5) minus those to cool season ET-T sensitivity. We added up the five processes' estimated contributions to SUB_{ETS} (brown curve, Figure 7a), which is quite close to the SUB_{ETS} (red curve, Figure 7a) directly calculated from model output, which confirms the accuracy of the approximation. The process with the largest fractional contribution to SUB_{ETS} is identified as the dominant process on a HUC-8 basin basis (Figure 7b).

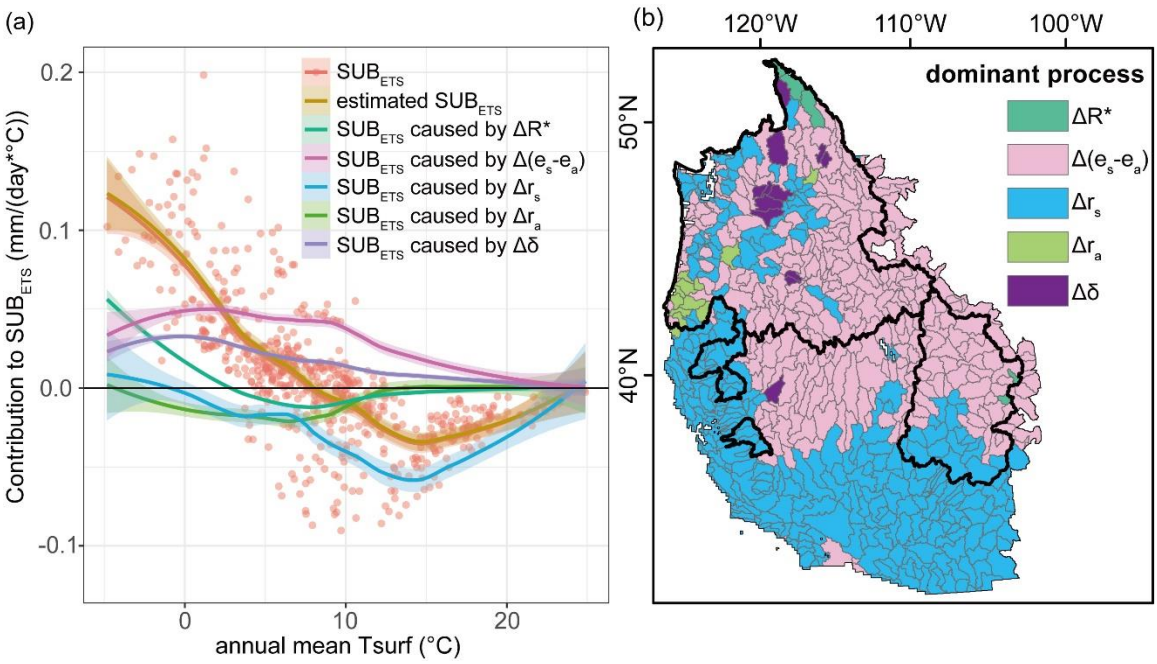

Chapter 2 Figure 7. (a) LOWESS-smoothed asymmetry of ET-T sensitivity (SUB_{ETS}, see Eq. 6 for definition), estimated SUB_{ETS}, and contribution of the five major ET-related processes to the estimated SUB_{ETS} across values for each of the 616 HUC-8 basins, as a function of annual mean surface temperature; The five processes: Available radiation (R*), vapor pressure deficit (e_s-e_a), surface resistance (r_s), aerodynamic resistance (r_a), and slope of saturated vapor pressure curve (δ). (b) Dominant processes controlling SUB_{ETS} for each HUC-8 basin. The LOWESS-smoothing span parameter and shading denotation are the same as the ones in Figure 5a.

Figure 7 suggests that different processes dominate the asymmetry of ET-T sensitivity (SUB_{ETS}) under seasonal warming at different temperatures. The contribution of available radiation change to the ET-T sensitivity asymmetry increases as cooler basins warm (Figure 7a). However, the difference in available radiation changes between warm and cool season warming contributes most to the asymmetry of ET-T sensitivity for only 5 of the 616 basins, all of which are at the highest latitudes (> 50°N) or very high elevations (> 3000m) (Figures 7b, S1e). This result is consistent with the more active snowmelt and albedo-radiation feedback, and therefore

enhanced potential evapotranspiration (Neto et al., 2020) in these basins' warm seasons. For basins with moderate temperatures, the difference in vapor pressure deficit change between warm and cool season warming contributes most to the asymmetry of ET-T sensitivity (293 basins), while changes in aerodynamic resistance and slope of saturated vapor pressure curve dominates fewer (12 for both) basins. For basins with the warmest temperatures, sensitivity of ET to warming-induced vapor pressure deficit change starts to decline, while the sensitivity of ET to surface resistance change remains relatively high at high temperatures (see supplement Figure S17 of Ban et al., 2020). Therefore, change in surface resistance becomes the dominant contributor to ET-T sensitivity's asymmetry (294 basins). Over the entire domain, changes in vapor pressure deficit and surface resistance contribute most to the asymmetry of ET-T sensitivity (587 of the 616 basins) and therefore dominate the annual streamflow response asymmetry.

5. Discussion

Milly and Dunne [2020] and Neto et al. (2020) concluded that increased net radiation from reflective snow loss under warming contributes most to the annual streamflow decline under annual warming for the UCRB. However, in our results, for the asymmetry of streamflow responses to seasonal warming, change in available radiation contributes less than change in vapor pressure deficit and surface resistance across most of the WUS (Figure 7). There are several reasons for this. First, our discussion focuses on the asymmetry of annual streamflow response to seasonal warming instead of the annual streamflow response to annual warming as in *Milly and Dunne* [2020]. Radiation-driven evapotranspiration increase is more evenly split by the warm and cool seasons than are evapotranspiration increases driven by changes in vapor pressure deficit or surface resistance (Figure S12, taking UCRB as an example). Therefore, changes in vapor pressure deficit and surface resistance contribute more substantially to the seasonal asymmetry of annual

streamflow response than do changes in available radiation (Figure S12). Second, we calculated contributions of vapor pressure deficit change and surface resistance change to evapotranspiration changes explicitly and separately in the Penman-Monteith expansion, while *Milly and Dunne* [2020] implicitly included contributions from the two processes together in the non-linear term category. Due to the feedback between elevated vapor pressure deficit and elevated surface resistance, if we consider the two factors' total effect on evapotranspiration changes, their contributions partially cancel out, and the remaining net contribution to annual evapotranspiration change under annual 1°C warming is smaller than the contribution from available radiation change in the study area (UCRB) of *Milly and Dunne* [2020] (Table S2). Nevertheless, discussing the two factors explicitly and separately is beneficial since the cancellation level varies across different hydroclimate conditions, and varies when discussing the response asymmetry instead of the annual response to annual warming (Figure 7).

We also show in Table S2 that when contributions from surface resistance change and vapor pressure deficit change partially cancel, the available radiation change still contributes less than the change in the slope of the saturated vapor pressure curve. This contribution ranking differs from *Milly and Dunne* [2020]'s finding that snow-albedo effect contributes more to streamflow decline than do temperature-associated changes in saturated vapor pressure. This difference in our results and theirs is probably due to differences in the evapotranspiration calculation framework. Our results come from a Penman-Monteith framework that considers the impact of vapor pressure deficit change on actual evapotranspiration, while *Milly and Dunne* [2020] used a Priestley-Taylor framework that discounts this impact. Under warming, reduced snowpack and albedo elevate net radiation, enhancing latent heat flux and bringing more moisture to the air, which reduces the vapor pressure deficit increment that directly comes from warming. This negative side effect of enhanced

radiation on vapor pressure deficit mitigates the radiation-driven evapotranspiration increase under warming somewhat. However, as mentioned above, the vapor pressure deficit impact on evapotranspiration is ignored in Priestley-Taylor framework. As a result, using a Priestley-Taylor framework results in a larger contribution of radiation (e.g., snowmelt-albedo feedback) to evapotranspiration increase and hence streamflow decline under warming.

We recognize that our land surface modeling does not consider the impact of elevated humidity from evapotranspiration increase on vapor pressure deficit, which could overemphasize vapor pressure deficit increase under temperature warming, leading to a larger contribution of vapor pressure deficit change to evapotranspiration increase. To check if this effect is substantial, we compared the relationship between vapor pressure deficit and air temperature in the VIC model and one high-resolution (50km) general circulation model (CNRM-CM6-1-HR) acquired from the Coupled Model Intercomparison Project (CMIP) version 6 multi-model ensemble [*Juckes et al.*, 2020; *Voldoire*, 2019]. We used the two models' daily historical period from 1950/01/01 to 2014/12/31 for the UCRB (using basin averages) and plotted the results in Figure S13. Vapor pressure deficit in the coupled model is slightly lower than that in the VIC model at moist pixels, and the two converge in regions with low soil moisture. In general, the difference between the slope of vapor pressure deficit vs. air temperature is not substantial between the two models, indicating the feedback between enhanced evapotranspiration and vapor pressure deficit should not substantially affect our findings based on the off-line implementation of the VIC model.

In addition to our model-based evaluation in section 4.4, we also utilized observation-based estimates (i.e., S_w and S_c in Eq. 4) to check their relationships with basin characteristics (Figure S11, detailed discussions see Text S1). Besides the similarity in a general context, the observation-based results are more inclined to have a stronger streamflow decrease under cool season warming

especially in moderate regions, and reflect a stronger suppressive effect of long-term snowpack reduction on streamflow sensitivity to warm season warming in cool regions, compared to results from model-simulations. Supposing the observation-based estimates can represent the reality, these differences may reflect how the real-world sensitivities could deviate from simulations.

Despite these differences, overall similarities between simulated and observation-based results (Figure 4, Figures S4-S7) suggest that the simulated results are not just reflecting how the model works, but also the streamflow response in the external world. Here, some differences between simulated and observation-based estimates of streamflow response are not unexpected, and we choose to rely on model outputs because: 1) Observation-based estimations treat each year as an individual realization of reference climates, which is less clear and informative than the model simulations treating baseline climatology as the reference climate; 2) Interannual variations in precipitation and their effect on streamflow generally dominate effects of temperature variation, complicating extraction of temperature effects from observations. This is a problem as well in observation-based estimations of elasticity, for example of annual streamflow to potential evapotranspiration [*Xiao et al.*, 2020]; 3) Some other issues in the observation-estimates, including shorter records, linear assumption, fewer predictors, and potential inevitable human disturbances to observations even after screening. There are also limitations in model simulations, such as static and smoothed parameters that may cause stronger spatial-smoothness of asymmetry than in reality.

The streamflow response asymmetry and its controlling mechanisms (characteristics) discussed in this paper represent a refinement of previous runoff-climate studies at much lower spatial resolution (Ban et al., 2020; Das et al., 2011) and for seasonal rather than annual scale of warming (e.g., Milly and Dunne, 2020). Future studies could follow the pathway we've developed to address additional issues such as implications of differential warming for seasonal water scarcity

(especially in the dry-season). Exploration of seasonal streamflow responses to differential warming might also explore the implications of vegetation dynamics, and atmosphere-land surface coupling.

6. Conclusions

We examined the complex spatial patterns of annual streamflow relative response to warm vs. cool season warming across the WUS. At a much higher granularity (HUC-8), we confirmed relationships between annual streamflow response asymmetry, temperature, and Gross Incoming Water found in our earlier work at much coarser spatial scales [*Ban et al.*, 2020]. We also evaluated the observation-based support for model-based sensitivity estimates; examined impacts of different basin surface characteristics on the patterns of annual streamflow relative response to seasonal warming; identified the processes that contribute most to the annual streamflow response asymmetry across the 616 HUC-8 basins, and discussed the relative role of net radiation as drivers to annual streamflow sensitivity to seasonal warming. All of these analyses expand on our previous work [*Ban et al.*, 2020]. Additionally, the smooth transition of results from west- to east- of the Continental Divide suggests that our findings could be applied to other similar basins (snow-dominated, asymmetrical seasonal warming).

Based on our work, we conclude that:

1. Using the ratio of annual streamflow decreases resulting from warm vs. cool season warming, moist basins with relatively low temperatures, high warm-to-cool-season Gross Incoming Water ratios, and moderate winter snow accumulation have the largest asymmetries (ratio > 1). These basins are mostly at high latitude (north of 37.5°N) or high elevation, especially the northern Columbia River basin and most of the Upper Colorado River Basin. Warmer coastal basins have smaller asymmetry (ratio < 1). Extremely warm and arid basins (e.g., those bordering

on the Mojave and Sonoran Deserts) and extremely cold basins with long snow seasons (e.g., three basins at the northern boundary of the Columbia River Basin) have negative asymmetries, with annual streamflow increases under warm season warming. Extremely arid but moderate temperature basins (e.g., those draining to the Great Basin) also have negative asymmetries, but with annual streamflow increases under cool season warming. Generally, stronger asymmetry occurs for cooler basins. This is because the ratio between warm and cool season evapotranspiration-temperature sensitivity which constrains the asymmetry is higher for cooler temperatures. *Ban et al.* [2020] found a similar pattern among four much larger river basins.

2. LOWESS-smoothed relationships between basin characteristics and asymmetry of annual streamflow responses from VIC indicate that cool (warm) basins streamflow has an asymmetrical tendency to be more sensitive to warm (cool) season warming. In both types of basins, increased vegetation (height, root depth, and density) enhances the above tendency by enhancing evapotranspiration and thus amplifies ET-T sensitivity. Runoff ratio and snow also enhance the tendency when runoff ratio<0.5, SWE<200mm, and snow cover fraction<0.6. Above these thresholds, net snowpack decrease causes additional snowmelt, a larger proportion of which occurs under warm season warming than cool season warming, mitigating the tendency of streamflow to decrease under warm season warming. Compared with model-based results, observation-based estimates show less asymmetry towards warm season warming.

3. Different warming-associated processes dominate the asymmetry of seasonal evapotranspiration-temperature sensitivity and hence the response asymmetry for annual streamflow across the 616 HUC-8 basins. In the extremely cold basins with the shortest snow-free season with 85% or more of snowmelt-generated streamflow occurring after Apr 1st, available radiation changes that primarily due to reduced snow cover dominate the streamflow response

asymmetry; in basins with intermediate temperature, vapor pressure deficit changes dominate, and in basins with the warmest temperatures, surface resistance increases under warmer temperature dominate.

Acknowledgments

We acknowledge Mr. Chandramauli Awasthi and Dr. Sankar Arumugam at North Carolina State University and Dr. Richard Vogel at Tufts University for their help in setting up panel regression with observations in our exploration for the paper. We acknowledge Chen Xin and Lu Su of UCLA Department of Geography for helpful discussions. We acknowledge the World Climate Research Programme, which, through its Working Group on Coupled Modelling, coordinated and promoted CMIP6. We thank the climate modeling groups for producing and making available their model output, which we used in the discussion section, the Earth System Grid Federation (ESGF) for archiving the data and providing access, and the multiple funding agencies who support CMIP6 and ESGF. Data and codes in this paper are publicly available at the following URLs:

GRanD v1.3 database: http://globaldamwatch.org/data/#core_global. USGS GAGESII: https://water.usgs.gov/GIS/metadata/usgswrd/XML/gagesII_Sept2011.xml#stdorder.

USGS WaterWatch: https://waterwatch.usgs.gov/index.php?id=wwds_runoff.

VIC-4.1.2.g: https://doi.org/10.5281/zenodo.4695040.

Other data (and information) used in this paper: https://doi.org/10.6084/m9.figshare.14349527.v5.

This work was funded in part by a grant from the NOAA Regional Integrated Sciences and Assessments (RISA) program to the California Nevada Climate Applications Program (CNAP) at the Scripps Institution of Oceanography, grant number NA17OAR4310284, under subaward to the University of California, Los Angeles.

References

Adam, J. C., Hamlet, A. F., & Lettenmaier, D. P. (2009). Implications of global climate change for snowmelt hydrology in the twenty-first century. Hydrological Processes: An International Journal, 23(7), 962-972.

Ban, Z., Das, T., Cayan, D., Xiao, M., & Lettenmaier, D. P. (2020). Understanding the asymmetry of annual streamflow responses to seasonal warming in the Western US. Water Resources Research, e2020WR027158.

Barnett, T. P., Adam, J. C., & Lettenmaier, D. P. (2005). Potential impacts of a warming climate on water availability in snow-dominated regions. Nature, 438(7066), 303-309.

Barnhart, T. B., Molotch, N. P., Livneh, B., Harpold, A. A., Knowles, J. F., & Schneider, D. (2016). Snowmelt rate dictates streamflow. Geophysical Research Letters, 43(15), 8006-8016.

Bohn, T. J., Livneh, B., Oyler, J. W., Running, S. W., Nijssen, B., & Lettenmaier, D. P. (2013). Global evaluation of MTCLIM and related algorithms for forcing of ecological and hydrological models. Agricultural and forest meteorology, 176, 38-49.

Brakebill, J. W., Wolock, D. M., & Terziotti, S. (2011). Digital Hydrologic Networks Supporting Applications Related to Spatially Referenced Regression Modeling 1. JAWRA Journal of the American Water Resources Association, 47(5), 916-932.

Condon, L. E., Atchley, A. L., & Maxwell, R. M. (2020). Evapotranspiration depletes groundwater under warming over the contiguous United States. Nature communications, 11(1), 1-8.

Das, T., Pierce, D. W., Cayan, D. R., Vano, J. A., & Lettenmaier, D. P. (2011). The importance of warm season warming to western US streamflow changes. Geophysical Research Letters, 38(23).

Dettinger, M. D., Cayan, D. R., Meyer, M. K., & Jeton, A. E. (2004). Simulated hydrologic responses to climate variations and change in the Merced, Carson, and American River basins, Sierra Nevada, California, 1900–2099. Climatic Change, 62(1), 283-317.

Falcone, J. A. (2011). GAGES-II: Geospatial attributes of gages for evaluating streamflow. US Geological Survey.

Forbes, W. L., Mao, J., Jin, M., Kao, S.-C., Fu, W., Shi, X., et al. (2018). Contribution of environmental forcings to US runoff changes for the period 1950–2010. Environmental Research Letters, 13(5), 054023.

Gesch, D. B., Verdin, K. L., & Greenlee, S. K. (1999). New land surface digital elevation model covers the Earth. Eos, Transactions American Geophysical Union, 80(6), 69-70.

Hansen, M. C., DeFries, R. S., Townshend, J. R., & Sohlberg, R. (2000). Global land cover classification at 1 km spatial resolution using a classification tree approach. International journal of remote sensing, 21(6-7), 1331-1364.

Hayhoe, K., Cayan, D., Field, C. B., Frumhoff, P. C., Maurer, E. P., Miller, N. L., ... & Verville, J. H. (2004). Emissions pathways, climate change, and impacts on California. Proceedings of the national academy of sciences, 101(34), 12422-12427.

Juckes, M., Taylor, K. E., Durack, P. J., Lawrence, B., Mizielinski, M. S., Pamment, A., et al. (2020). The CMIP6 data request (DREQ, version 01.00. 31). Geoscientific Model Development, 13(1), 201-224.

Lehner, B., Liermann, C. R., Revenga, C., Vörösmarty, C., Fekete, B., Crouzet, P., et al. (2011). High-resolution mapping of the world's reservoirs and dams for sustainable river-flow management. Frontiers in Ecology and the Environment, 9(9), 494-502.

Li, D., Wrzesien, M. L., Durand, M., Adam, J., & Lettenmaier, D. P. (2017). How much runoff originates as snow in the western United States, and how will that change in the future? Geophysical Research Letters, 44(12), 6163-6172.

Liang, X., Lettenmaier, D. P., Wood, E. F., & Burges, S. J. (1994). A simple hydrologically based model of land surface water and energy fluxes for general circulation models. Journal of Geophysical Research: Atmospheres, 99(D7), 14415-14428.

Livneh, B., Rosenberg, E. A., Lin, C., Nijssen, B., Mishra, V., Andreadis, K. M., et al. (2013). A long-term hydrologically based dataset of land surface fluxes and states for the conterminous United States: Update and extensions. Journal of Climate, 26(23), 9384-9392.

Milly, P. C., & Dunne, K. A. (2020). Colorado River flow dwindles as warming-driven loss of reflective snow energizes evaporation. Science, 367(6483), 1252-1255.

Mote, P. W., Hamlet, A. F., Clark, M. P., & Lettenmaier, D. P. (2005). Declining mountain snowpack in western North America. Bulletin of the American Meteorological Society, 86(1), 39-50.

Mote, P. W., Li, S., Lettenmaier, D. P., Xiao, M., & Engel, R. (2018). Dramatic declines in snowpack in the western US. Npj Climate and Atmospheric Science, 1(1), 1-6.

Neto, A. A. M., Niu, G. Y., Roy, T., Tyler, S., & Troch, P. A. (2020). Interactions between snow cover and evaporation lead to higher sensitivity of streamflow to temperature. Communications Earth & Environment, 1(1), 1-7.

Qin, Y., Abatzoglou, J. T., Siebert, S., Huning, L. S., AghaKouchak, A., Mankin, J. S., et al. (2020). Agricultural risks from changing snowmelt. Nature Climate Change, 10(5), 459-465.

Rupp, D. E., Li, S., Mote, P. W., Shell, K. M., Massey, N., Sparrow, S. N., et al. (2017). Seasonal spatial patterns of projected anthropogenic warming in complex terrain: a modeling study of the western US. Climate Dynamics, 48(7-8), 2191-2213.

Simley, J.D., Carswell Jr., W.J., 2009, The National Map—Hydrography: U.S. Geological Survey Fact Sheet 2009-3054, 4 p.

Stewart, I. T., Cayan, D. R., & Dettinger, M. D. (2004). Changes in snowmelt runoff timing in western North America under abusiness as usual'climate change scenario. Climatic Change, 62(1), 217-232.

Su, L., Cao, Q., Xiao, M., Mocko, D. M., Barlage, M., Li, D., et al. (2021). Drought Variability over the Conterminous United States for the past century. Journal of Hydrometeorology.

Vano, J. A., & Lettenmaier, D. P. (2014). A sensitivity-based approach to evaluating future changes in Colorado River discharge. Climatic Change, 122(4), 621-634.

Vano, J. A., Nijssen, B., & Lettenmaier, D. P. (2015). Seasonal hydrologic responses to climate change in the P acific N orthwest. Water Resources Research, 51(4), 1959-1976.

Voldoire, A. (2019). CNRM-CERFACS CNRM-CERFACS CNRM-CM6-1-HR model output prepared for CMIP6 CMIP historical. Version 20200130. Earth System Grid Federation. doi:https://doi.org/10.22033/ESGF/CMIP6.4067 .

Xiao, M., Gao, M., Vogel, R. M., & Lettenmaier, D. P. (2020). Runoff and Evapotranspiration Elasticities in the Western United States: Are They Consistent With Dooge's Complementary Relationship? Water Resources Research, 56(8), e2019WR026719.

Yang, Y., Roderick, M. L., Zhang, S., McVicar, T. R., & Donohue, R. J. (2019). Hydrologic implications of vegetation response to elevated CO 2 in climate projections. Nature Climate Change, 9(1), 44-48.

Chapter 3 The Increasing Role of Seasonal Rainfall in Western U.S. Summer Streamflow

(This chapter has been published in *Geophysical Research Letters*: Ban, Z., Li, D., & Lettenmaier, D. P. (2023). The Increasing Role of Seasonal Rainfall in Western U.S. Summer Streamflow. Geophysical Research Letters, 50(9), e2023GL102892.

Abstract: Summer streamflow variations strongly affect water supply reliability and ecological functioning of western U.S. (WUS) streams. Traditional snow-based forecasts of summer streamflow are becoming less accurate with warming-induced reductions in winter snow accumulation. This reflects a rising importance of competing runoff-generating processes in controlling summer streamflow variations, primarily an increasing role of rainfall in contrast to snowmelt. Here, based on a snowmelt-rainfall tracking algorithm applied to two hydrological models, we show that cool-season rainfall provides an important volumetric contribution to summer streamflow for many WUS streams in the current climate, and this contribution will increase under climate warming, especially in years with warm snow droughts and abnormally dry summers. We also show that seasonal rainfall (warm-/cool-seasons) dominates the variability of summer streamflow across ~70% area of WUS. We show that an increasing warm-season rainfall contribution to summer streamflow (largely replacing snowmelt) results in reduced summer streamflow predictability.

Plain Language Summary: Summer streamflow is a critical water resource in the generally dry summers of the western U.S. (WUS), and is routinely forecasted using spring snowpack and/or winter total precipitation as primary predictors. However, climate warming leads to reduced snowpacks, exacerbates summer low flows, and reduces the accuracy of snow-based summer streamflow forecasts. On the other hand, the role of winter rainfall as a control on summer streamflow increases in a warmer climate. Here, we explicitly quantify the contributions from

cool-season rainfall, warm-season rainfall, and snowmelt to summer streamflow across the WUS, and how they change under a uniformly 1°C warmer climate. We show that the cool-season rainfall contribution to summer streamflow increases under warming across WUS, especially in streams that currently have low-to-moderate snow contributions to runoff, and in years with anomalously warm winters and/or dry summers. We also show that the warm-season rainfall contribution to summer streamflow increases widely, especially in the southern interior of WUS in a warmer climate, and that increasing warm-season rainfall contribution to summer streamflow (largely replacing snowmelt) results in reduced summer streamflow predictability.

1 Introduction

Summer (Jul-Sep) streamflow is a critical water resource for aquatic ecosystems, agriculture, industry, and municipal water supply in the Western U.S. (WUS). Although Jul-Sep streamflow for most WUS river basins is not a major part of annual runoff volume, it is a period when the lowest flow generally occurs, and therefore is especially ecologically important and arguably will become more so as the climate warms. Summer streamflow represents a balance between snow and soil water storage accumulated in the previous winter, and peaking water demand driven by seasonally high net radiation and vapor pressure deficit [*Cooper et al.*, 2018; *Crozier et al.*, 2008; *Li et al.*, 2017; *Palmer et al.*, 2009]. This tension is exacerbated as climate warming causes earlier snowmelt and soil moisture depletion, resulting in reduced summer streamflow. This change in summer water availability adversely impacts wildlife and water supply, and accentuates seasonal drought and wildfires [*Stewart et al.*, 2005]. Worse still, reduced snowmelt challenges the predictability of summer streamflow for snow-based forecasting/management systems [*He et al.*, 2016; *Livneh and Badger*, 2020; *Mote*, 2003; *Shrestha et al.*, 2022; *Tsuruta and Schnorbus*, 2021] (see also Supporting Information Figs. S1-S3 which

show smaller correlations between summer streamflow and spring snowpacks in less snow-covered river basins across WUS). These adverse consequences associated with ongoing trends in snowmelt and summer streamflow heighten the need for better understanding of controls on summer streamflow variations. They also bring attention to bear on streamflow contributing processes other than snowmelt that might better constrain forecasts of summer streamflow in a reduced snow future.

Tague and Grant [2009] proposed a simple conceptual model that relates summer streamflow sensitivity to warming to two factors: timing of peak snowmelt relative to late season flows, and drainage efficiency. More recently, understanding of summer streamflow variations has focused on long-term elasticities/sensitivities of summer low flows to spring snowmelt, winter accumulative water supply, and summer evapotranspiration [*Cooper et al.*, 2018; *Safeeq et al.*, 2013; *Safeeq et al.*, 2014]. However, rainfall in winter and the following warm season (Apr-Sep) can make nontrivial contributions to summer streamflow by replenishing soil moisture, a mechanism that generally has received less attention than snowmelt. For example, *Lapides et al.* [2022] found that warm season runoff generation is strongly tied to root-zone water storage deficits, which must be replenished by snowmelt or rainfall before substantial runoff occur. Moreover, *Cooper et al.* [2018] found a larger percentage change of summer low flows per percentage change of winter precipitation for rain-dominated catchments as compared with snow-dominated catchments in maritime WUS mountains. Furthermore, quality-controlled SNOTEL data show a significant decrease in annual maximum snowmelt but a significant increase in the frequency of rain-on-snow events across the WUS over the period 1979–2017 [*Yan et al.*, 2019]. These findings suggest a future in which cool-season (Oct-Mar) rainfall will be increasingly important to streamflow in the following summer and will at least partly displace the contribution of snowmelt

to summer streamflow. Despite many previous studies that have discussed ongoing precipitation delivery (i.e., composition of rainfall and snowmelt fraction) change impacts on annual streamflow (e.g., *Kiewiet et al.* [2022]), knowledge of how precipitation delivery impacts sub-annual (e.g., summer) streamflow is still limited, especially for large spatial domains. How the water source (rainfall and snowmelt) composition of summer streamflow will evolve under warming, and how the warming-induced change in precipitation delivery affects summer streamflow predictability across the WUS has received little previous attention, and is our focus here.

We focus on the water source composition of summer streamflow across WUS to (i) quantify the contribution to summer (Jul-Sep) streamflow from cool-season (Oct-Mar) rainfall, warm-season (Apr-Sep) rainfall, and snowmelt; (ii) assess the change in contribution from these three components under climate warming, and (iii) examine whether and how the summer streamflow predictability relates to above precipitation delivery change.

2 Methods

We derive explicit quantifications of contributions to summer streamflow from snowmelt (F_snow), cool-season rainfall (F_rainc) and warm-season rainfall (F_rainw). We do so by further developing the snowmelt-tracking system of *Li et al.* [2017] to allow custom-period tracking (details in Text S1). Our modification separates the contribution to summer streamflow from cool and warm-season rainfall temporally by the time the rainfall occurs. This temporal partitioning also separates snowmelt from rainfall (the rain-on-snow refreeze effect on the tracking is negligible (see *Li et al.* [2017]). This modification maintains the reliability of the original algorithm in *Li et al.* [2017], for which the snowmelt contribution showed good agreement with isotope measurements.

We applied the custom-period tracking algorithm to two land surface models: the Variable Infiltration Capacity model (VIC) version 4.1.2g [*Liang et al.*, 1994] and Noah-MP (HRLDAS-v3.9, with Jordan's snowfall-rainfall partitioning scheme) [*Niu et al.*, 2011] to account for uncertainty related to model specifics. We note that both models use physics-based snow parameterizations relying on first principles and are generally non-adjustable, unlike the models' runoff response algorithms that require calibration for parameters such as soil water holding capacity. Such calibrations have been performed in previous studies (notably for VIC [*Livneh et al.*, 2013]). Furthermore, comparisons of simulated and observed snow water equivalent (SWE) and streamflow from numerous previous studies using standard versions of VIC in particular have shown plausible consistency with observations [*Chen et al.*, 2014; *Li et al.*, 2017; *Livneh et al.*, 2013].

We ran both models from water year 1951-2018 with ten repeats of the first year as spin up. Both models were forced by 1/16th degree lat-long degree meteorological forcings from *Livneh et al.* [2013], which were extended to 2018 by *Su et al.* [2021]. Simulated results of summer streamflow from the two models show a plausible consistency (albeit with slight underpredictions at low values in Noah-MP) with observations (Fig. S4). Based on the simulations, we calculated the contributions from the three sources (cool/warm season rainfall, snowmelt) to summer streamflow on a grid-cell level across the WUS. To avoid initialization issues with the tracking algorithm, we excluded early years 1950-1958 from our analysis which was performed for the 60-year period from water year 1959-2018.

To assess the climate warming impact on the role of each contributor, we applied uniform 1°C warming to the historical (baseline) simulations for each of the two models. Furthermore, we assessed the contributions' spatial pattern by categorizing the WUS into different land surface

conditions by three factors: elevation, precipitation ratio (defined as the ratio of cool-season precipitation to warm-season precipitation), and long-term average summer streamflow volume. Temporally, we separated the 60 years for each grid-cell into two categories: (1) percentile of the summer streamflow historical distribution (<33.3%, 33.3%-66.7%, and >66.7%), and (2) We defined warm snow drought years as having below-median peak SWE (i.e., maximum depth of snow water equivalent within a year), but above-median cool-season temperature and precipitation, dry snow drought years as having below-median peak SWE, cool-season temperature and precipitation, and warm-and-dry snow drought years as having below-median peak SWE and cool-season precipitation, and above-median cool-season temperature. We defined no snow drought years as having above-median peak SWE.

To assess the relationship between precipitation delivery (the contributors) and summer streamflow predictability, at each grid cell, we conducted a stepwise regression between summer streamflow (dependent variable) and cool-season rainfall, warm-season rainfall, and peak SWE as predictors across the 60 years. Among the predictors selected from the stepwise regression, we removed the ones without statistically significant coefficients (t-test, significance level = 0.05). Then, from the predictors remaining in the equation, we identified the predictor that explained most of the summer streamflow variance, as found by the analysis of variance of the stepwise regression (ANOVA) as the dominant predictor. Finally, we assessed how different contributors and how their warming-driven changes impact summer streamflow predictability by conducting (i) linear regression using peak SWE as the only predictor, and (ii) multiple linear regressions that additionally included cool-season rainfall and/or Apr-Jun rainfall as predictors. We note that although our warm season is Apr-Sep, we avoid using summer months' rainfall in analyzing summer streamflow predictability under both baseline and uniform 1°C warming scenarios. We

use adjusted-R^2 (Eq. 1) to measure the regression performance. We calculated adjusted-R^2 using 60-years leave-one-year-out summer streamflow predictions based on predictor variables from model simulations.

$$\bar{R}^2 = 1 - \frac{SS_{res}/(n-p-1)}{SS_{tot}/(n-1)} \quad \text{(Eq. 1)}$$

where p is the number of predictors, n is the population size, SS_{res} is the sum of squares of residuals, and SS_{tot} is the sum of squares.

3 Results

3.1 Contribution of cool-season rainfall to summer streamflow

Fig. 1a shows the contributions from cool-season rainfall to summer streamflow (F_rainc) from the tracking algorithm applied to the VIC simulation results. Across the WUS, cool-season rainfall substantially contributes to summer streamflow, on average accounting for 10.5% (corresponding Noah-MP result: 4.0%, hereafter in parentheses) of the entire WUS summer streamflow. Cool-season rainfall contributes the most to summer streamflow in maritime basins (Fig. 1a), where most of the annual precipitation occurs in the cool-season. The contributions from warm-season rainfall and snowmelt to summer streamflow are shown in the supplement (Fig. S5). Warm-season rainfall contributes most in the southeast part of the region where the North American Monsoon contributes substantially to annual precipitation and hence the ratio of warm to cool-season precipitation is the highest (Figs. S5a, S7c); this region accounts for 33.0% (23.7%) of the entire WUS summer streamflow (Figs. S5a, S5c). Snowmelt is the greatest contributor to summer streamflow in snow-dominant mountainous regions, accounting for 57.5% (72.1%) of WUS summer streamflow (Figs. S5b, S5d). Our results are comparable to the snowmelt contribution to annual streamflow in *Li et al.* [2017] (53% for WUS excluding the Canadian part).

Across different subregions of the WUS, cool-season rainfall plays an especially important role in summer streamflow generation at low elevations (Figs. 1c, 1f), in areas with precipitation highly concentrated in winters (Figs. 1d, 1g), and dry summers (Figs. 1e, 1h). For some low-lying coastal regions with precipitation concentrated in winter, cool-season rainfall contributes over half of the summer streamflow (Figs. 1c-1d, 1f-1g). A simple prediction of the long-term average cool-season and warm-season rainfall contributions to summer streamflow can be made using multiple linear regression with cool-season and Apr-Jun precipitation and temperature, averaged across water years 1959-2018 for each grid cell in the WUS as predictors (see Supporting Information Tab. S1). The resulting prediction equations reveal that grid cells with higher cool-season temperatures favor higher cool-season rainfall contribution, and higher Apr-Jun temperature and precipitation favor a higher warm-season rainfall contribution. Noah-MP results have patterns that are generally consistent with VIC (Figs. S5-S6).

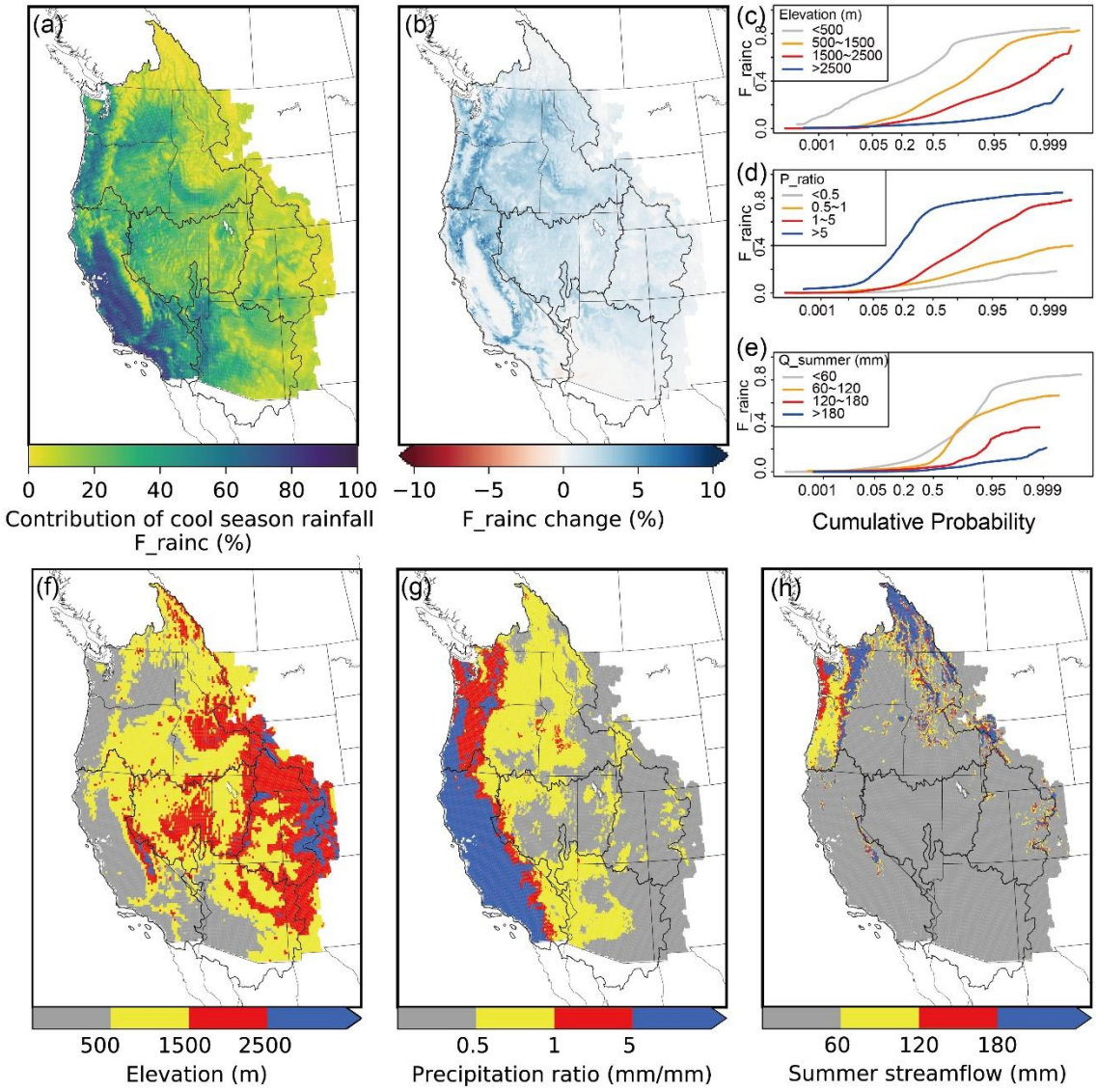

Chapter 3 Figure 1. Contribution of long-term (water years 1959-2018) average cool-season rainfall (F_rainc) to summer streamflow (a), changes under uniform 1°C warming (b), and their baseline cumulative distribution function across regions with different elevations, precipitation ratios, and long-term average summer streamflow volumes (c-e). Panels (f-h) show maps of elevation, precipitation ratio (cool-season precipitation divided by warm-season precipitation), and long-term average summer streamflow volume. Results are from VIC simulation; corresponding comparison with Noah-MP results is shown in Supplement Fig. S6.

3.2 Change in seasonal rainfall contribution to summer streamflow under warming

We find that the cool-season rainfall's contribution to summer streamflow increases almost everywhere in the WUS under warming, with a maximum increase of about 10% of summer streamflow volume in maritime regions (Fig. 1b) for 1°C warming. Warm-season rainfall contribution to summer streamflow increases mostly in snow-covered regions (Fig. S7), and snowmelt contribution decreases almost everywhere (Fig. S8). Fig. 2 shows the spatial-temporal classified contributions from seasonal rainfall and snowmelt to summer streamflow, and their changes for uniform 1°C warming. Spatially, across subregions binned by long-term average peak SWE (<150mm, 150-500mm, 500-1000mm, >1000mm), contributions from both warm and cool-season rainfall increase under warming, the sum of which approximately cancels the decrease in contribution of snowmelt (Fig. 2a). For regions with relatively low snow accumulations (peak SWE < 500 mm), cool-season rainfall has comparable or higher contribution increases than does warm-season rainfall (Fig. 2a). For regions with relatively high peak SWE, the contribution of warm-season rainfall to summer streamflow increases more than cool-season rainfall (Fig. 2a).

Across water years with different percentiles of summer streamflow, cool-season rainfall contribution (F_rainc) and sensitivity of the contribution to warming are larger in years with lower summer streamflow volumes (i.e., drier summers), probably because such years have less available snowmelt and warm-season rainfall than other years (Fig. 2b).

Across water years with different snow drought conditions, years with snow drought due to abnormally warm temperatures (type warm) have a larger contribution from cool-season rainfall to summer streamflow, and also a larger sensitivity of the contribution to warming than other categories (Fig. 2c). This is because more precipitation is partitioned into rainfall than snowfall, resulting in a decline in snowmelt (and its contribution) to summer streamflow under warm snow

drought conditions. On the other hand, we found substantial increases in F_rainc under warming even without snow drought (Fig. 2c), indicating that warming leads to an increasingly important role of cool-season rainfall in summer streamflow even during normal snow years. Additional analysis (results not shown) of wet years (top 10% cool-season precipitation) and large snow years (top 10% peak SWE) also shows substantial increases in seasonal rainfall's contribution (i.e., F_rainc and F_rainw), albeit the increments are smaller than for the four cases discussed above. Noah-MP results (Fig. S9) exhibit similar patterns.

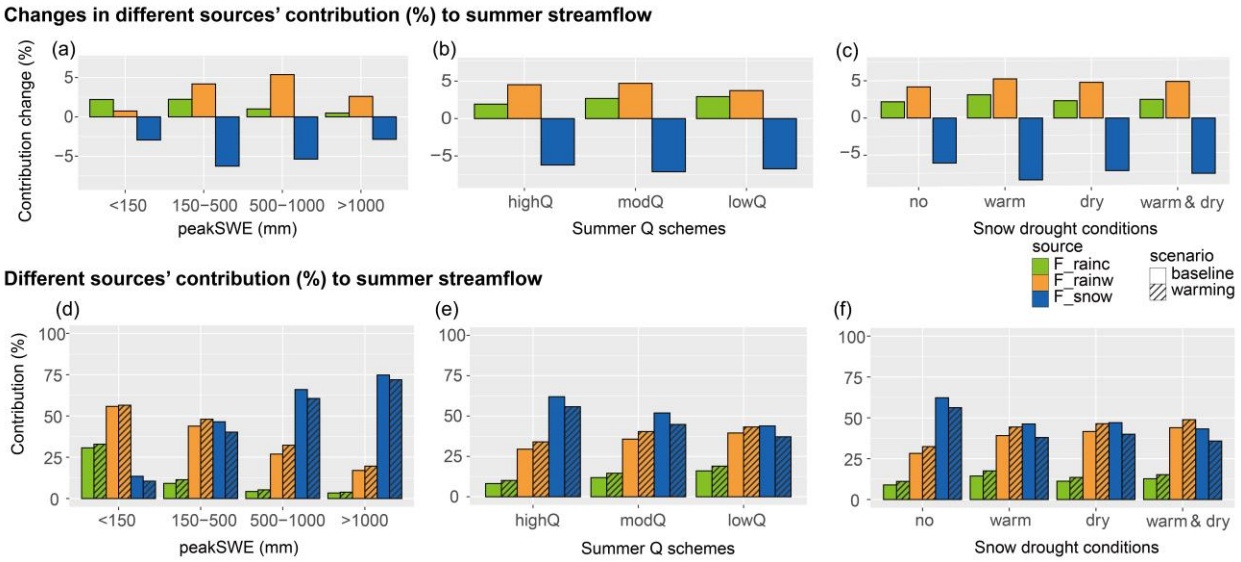

Chapter 3 Figure 2. Changes in contributions from cool-season rainfall, warm-season rainfall, and snowmelt to summer streamflow under uniform 1°C warming, summarized for areas with different long-term (water years 1959-2018) average peak SWE bins (a), and for years categorized by different summer streamflow volumes, divided by terciles over the 60 years (Q_scheme) (b), and different snow drought categories (c). Subplots (d, e, f) show the contributions from the three sources under baseline and warming scenarios across the same region/periods corresponding to a-c. All contributions were calculated as a fraction of the area-weighted average summer streamflow

volume summarized within the regions/periods. Results are from VIC simulations; corresponding Noah-MP results are shown in Fig. S9.

3.3 Role of precipitation delivery in summer streamflow predictability

We find that rainfall dominates summer streamflow variations over much of the western U.S. in VIC results aside from high mountain areas (Fig. 3a). Generally, cool-season rainfall dominates in the mid-south part of Pacific Northwest (PNW) and other low elevation areas in the coast range and the Cascades and some southern parts of the WUS (Fig. 3a), where summer streamflow is low (Fig. 1h). Warm-season rainfall dominates most of the rest of the domain, aside from high elevation regions where much of the annual precipitation accumulates as SWE during the winter months (Fig. 3a). Noah-MP results show similar patterns to VIC, except that cool-season rainfall dominated parts are more centered in the southern part of WUS (Fig. S12a) due to two models' difference in simulated summer streamflow spatial patterns. Both VIC and Noah-MP results show that cool and warm season rainfall contribute to the summer streamflow variations more than across ~70% of WUS, including the main streamflow-generation regions (Fig. S11).

Figs. 3b-3d show the changes in summer streamflow predictability (measured by adjusted-R^2 of regressions) for different predictors added compared with baseline regressions using peakSWE as the only predictor, based on VIC model simulations. Adding cool-season rainfall (rain_c, mm) as a predictor substantially increases summer streamflow predictability, especially in the central and southern parts of the PNW, and California's Central Valley (Fig. 3b). Adding Apr-Jun rainfall (AJrain, mm) as a predictor causes a smaller increment in predictability for the rest of the domain (Fig. 3c). Adding both predictors effectively sums the predictability improvement effects of the two individual predictors (Fig. 3d, compared with Figs. 3b-3c). Noah-MP results show similar patterns (Figs. S12b-S12d).

We further checked whether summer streamflow predictability varies with changes in precipitation delivery (measured by a combination of F_rainc, F_rainw, and F_snow) in Figs. 3e-3h. Across all four prediction frameworks, summer streamflow predictability is reduced with decreasing fractions of snowmelt (Figs. 3e-3h). Adding cool-season rainfall as a predictor increases predictability in some regions with low snow but high cool-season rainfall contribution (Fig. 3f, as compared to Fig. 3e). Adding Apr-Jun rainfall as a predictor similarly increases summer streamflow predictability in regions with low snow but high warm-season rainfall contribution (Fig. 3g, as compared to Fig. 3e). Again, adding both predictors roughly sums the predictability improvements caused by the individual predictors (Fig. 3h). Again, Noah-MP results are qualitatively similar (Figs. S12e-S12h).

Fig. 2d shows a switch in the relative importance of warm-season rain and snow for peakSWE in the 150-500 mm range. As warm-season rain becomes more important than snow, the prediction with regression based on peakSWE and cool-season rain (aligns with common streamflow forecast predictors) becomes less skillful (i.e., lower adjusted-R^2, see Figs. 3f, S10a and S10c). Across different snow drought scenarios, years with warm snow droughts have greater predictability than dry snow droughts, followed by no droughts (Figs. S10b and S10d).

Under uniform 1°C warming, the change in adjusted-R^2 of predictions based on peakSWE and cool-season rain (which aligns with common operational streamflow forecast predictors) has the largest correlation to F_rainw change compared to correlations with F_rainc and F_snow change (see cg_cor in Fig. 3f), which indicates that the reduced summer streamflow predictability under warming is most strongly tied to increased relative importance of warm season rainfall. Noah-MP results are similar (Fig. S12f).

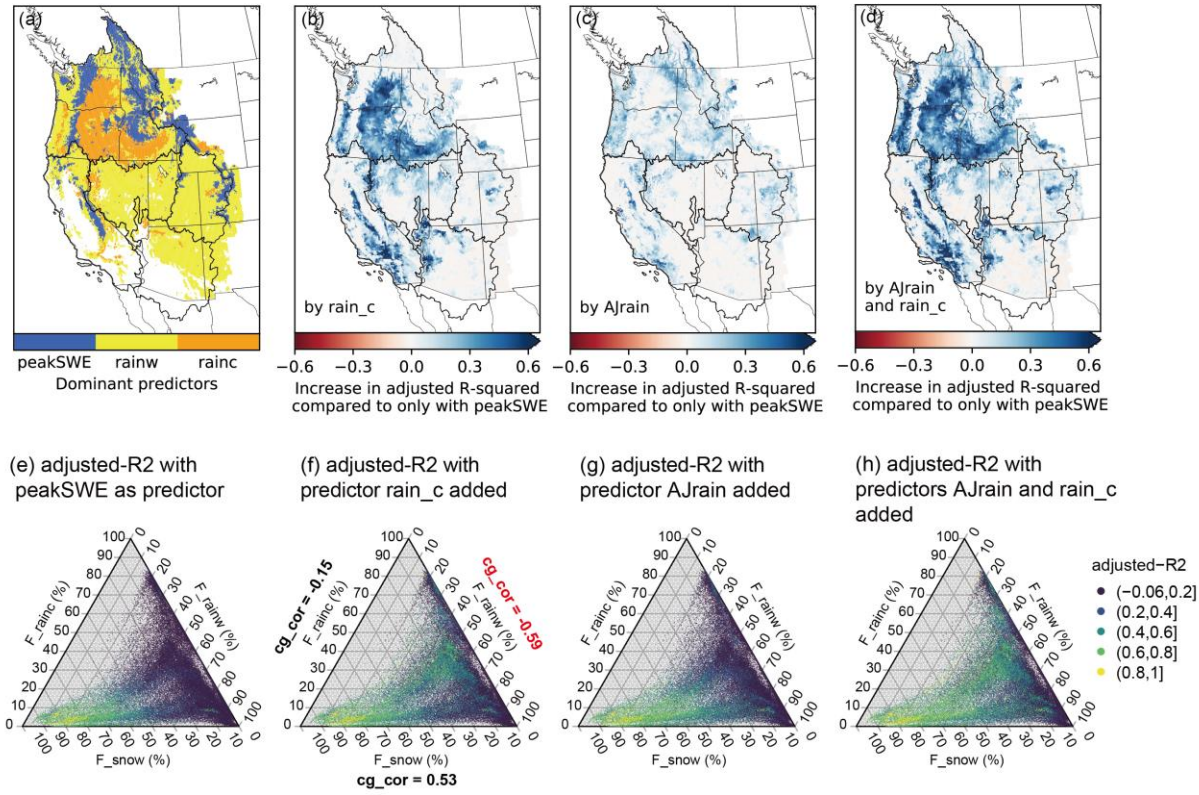

Chapter 3 Figure 3. (a) predictors that explain most variance of summer streamflow variation among variables selected by analysis of variance (ANOVA) of the stepwise regression (and with statistically significant coefficients, significance level = 0.05); (b-d) absolute increase in adjusted-R2 by adding cool-season rainfall (rain_c), Apr-Jun rainfall (AJrain), or both rain_c and AJrain as predictors compared to adjusted-R^2 in regression with only peakSWE as a predictor. Here we consider Apr-Jun rather than warm-season to ensure no summer data are used in the prediction. (e-h) ternary plots showing baseline adjusted-R^2 as a function of F_rainc, F_rainw, and F_snow across every grid cell of the WUS. Correlation values (cg_cor) in (f) are calculated between adjusted-R^2 changes (with peakSWE and rain_c as predictors in operational streamflow forecast practice) and the changes of F_rainc, F_rainw and F_snow under uniform 1°C warming relative to baseline. Results are from VIC simulations, corresponding Noah-MP results are in Fig. S12. Blank regions

in (a) indicate no predictor with statistically significant coefficients remains after predictor selection by stepwise regression. All predictions are for summer streamflow.

4 Discussion

We have explicitly quantified the contributions from cool-season rainfall, warm-season rainfall, and snowmelt to summer streamflow. The substantial contributions from cool-season rainfall to summer streamflow revealed long-span memory of soil that can store water from cool season augmenting the following summer's streamflow, as also found by *Frisbee et al.* [2011] and *Shaw et al.* [2014]. This is especially the case for low mountain or valley regions. This alternative inter-season water transport process is expected to become increasingly important in a warming climate. As we found in a uniformly 1°C warming scenario, the contribution to summer streamflow from cool-season rainfall increases almost everywhere in the WUS, and takes the place of near half of the decreased contribution from snowmelt (the other half is an increased contribution of warm-season rainfall).

We found substantial improvement in the adjusted-R^2 for regression-based summer streamflow prediction by introducing cool-season rainfall (Fig. 3b), supporting the current usage of cool-season rainfall (or precipitation) as a predictor in some summer streamflow forecast practices [*Godsey et al.*, 2014]. However, under 1°C uniform warming, we found the predictability using solely peakSWE and cool-season rainfall decreased mainly due to the increasing relative importance of warm season rainfall (Figs. 3f and S12f), which usually is not included as a predictor in operational streamflow forecast methods (practically, forecasts are made before summer precipitation. Apr-Jun rainfall may be used as an alternative, but it provides a shorter lead time than cool-season rainfall or peakSWE). As a result, in addition to common processes (snowmelt, evapotranspiration, or total precipitation), it would be beneficial to consider seasonal precipitation

delivery change (rainfall rather than snowmelt), and/or soil moisture more carefully to capture future streamflow variability. Additionally, we show the adjusted-R^2 of peak SWE-based predictions for baseline and uniform 1°C warming scenarios in supplement Fig. S15 to indicate predictability reduction.

Our tracking results (from VIC simulations) suggest that snowmelt generates about 60% of summer streamflow for the entire WUS, slightly higher than 53%, which is the contribution of snowmelt to total runoff in the region from *Li et al.* [2017]. This slightly higher contribution from snowmelt to summer streamflow than annual streamflow is consistent with the fact that snowmelt peaks in the (early) warm-season and contributes more to streamflow during spring and summer than winter. A check of snowmelt contribution to annual streamflow also reproduced results in *Li et al.* [2017] (Fig. S13). Our tracking system partitioning occurs at seasonal scale, but arguably could be applied to any temporal subdivision that is larger than model steps to perform more detailed analyses. Additionally, it can be applied to other land surface hydrology models given the required outputs available. Therefore, it has the potential to be applied to fields such as geochemistry and agriculture that need to consider pollution or nutrient release within a certain period, or as a bridge to connect pollution with the natural precipitation and soil water transport processes.

Our work is based entirely on (and therefore is limited by limitations of) model simulations. We do note that the original version of the tracking algorithm was compared with observations via isotope tracking (*Li et al.* [2017], see also *Beria et al.* [2018]). Additionally, we applied our tracking algorithm to two widely-used land surface models, to evaluate the extent to which our results are model-dependent. Notably, despite some differences in large-scale average statistics, the grid-cell scale patterns of the three sources' contribution to summer streamflow and their

changes are qualitatively similar for the two models. Nonetheless, application of the tracking algorithm to other land surface models should be feasible. As for our regression-based analysis, we intend to explore how warming-induced precipitation delivery change impacts summer streamflow predictability, and hence our regressions are based on model-simulated results, rather than observations. The core value of this study is not specific predictions or their spatial patterns, but rather the broad shifts in the roles of different water sources in generating and predicting summer streamflow. In this context, the two models give consistent first-order messages as to the relative importance of precipitation delivery forms in summer streamflow generation under climate warming in the WUS.

Our focus here has been the role of water sources (rainfall and snowmelt) in summer streamflow variability, rather than water sinks (most notably evapotranspiration (ET)), despite ET being also important in controlling summer streamflow. We do not expand on ET here because its effect is incorporated (at every time step) in our tracking algorithm. From this we can infer that a) increased ET in the cool season can reduce the contribution of cool-season rainfall and snowmelt in summer streamflow, and b) increased ET in the warm season reduces the contribution of snowmelt and warm-season rainfall in summer streamflow (Text S1). Future studies could extend to more comprehensive forecasting practices with larger model ensembles and better calibrations, and logically would be based on observations (in-situ or remote-sensed for precipitation and streamflow in ungauged basins) to the extent possible. Furthermore, our analyses are based on 1°C (uniform) warming to focus on the derivative of changes, and therefore are not subject to new GCM versions as we do not attempt to make projections of future climate. Logical extensions might consider seasonal variations in warming and/or changes in precipitation seasonality.

5 Conclusions

Our snowmelt-rainfall tracking shows that seasonal rainfall provides important volumetric contributions to summer streamflow for many streams in the WUS. In low-elevation coastal streams, cool-season rainfall contributes the most, while warm-season rainfall dominates in the southern interior of our WUS domain. As the climate continues to warm and snowmelt declines, seasonal rainfall's contribution to summer streamflow will increase. This increase will be mostly from warm-season rainfall, offsetting two-thirds of the reduction in snowmelt contribution, with the other one-third offset by cool-season rainfall (the three sources' contributions are normalized to sum to one). The contribution increase from cool-season rainfall is especially large in years with warm snow droughts and abnormally dry summers.

Furthermore, we find that seasonal rainfall dominates summer streamflow variability across ~70% of WUS. By incorporating cool-season and Apr-Jun rainfall, we can substantially mitigate the loss of summer streamflow predictability due to reduced snowmelt contribution compared to predictions based solely on peak SWE. Our findings of the substantial contribution of seasonal rainfall to summer streamflow (even in catchments with substantial spring snowmelt) highlight the increasing value in studying these alternative contributions and associated hydrologic processes (rainfall) as the control of summer streamflow, especially with continued climate warming and declining snowpacks.

Acknowledgments

This work was supported in part by the Center for Western Weather and Water Extremes (CW3E) at the Scripps Institution of Oceanography, via AR Program Phase 3, Grant 4600014294, sponsored by the California Department of Water Resources. We thank Qian Cao of CW3E for her assistance with our implementation of the Noah-MP model.

Open Research

Data and codes in this paper are publicly available at:

https://doi.org/10.6084/m9.figshare.20739025.v2.

References

Beria, H., J. R. Larsen, N. C. Ceperley, A. Michelon, T. Vennemann, and B. Schaefli (2018), Understanding snow hydrological processes through the lens of stable water isotopes, Wiley Interdisciplinary Reviews: Water, 5(6), e1311.

Chen, F., M. Barlage, M. Tewari, R. Rasmussen, J. Jin, D. Lettenmaier, B. Livneh, C. Lin, G. Miguez-Macho, and G. Y. Niu (2014), Modeling seasonal snowpack evolution in the complex terrain and forested Colorado Headwaters region: A model intercomparison study, Journal of Geophysical Research: Atmospheres, 119(24), 13,795-713,819.

Cooper, M., J. Schaperow, S. Cooley, S. Alam, L. Smith, and D. Lettenmaier (2018), Climate elasticity of low flows in the maritime western US mountains, Water Resources Research, 54(8), 5602-5619.

Crozier, L. G., A. Hendry, P. W. Lawson, T. Quinn, N. Mantua, J. Battin, R. Shaw, and R. Huey (2008), Potential responses to climate change in organisms with complex life histories: evolution and plasticity in Pacific salmon, Evolutionary Applications, 1(2), 252-270.

Frisbee, M. D., F. M. Phillips, A. R. Campbell, F. Liu, and S. A. Sanchez (2011), Streamflow generation in a large, alpine watershed in the southern Rocky Mountains of Colorado: Is streamflow generation simply the aggregation of hillslope runoff responses?, Water Resources Research, 47(6).

Godsey, S. E., J. W. Kirchner, and C. L. Tague (2014), Effects of changes in winter snowpacks on summer low flows: case studies in the Sierra Nevada, California, USA, Hydrological Processes, 28(19), 5048-5064.

He, M., M. Russo, and M. Anderson (2016), Predictability of seasonal streamflow in a changing climate in the Sierra Nevada, Climate, 4(4), 57.

Kiewiet, L., E. Trujillo, A. Hedrick, S. Havens, K. Hale, M. Seyfried, S. Kampf, and S. E. Godsey (2022), Effects of spatial and temporal variability in surface water inputs on streamflow generation and cessation in the rain–snow transition zone, Hydrology and Earth System Sciences, 26(10), 2779-2796.

Lapides, D. A., W. J. Hahm, D. M. Rempe, J. Whiting, and D. N. Dralle (2022), Causes of missing snowmelt following drought, Geophysical Research Letters, e2022GL100505.

Li, D., M. L. Wrzesien, M. Durand, J. Adam, and D. P. Lettenmaier (2017), How much runoff originates as snow in the western United States, and how will that change in the future?, Geophysical Research Letters, 44(12), 6163-6172.

Liang, X., D. P. Lettenmaier, E. F. Wood, and S. J. Burges (1994), A simple hydrologically based model of land surface water and energy fluxes for general circulation models, Journal of Geophysical Research: Atmospheres, 99(D7), 14415-14428.

Livneh, B., and A. M. Badger (2020), Drought less predictable under declining future snowpack, Nature Climate Change, 10(5), 452-458.

Livneh, B., E. A. Rosenberg, C. Lin, B. Nijssen, V. Mishra, K. M. Andreadis, E. P. Maurer, and D. P. Lettenmaier (2013), A long-term hydrologically based dataset of land surface fluxes and states for the conterminous United States: Update and extensions, Journal of Climate, 26(23), 9384-9392.

Mote, P. W. (2003), Trends in snow water equivalent in the Pacific Northwest and their climatic causes, Geophysical Research Letters, 30(12).

Niu, G. Y., Z. L. Yang, K. E. Mitchell, F. Chen, M. B. Ek, M. Barlage, A. Kumar, K. Manning, D. Niyogi, and E. Rosero (2011), The community Noah land surface model with

multiparameterization options (Noah-MP): 1. Model description and evaluation with local-scale measurements, Journal of Geophysical Research: Atmospheres, 116(D12).

Palmer, M. A., D. P. Lettenmaier, N. L. Poff, S. L. Postel, B. Richter, and R. Warner (2009), Climate change and river ecosystems: protection and adaptation options, Environmental management, 44(6), 1053-1068.

Safeeq, M., G. E. Grant, S. L. Lewis, and C. L. Tague (2013), Coupling snowpack and groundwater dynamics to interpret historical streamflow trends in the western United States, Hydrological Processes, 27(5), 655-668.

Safeeq, M., G. E. Grant, S. L. Lewis, M. G. Kramer, and B. Staab (2014), A hydrogeologic framework for characterizing summer streamflow sensitivity to climate warming in the Pacific Northwest, USA, Hydrology and Earth System Sciences, 18(9), 3693-3710.

Shaw, G. D., M. H. Conklin, G. J. Nimz, and F. Liu (2014), Groundwater and surface water flow to the Merced River, Yosemite Valley, California: 36Cl and Cl− evidence, Water Resources Research, 50(3), 1943-1959.

Shrestha, R. R., Y. B. Dibike, and B. R. Bonsal (2022), Snowpack driven streamflow predictability under future climate: contrasting changes across two western Canadian river basins, Journal of Hydrometeorology.

Stewart, I. T., D. R. Cayan, and M. D. Dettinger (2005), Changes toward earlier streamflow timing across western North America, Journal of climate, 18(8), 1136-1155.

Su, L., Q. Cao, M. Xiao, D. M. Mocko, M. Barlage, D. Li, C. D. Peters-Lidard, and D. P. Lettenmaier (2021), Drought variability over the conterminous United States for the past century, Journal of Hydrometeorology, 22(5), 1153-1168.

Tague, C., and G. E. Grant (2009), Groundwater dynamics mediate low-flow response to global warming in snow-dominated alpine regions, Water resources research, 45(7).

Tsuruta, K., and M. A. Schnorbus (2021), Exploring the operational impacts of climate change and glacier loss in the upper Columbia River Basin, Canada, Hydrological Processes, 35(7), e14253.

Yan, H., N. Sun, M. Wigmosta, R. Skaggs, L. R. Leung, A. Coleman, and Z. Hou (2019), Observed spatiotemporal changes in the mechanisms of extreme water available for runoff in the western United States, Geophysical Research Letters, 46(2), 767-775.

Chapter 4 Weakening Runoff Response to Warming with Snowpack Reduction in the Montane Western U.S.

Abstract: Snow loss under climate warming has been a prominent hydrologic signature across the western United States (WUS), posing a threat to the stability and availability of water supplies. Numerous studies have discussed the mechanisms linking WUS warming-driven snow loss to annual runoff declines, especially in the Upper Colorado River Basin (UCRB). However, the dynamics of how the rate of snow loss and subsequent annual runoff decline will evolve under warming remains unknown. Here we show that the snow and subsequent annual runoff declines will be smaller (in absolute value) under a warmer reference climate than for a cooler reference climate, given unchanged precipitation. Our analyses are based on controlled warming experiments with land surface models (LSMs) and analysis of LSM-coupled downscaled global climate model (GCM) ensembles, over three major river basins in the WUS. We discovered a hint of decelerated streamflow decline in the historical record (for UCRB). Then, with controlled warming experiments, we further confirmed the weakening warming sensitivity of streamflow, snow, and evapotranspiration under warming with fixed precipitation. From GCM-LSM simulations (off-line forcing of LSMs with bias corrected and downscaled GCM output), we also detected a hint of deceleration in runoff ratio decline in the SSP245 scenario. A sub-basin analysis suggests a slower snow loss at lower-elevation/less-snow regions, which analogs to a warmer future. At the end, we raised several hypotheses about the weakening warming sensitivity in streamflow and snow. Further research is required to examine the hypotheses and isolate the related mechanism's effect with more idealized experiments.

Main

Declining runoff poses a threat to western U.S. (WUS) water and energy security, including water availability for agriculture and municipal water supplies, hydropower generation, and water quality related to increased concentration of nutrient and sediment loading [*Johnson et al.*, 2015]. Previous studies have shown that declining springtime snowpack and associated net radiation increase are the predominant drivers of increased evapotranspiration, ultimately causing loss of annual runoff, especially in the Upper Colorado River Basin (UCRB) [*Milly and Dunne*, 2020; *Neto et al.*, 2020]. Our earlier study [*Ban et al.*, 2023] further showed that the snowmelt-radiation feedback dominates the annual runoff sensitivity to warming for over 50% of the area of the WUS. Previous studies have mostly summarized the annual runoff decline mechanism/sensitivity from a static view, but whether and how the mechanisms will evolve remain uncertain [*Milly and Dunne*, 2020; *Neto et al.*, 2020]. We envision that, under a low-to-no snow future, the snow-related mechanism/sensitivity will be strongly non-stationary.

Slower snowmelt is expected under a warming future due to the earlier shift of snowmelt season to a period with lower available energy, which could reduce evapotranspiration energized by snowmelt-radiation feedback, and cause a slower runoff decline [*Musselman et al.*, 2017]. For example, despite the common perception of declining annual runoff in the UCRB over the last ~100 years (1906-2018), the decreasing trend in streamflow is mostly dominated by the record before 1970. This is also the case for simulated runoff from Variable Infiltration Capacity (VIC) hydrologic model [*Liang et al.*, 1994] driven by trend-corrected H&L forcing [*Hamlet and Lettenmaier*, 2005] during 1916-1970, see Methods "Historical Simulations" for details (Fig. 1e). Similarly, the dominant decreasing trend before 1970 is also found in VIC-simulated runoff driven by an ensemble of historical forcings downscaled from seven Global Climate Models (GCMs) in

Coupled Model Intercomparison Project Phase 6 (CMIP6) (see Methods "GCM-LSM Simulations" for details) (1950-1970) (Fig. 1e), as well as the naturalized flow records (1916-1970) (Fig. 1f). After 1970, the decreasing trend has become much less obvious or even reversed (Figs. 1e-1f). One reason for the apparent decelerating runoff decline comes from the decelerating precipitation decline after water year 1970 (Fig. 1a). Additionally, snow extent decrease and subsequent net radiation increase also appear to have decelerated over the last half century (Figs. 1c-1d), which may lead to decelerated radiation-energized evapotranspiration loss and could be another reason for the slower annual runoff decline [*Ban et al.*, 2023; *Milly and Dunne*, 2020]. The decelerating runoff decline after 1970 contrasts with the accelerating temperature warming after 1970 (Fig. 1b), suggesting a possibly smaller sensitivity of runoff, net radiation, and snow change to warming. It is important to understand whether these changes reflect a more general signal of less warming sensitivity of key hydrologic processes at an annual scale under a warmer reference climate, given the critical importance of annual runoff to water supplies across the WUS.

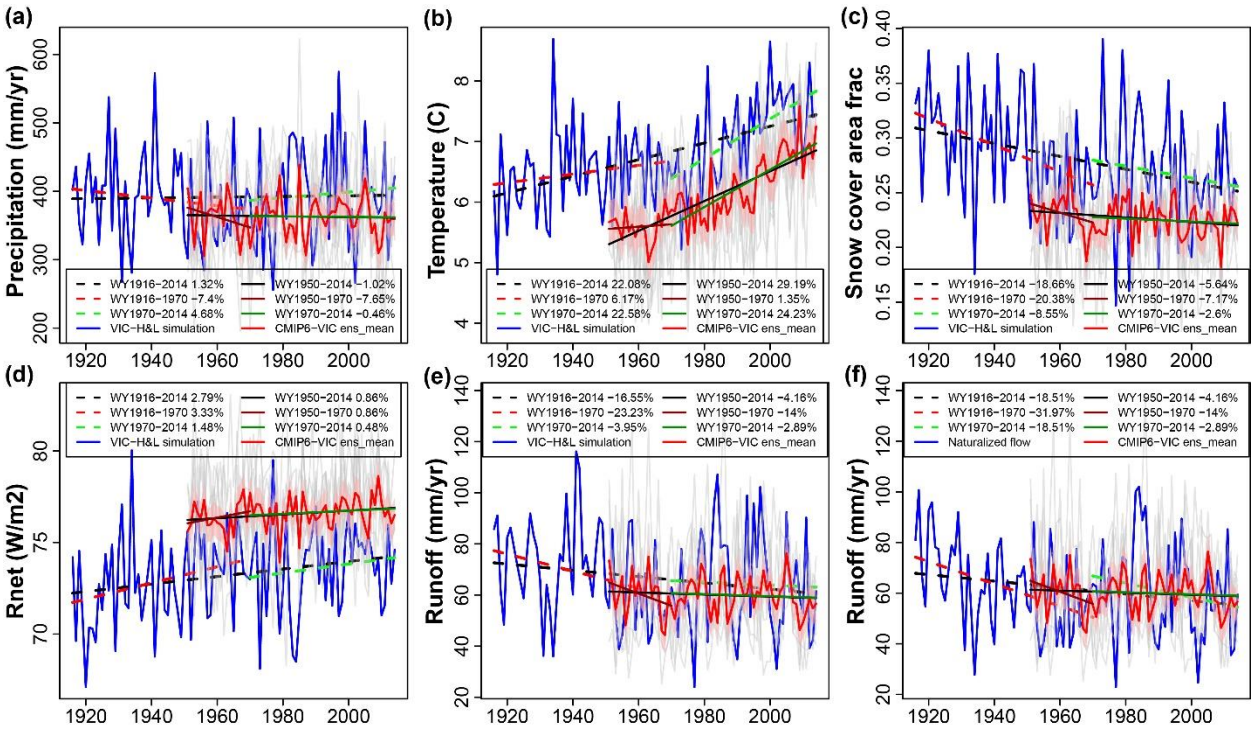

Chapter 4 Figure 1. Time series of annual precipitation (a), annual average temperature (b), annual average snow cover area fraction (c), annual average net radiation (d), annual runoff (e), and naturalized annual flow (f) in the UCRB from 1916 to 2014, and trends in different periods. Blue lines in (a-e) show VIC model outputs driven by 1916-2014 H&L forcing (see Methods for details) [*Hamlet and Lettenmaier*, 2005], and blue line in (f) shows naturalized flow. Dashed lines in (a-f) are linear fit lines of VIC historical simulations during 1916-1970, 1970-2014, and 1916-2014. Red lines show ensemble average of VIC outputs driven by seven CMIP6 GCMs' downscaled forcings during 1950-2014 (see Methods "GCM-LSM Simulations" for GCM selection details), with light grey lines denote each of the seven members. Shadings show the ±1 standard error of the ensemble means. Solid straight lines show the corresponding linear fit lines of GCM-VIC simulation ensemble average results during 1950-1970, 1970-2014, and 1950-2014. The values of change in the legend are relative to the first water year of the linear fit.

Herein, we address the following questions using hydrological model simulations driven

by an ensemble of forcings (CMIP6), as well as naturalized flow records for three major river basins across WUS: a) Are trends in annual runoff evolving, and if so, how? b) Where trends are evolving, how are they related to changes in snow, and in climate warming? c) What is the main mechanism controlling changes in the rates of annual runoff declines, where present?

To fully sample the spatial variability of montane hydroclimate across the WUS in answering the above questions, we considered three major river basins: Columbia (Pacific Northwest, hereafter PNW), Sacramento – San Joaquin (California, hereafter CA), and UCRB. We used naturalized flow records (records based on observed streamflow corrected for upstream reservoir storage and diversions) from the California Data Exchange Center (CDEC) for CA, U.S. Bureau of Reclamation (UCRB), and Bonneville Power Administration (PNW). The spatial domain is shown in Fig. 2. The stream gages (in total 60) within each of the three major river basins are listed in Appendix Table C1.

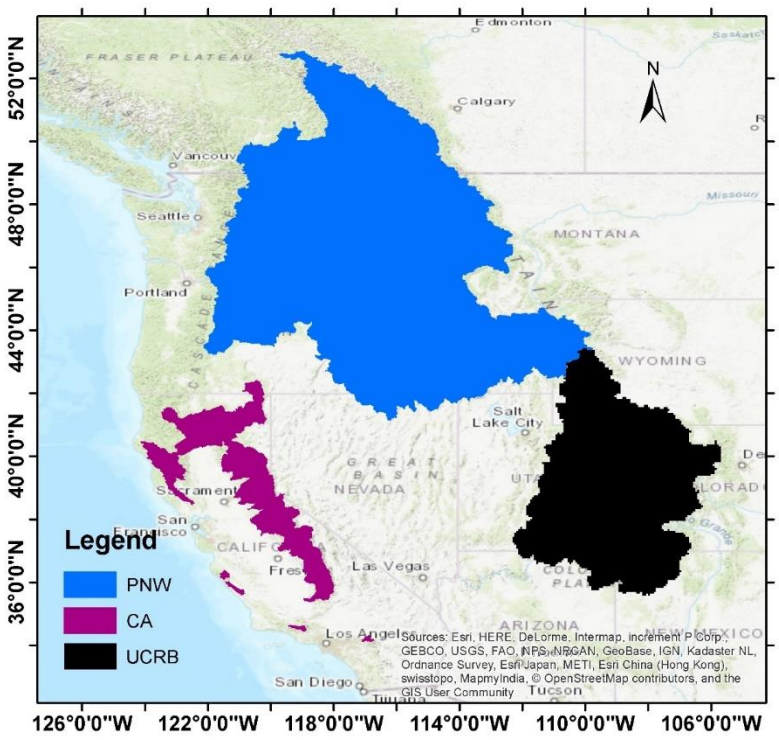

Chapter 4 Figure 2. Map of the three major WUS river basins, within which we analyzed naturalized flows for the 60 tributaries.

1-degree Controlled Warming Experiments

To determine changes in the rate of the snow and annual runoff declines as they might be affected by warming rates, we conducted a controlled warming experiment using two Land Surface Models (LSMs): the Variable Infiltration Capacity (VIC) model [*Liang et al.*, 1994], and the Noah-multiparameterization (Noah-MP) [*Niu et al.*, 2011; *Yang et al.*, 2011]. We initially conducted a baseline simulation for the historical period (1950-2018) with Livneh meteorological forcings [*Livneh et al.*, 2013] (extended to 2018 by *Su et al.* [2021]). Then, we applied one-degree warming to both daily maximum and minimum temperature for every day in the historical simulation historical period (1950-2018) while keeping precipitation unchanged. We used two warming

magnitudes (1°C and 2°C), constituting two 1-degree warming cases with different reference climates (baseline to 1°C, and 1°C-2°C). Table 1 summarizes changes in annual runoff (Q), evapotranspiration (ET), and average snow water equivalent (SWE) for the two warming cases. Comparing the changes between the two warming cases in Table 1, there are consistently smaller changes for 1°C-2°C warming case than for baseline to 1°C warming case across all variables, models, and basins. This general pattern confirms that the tendency toward weaker warming sensitivity as the climate warms is not model-dependent and occurs for all three of the major river basins discussed here. A more general map of the difference of the three variable's warming sensitivity between the two warming cases is shown in Fig. C1, where we see the weakening of warming-sensitive signal is strongest in moderately snow-covered regions, and less strong in colder/snowier and low snow regions.

Chapter 4 Table 1. Results of controlled warming experiment differences for 0-1°C and 1-2°C over the historical period (water years 1951-2018). Percent deceleration is calculated as 1-2°C changes (in means) minus 0-1°C changes in means, divided by 0-1°C change.

Long-term annual average/sum value over WY 1951-2018										
Basin-average		**PNW**			**UCRB**			**CA**		
Model	**T-change**	**0-1°C**	**1-2°C**	**Percent Deceleration (%)**	**0-1°C**	**1-2°C**	**Percent Deceleration (%)**	**0-1°C**	**1-2°C**	**Percent Deceleration (%)**
VIC	**ΔQ (mm)**	-12.02	-11.75	-2	-3.82	-3.39	-11	-14.31	-13.96	-2
	ΔET (mm)	13.51	12.55	-7	3.81	3.36	-12	14.48	14.03	-3
	ΔSWE (mm)	-13.68	-13.34	-2	-2.65	-2.56	-3	-16.73	-13.49	-19
Noah-MP	**ΔQ (mm)**	-12.25	-12.02	-2	-5.57	-5.20	-7	-16.46	-16.28	-1
	ΔET (mm)	12.22	12.00	-2	5.54	5.17	-7	16.47	16.28	-1
	ΔSWE (mm)	-13.05	-12.22	-6	-2.44	-2.31	-5	-15.27	-12.73	-17

GCM-VIC Simulations for Future Warming

The controlled warming historical experiments confirmed the existence of a weakening

warming sensitivity under a warmer climate, given fixed precipitation. To get a sense of how future snowpacks and runoff may evolve, we simulated the hydrologic responses to future climate projections. In particular, we used GCM-based LOCA2 hybrid downscaled daily temperature and precipitation archived at https://loca.ucsd.edu/ [*Livneh et al.*, 2015; *D Pierce and Cayan*, 2016; *D W Pierce et al.*, 2014; *D W Pierce et al.*, 2023; *D W Pierce et al.*, 2015] and wind speed downscaled from the National Centers for Environmental Prediction (NCEP)–National Center for Atmospheric Research (NCAR) reanalysis [*Livneh et al.*, 2013], to drive the VIC model for the period 1950-2100 (using 1950-2018 wind climatology for 2015-2100 simulation). To average out sub-century scale variability in the historical record, we performed VIC simulations driven by downscaled forcings from the seven "best" CMIP6 GCMs for the three major river basins, taking the first available member from each of the GCMs, resulting in a seven-member ensemble of GCM-VIC outputs (see Methods "GCM-LSM Simulations" for details including how the seven "best" GCMs were identified).

To better visualize the long-term evolution of hydrology inferred from the GCM simulations, we applied 30-yr moving averages throughout the time series of output variables. To evaluate the effects of alternative warming rates, we used both SSP245 (with an additional radiative forcing of 4.5 W/m² by the year 2100, assuming climate protection measures are taken) and SSP585 (with an additional radiative forcing of 8.5 W/m² by the year 2100) warming scenarios. The moving averaged results under the two SSP scenarios are shown in Fig. 3. The results are somewhat difficult to interpret, because the projected precipitation changes tend to overwhelm all other factors' impact on runoff evolution. However, at least for SSP245, we do see that there is no acceleration in runoff decline (blue line) and there seems to show a hint of deceleration. A similar hint of deceleration in change rates are also shown in SSP245's runoff ratio, SWE, and net radiation.

Future work to better separate the precipitation and temperature warming effect and isolate the temperature-related mechanism of the decelerated runoff sensitivity under warming with more idealized experiments, is outlined in the Section "Further Research".

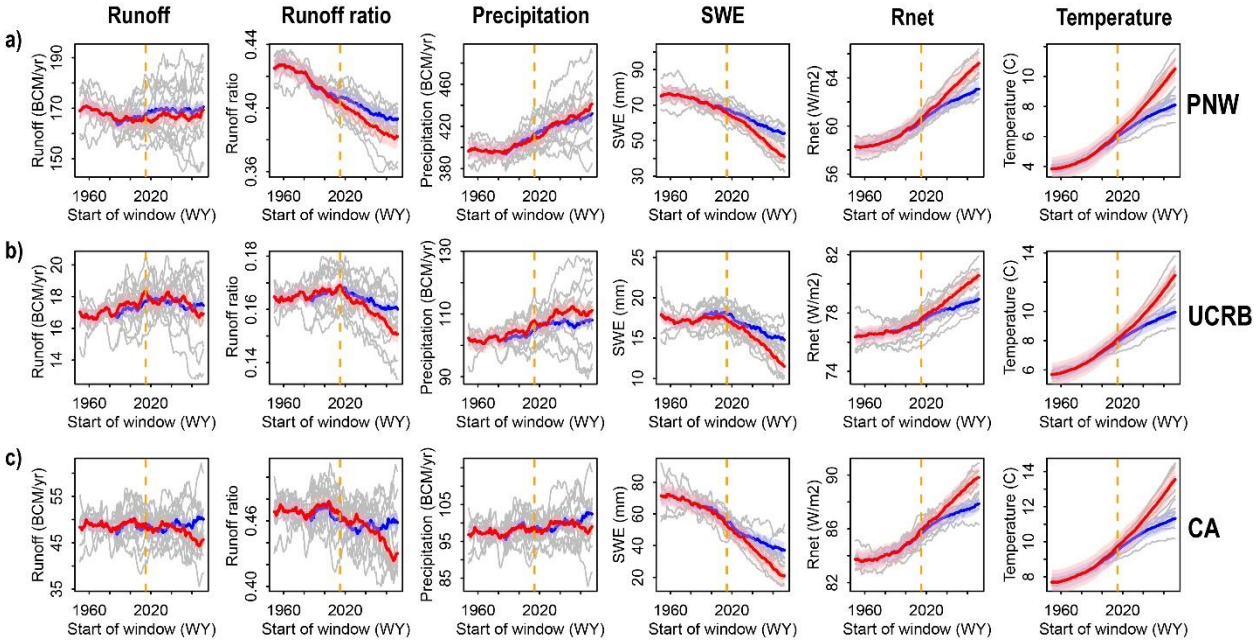

Chapter 4 Figure 3. The evolution of 30-yr moving average time series of annual runoff (billion cubic meters per year, BCM/yr), annual runoff ratio, annual precipitation (BCM/yr), annual-average SWE (mm), annual-average net radiation (W/m^2), and annual-average temperature (°C) for water years 1951-2100. Shading shows the ±1 standard error of the ensemble means. Orange dashed lines partition the results of the historical simulation (1950-2014) from that of future projections (2014-2100). Blue and dark red lines show the ensemble average from SSP245 and SSP585 scenarios and grey lines represent each of the ensemble members.

Sub-basin Scale SWE Loss Evolution

Considering the obscuring effect of non-constant warming rate and precipitation change on the evolution of hydrologic warming sensitivity (specifically, for runoff in Fig. 3), we refined the evaluation to focus on the evolution of SWE loss at the sub-basin level. We take SSP585 as an

example, splitting the three major river basins into major tributaries for which historical naturalized flow records were available. We further segregated by sub-basin mean elevations and snow amounts, as shown in Fig. 4. Fig. 4 shows that the SWE loss is slower under warming at lower-elevations and/or less-snowy sub-basins, which can be considered analogs to warmer reference temperatures. This result serves as further substantiation of the weakening warming sensitivity of SWE loss under a warmer reference climate, as suggested by the control warming experiments. Fig. C2 shows similar plots for SSP245.

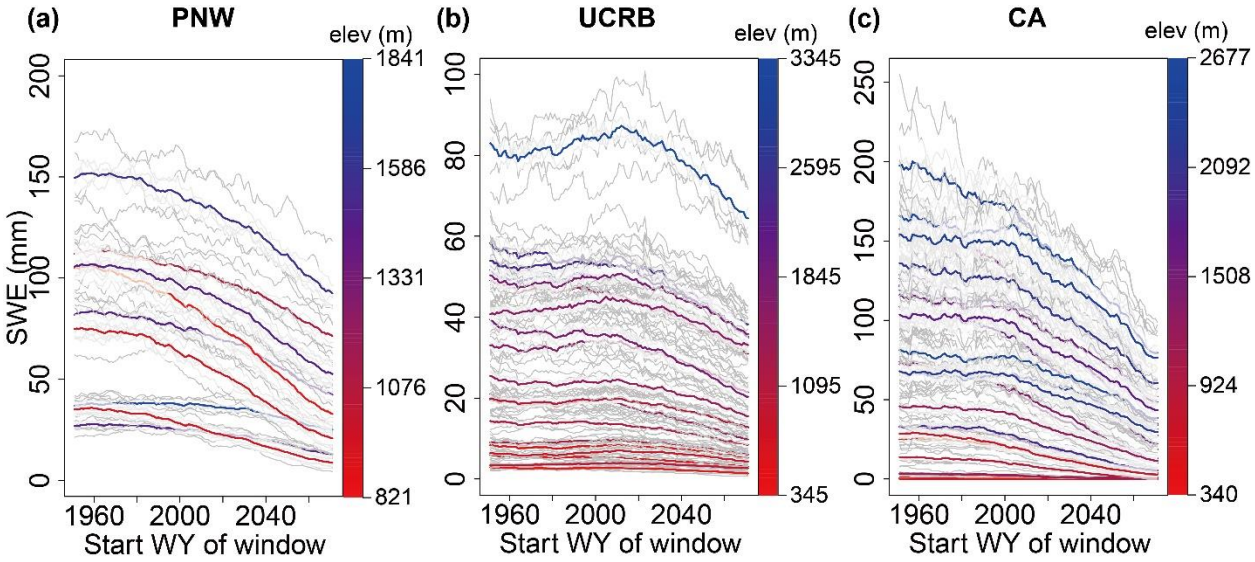

Chapter 4 Figure 4. Time series of SSP585-driven VIC output SWE in sub-basins with naturalized flow records, averaged by a 30-year moving window over water years 1951 to 2100 in (a) PNW, (b) UCRB, and (c) CA.

After confirming the weaker warming sensitivity under a warmer climate, we further evaluate which season dominates the change. A temporal analysis in Fig. 5 shows that the increasing fraction of ET from precipitation, decreasing snow cover ratio (fraction of area covered by snow), and increasing net radiation with temperature are all dominated by melt period changes, when the snowmelt-radiation feedback is strongest. This temporal analysis underlines the

substantial contribution of melt-period (and likely the snowmelt-radiation feedback) to annual SWE loss, ET increase, and radiation change, which is consistent with findings in *Ban et al.* [2023] that snowmelt-radiation feedback is the dominant contributor to annual runoff response to warming for most montane, runoff-sensitive basins. Further actions to assess the relationship more rigorously between the evolving warming sensitivity and snowmelt-radiation feedback are outlined in the "Further Research" section.

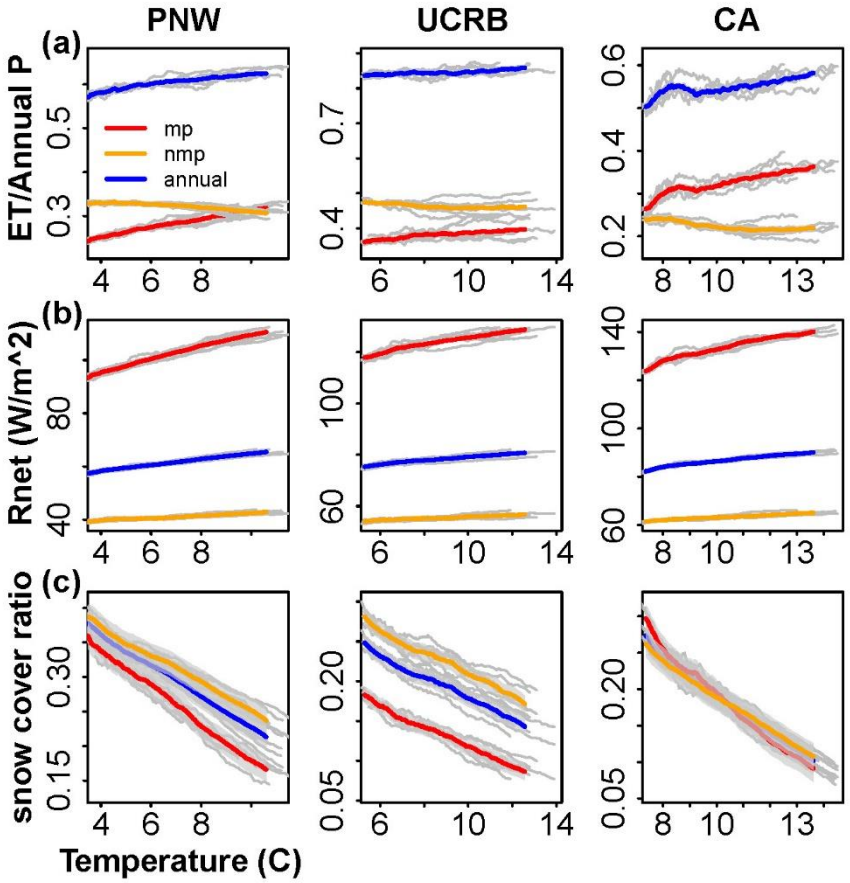

Chapter 4 Figure 5. (a) Ratios of annual ET, melt-period (mp, Mar-May) ET, and non-melt-period (nmp, Jun-Feb) to annual precipitation (P) as a function of temperature, derived from the pooled GCM-driven VIC outputs for water years 1951 to 2100; (b) same as (a), but for net radiation averaged over annual period, melt-period, and non-melt-period; (c) same as (b), but for snow cover

ratio (fraction of area covered by snow). Note that our definition of melt period (Mar-May) did not consider the timing shift caused by earlier snowmelt. Results are from SSP585 scenario; corresponding results for SSP245 are shown in Fig. C3.

Summary and discussion

Using a combination of LSM-based 1°C/2°C controlled warming in the historical period (1950-2018) and sub-basin analysis of GCM-LSM output (1950-2100), we found a weaker warming sensitivity of SWE loss, ET increase, and Q loss under a warmer reference climate in three major montane river basins of the WUS. In our GCM experiments, under near-linear warming in SSP245, the runoff ratio decrease, SWE loss, and related net radiation increase show a hint of deceleration across time. In contrast, no hint of deceleration is shown in SSP585 scenario, which is probably due to the accelerating warming rate in SSP585, which cancels (or reverses) deceleration in the hydrologic response. The above differences between SSP245 and SSP585 imply that with slower warming (e.g., SSP245), we could witness smaller annual runoff declines accompanied by decelerating snow loss, and even increasing annual runoff given more precipitation.

A few potential mechanisms are responsible for the less warming-sensitive SWE and annual runoff loss: 1) Under a warmer reference climate, the higher snowline may elevate slower (i.e., with less area additionally exposed below the snowline), which translates to less snow loss per unit degree of warming; 2) An earlier shift of the snowmelt season to a period with lower available energy [*Musselman et al.*, 2017], reduces the overall efficiency of energizing evapotranspiration by the snowmelt-radiation feedback, which contributes to a slower (per °C warming) runoff decline; 3) Less snow coverage under a warmer reference climate causes reduced effect of albedo change during the melt season under a warmer reference climate. Further actions

to examining these hypotheses are outlined in the "Further Research" section.

In our earlier study [*Ban et al.*, 2023], we found that the region dominated by snowmelt-radiation feedback comprises about 53% of the area of the entire WUS. These regions are mainly snow-covered with strong annual runoff change in response to warming. For the highly warming-sensitive (>5% change/°C) basins, 74% of them have more than half of the runoff change caused by the snowmelt-radiation feedback. For the remaining basins, the runoff sensitivity could be attributed to other factors, such as the saturation-vapor pressure effect, which can hold more ET from elevated saturated vapor pressure with warming, elevated vapor pressure deficit, and changes in aerodynamic and surface resistance that affect ET and thus the runoff decline. In this paper, while acknowledging other possible factors' effects, we focus on the major runoff generation basin (snow-affected, warming-sensitive mountainous basin) and the non-stationarity of the major driver (snowmelt-radiation feedback [*Ban et al.*, 2023]) of these basins' runoff sensitivity.

The work we cited for selecting GCM [*Ashfaq et al.*, 2022; *Krantz et al.*, 2021; *D W Pierce et al.*, 2022] mainly conducted assessments based on temperature and precipitation fields, and the snow performance was not considered because GCMs do not generally archive snow-related variables in their standard output. However, the better performance in GCMs' simulation of temperature and precipitation field should indirectly benefit a better snow simulation when coupled with a land surface model, as those two variables are the most important drivers of snow melt among the GCM outputs. Acknowledging this potential effect, we selected seven best GCMs in temperature and precipitation performance to capture a more realistic spread of snow simulation while also accounting for the uncertainties in temperature and precipitation fields.

Our analysis primarily emphasizes annual values of runoff, rather than the timing of peak flow, which is widely recognized to occur earlier under climate warming. Additionally, we have

not specifically examined the extremes of runoff, which could be influenced by other factors, such as variability in precipitation patterns. Regarding the seasonal timing of runoff, we hypothesize that the observed earlier shift may be slowing down in response to a warmer climate. Conducting further analysis to investigate this potential change and its impacts would provide valuable insights for future research endeavors.

Further research

Idealized experiment with expanded control warming using LSM

In the current paper, we only conducted 1~2°C and 0~1°C warming experiments and changes in sensitivity are small for some basins (e.g., ~2% change in annual runoff for PNW and CA in Chapter 4 Table 1). To get a better view of the evolving sensitivity at different levels of warmer reference climate, further study could include more control warming steps (3°C, 4°C, 5° C, and 6°C) with fixed precipitation. These fixed-precipitation warming experiments would serve to better elucidate runoff sensitivity evolution under a constant warming rate meanwhile control for precipitation changes.

Detection of evolving snowmelt-radiation feedback impact on runoff

The 1~6°C control warming experiment could be used in conjunction with the attribution method developed by *Ban et al.* [2023] to isolate the mechanism as specific to the snowmelt-radiation feedback (SRF) and quantify the SRF's contribution to the ET and runoff sensitivity change among the different warming cases.

For GCM-VIC simulations, further analysis could use the attribution method [*Ban et al.*, 2023] to obtain the time series of SRF contribution to runoff and back out the remaining part of runoff evolution (caused by other factors) as another time series. Plotting the two separate time

series together with the runoff time series through the 1950-2100 period would provide insight into how the SRF-driven ET loss (thus runoff loss) will evolve in the projected future and whether and when the future dominant mechanism will be replaced by the remaining factors (e.g., precipitation). Please note that here the interpretation of the CMIP6 GCM-VIC simulations focuses more on the reference value of projection rather than re-interpret/re-identify the pattern of weakening sensitivity. This is because the GCM-VIC simulated results are essentially VIC outputs driven by GCM-LOCA downscaled temperature and precipitation rather than GCM output. Therefore, adjusting the downscaled temperature to a constant warming rate or detrending downscaled precipitation will eventually route back to the idealized experiment described above.

Examining hypotheses of less warming-sensitive snow loss and streamflow decline

The LSM results from the control warming experiment could be used to examine the three hypotheses of the less warming-sensitive snow loss and streamflow decline under a warmer reference climate, as specified below:

Hypothesis 1): Under a warmer reference climate, the higher snowline may elevate slower (i.e., with less area additionally exposed below the snowline) per unit degree of warming and may lead to a slower snow loss per unit of temperature warming.

Further study could collect the three major basins' elevation-area profile, their average elevation of snow-covered grid cells, and the difference in total area of snow-covered grid cells across different magnitudes of warming. If under a warmer reference climate, the average elevation is progressively higher; shrinkage in the area of snow-covered grid cell by 1°C warming is progressively smaller; and the additionally exposed area between elevated snowlines by 1°C lapse rate is also progressively smaller, we can confirm the hypothesis.

Hypothesis 2): earlier snowmelt shifts to a period with lower available radiation, leading to less efficient ET loss and a slower runoff decline with the weaker snowmelt-radiation feedback.

Further study in this paper can collect the snowmelt timing and the average radiation during the snowmelt period and calculate the snowmelt-radiation feedback (SRF) contribution to ET loss. If under a warmer reference climate, the snowmelt timing is progressively earlier, average radiation smaller, and the decreasing SRF contribution largely accounts for the smaller runoff change, we can confirm the hypothesis.

Hypothesis 3): less snow coverage under warmer reference climate leads to less total snow coverage and albedo change during the melt season under a warmer reference climate.

Further study in this paper can calculate the snow coverage area and albedo and their change across the control warming experiments. If the snow coverage and albedo change are progressively smaller under a warmer reference climate, we can confirm the hypothesis.

Effect of net longwave radiation change in response to atmospheric opacity change

Our earlier study [*Ban et al.*, 2023] found that accounting for the atmospheric opacity change can substantially affect the runoff response to warming. In a parallel set of 1~6°C control warming experiments, further study could include the atmospheric opacity effect by modifying the model's atmospheric opacity-driven increment in incoming longwave per °C to a reasonable value (comparable to the median of IPCC6 estimate of net longwave change per warming). By comparing the findings with the warming experiment without considering the effect, we can assess the atmospheric opacity effect on the results.

Methods

Historical Simulations

In our simulations, we used Variable Infiltration Capacity (VIC) model version 4.1.2g. The VIC model is driven by gridded daily precipitation, maximum temperature, minimum temperature, and wind speed at 1/16th degree resolution from the Hamlet & Lettenmaier forcing, hereafter H&L forcing (Hamlet & Lettenmaier, 2005) from 1915 to 2014. The meteorological data for the H&L forcing come from National Climatic Data Service's Cooperative Observer (NCDC Co-op) network, Environment Canada station data (ECAN), monthly U.S. Historical Climatology Network (HCN) and the Historical Canadian Climate Database (HCCD) station data for temporal adjustment, and monthly precipitation maps from Precipitation Regression on Independent Slopes Method (PRISM) method [*Daly et al.*, 1994] for topographic adjustment [*Hamlet and Lettenmaier*, 2005]. The H&L forcing adjusted the artificial trend in gridded daily precipitation and temperature maxima and minima over the continental United States based on electronic form NCDC Co-op station data from the early 1900s on, and therefore is suitable to be used with hydrologic modeling for long-term trend analysis of simulated variables [*Hamlet and Lettenmaier*, 2005]. The VIC simulation with H&L forcing uses the full-energy balance mode, which means that the effective surface temperature is estimated to solve the surface energy budget at every time step.

Control Warming Experiments

We used Livneh forcing [*Livneh et al.*, 2013] (1915-2013, extended to 2018 by *Su et al.* [2021]) to drive the VIC model as baseline simulation. We apply two warming scenarios, applying 1°C and 2°C warming uniformly to daily maximum and minimum temperatures, respectively. We compared outputs from the baseline scenario with the 1°C warming outputs to calculate sensitivity under the baseline condition. We compared the 2°C warming outputs with the 1°C warming

outputs to calculate sensitivity under a warmer reference climate (1°C warming). Across the warming scenarios, we kept the precipitation unchanged to isolate the warming impact on temperature sensitivity.

GCM-LSM Simulations

The same VIC version (4.1.2g) was used as in the controlled warming experiments. We included a 10-yr spin-up at the beginning of both historical (1950-2014) and future projection (2015-2100) runs, which we discarded. We used a (daily) wind climatology (taken from *Livneh et al.* [2013] and extended by *Su et al.* [2021] to 2018) summarized from the historical period (1950-01-01 – 2018-12-31), which is applied to the future period 2015-2100. For the historical run, we used the original wind speed time series from *Livneh et al.* [2013]. Daily maximum/minimum temperatures and precipitation from the GCMs' LOCA2 hybrid downscaled dataset [*Livneh et al.*, 2015; *D Pierce and Cayan*, 2016; *D W Pierce et al.*, 2014; *D W Pierce et al.*, 2023; *D W Pierce et al.*, 2015] were used to generate other VIC forcings (downward solar and longwave radiation, humidity) following methods summarized by *Bohn et al.* [2013]. From the model output, we collected the runoff on a grid cell basis without routing, whereas the streamflow (subject to adjustment via naturalization) is observed within river channels. However, on the annual basis (the time scale in our study), it makes very little difference as the routing effect is small.

The best five GCMs selected for the three major river basins are:

PNW: GFDL-CM4, EC-Earth3-Veg, NorESM2-MM, HadGEM3-GC31-MM, ACCESS-CM2; **UCRB**: IPSL-CM6A-LR, GFDL-ESM4, MPI-ESM1-2-HR, NorESM2-MM, ACCESS-CM2; **CA**: EC-Earth3-Veg, MPI-ESM1-2-HR, MRI-ESM2-0, IPSL-CM6A-LR, ACCESS-CM2.

Different GCMs were selected for each of the three river basins based on *Ashfaq et al.* [2022] for the PNW, *Krantz et al.* [2021] for CA, and *D W Pierce et al.* [2022] for UCRB,

respectively. To ensure the GCM consistency among basins and scenarios, we took the union of the five best models for each of the three basins, resulting in 10 GCM models. From the 10 models, we removed the HadGEM3-GC31-MM, for which downscaled results were not available in the LOCA downscaled dataset as of the date of retrieval (2023-06-10) for SSP245. We also removed EC-Earth3 and GFDL-ESM4 to avoid including multiple models from the same institution (with similar performance) in the ensemble. We chose to keep EC-Earth3-Veg and GFDL-CM4 instead due to their generally better performance than EC-Earth3 and GFDL-ESM4 in the WUS [*Ashfaq et al.*, 2022].

Naturalized Flow Subbasin Delineations

Colorado River Basin

We obtained the natural flow polygon for the entire Colorado River Basin (data provided below archived with other data) from James R. Prairie at the Bureau of Reclamation. Our focus was on the UCRB (equivalent to the USGS hydrologic region: upper Colorado, except the great divide subbasin), so we only used information for that part of the Colorado River basin (which accounts for about 90% of the average annual flow of the entire basin).

California

Our California domain covers the stream basins with available long-term full-naturalized-flow gauges from CDEC, which coverage is different from the USGS California hydrologic region. We delineated the CDEC long-term full-naturalized-flow gauges' associated basin polygon shapefiles using 3 arc-second MERIT Hydro flow direction in GIS and gauge coordinates obtained from CDEC (https://cdec.water.ca.gov/reportapp/javareports?name=MonthlyFNF). The results were carefully checked against other papers [*Bass et al.*, 2023; *VanRheenen et al.*, 2004] and data sources (listed below):

1. Margulis dataset [*Margulis et al.*, 2016]

2. WBD HUC8 and HUC10, watershed description and polygons [*Jones et al.*, 2022].

3. CNRFC watershed dataset, retrieved at (CNRFC - California Nevada River Forecast Center (noaa.gov)).

4. MERIT Hydro flow accumulation raster (to double-check that the watershed drains into the gauge) [*Yamazaki et al.*, 2019].

A total of 31 basins remained after all the above steps, which provide good coverage of the central Sierra Nevada, eastern Sierra Nevada, and maritime basins. It contains all 16 watersheds used in *Bass et al.* [2023] except Calaveras (long-term full-naturalized-flow not available), and covers all 16 watersheds in *VanRheenen et al.* [2004] except Calaveras and Bear Rivers, which are small. We believe this dataset provides comprehensive and complete coverage for California's available long-term full-naturalized-flow gauges from CDEC. The shapefiles are provided as described in Data Availability. The gauges list can be found in Table C1 in the supplement.

Pacific Northwest (PNW)

The PNW covers the PNW hydrologic region less coastal tributaries (beyond the Columbia River at Bonneville). We obtained the watershed polygons for PNW major tributaries in BPA-modified flow gages from USGS WBD HUC-4 and HUC-6, and the stations of the tributaries' outlets are selected based on the:

1. MERIT Hydro 90m flow accumulation dataset [*Yamazaki et al.*, 2019].

2. Streamflow routing network in *Payne et al.* [2004].

3. BPA provided flow point location and upstream watershed area (Historical Streamflow Reports - Bonneville Power Administration (bpa.gov)).

The watersheds are carefully cross-checked against the above resources to confirm they make sense.

A total of 9 major tributaries (and associated gauges) were obtained after the above steps. Among the nine gauges, five were used by *Hamlet et al.* [2002] and *Payne et al.* [2004], including Hells Canyon as the Middle Snake outlet, Ice Harbor as Lower Snake outlet, Priest Rapid as Upper Columbia outlet, Watena as Pend Oreille outlet, and Bonneville as the overall outlet at the boundary of middle Columbia (more perfectly located at the boundary of USGS WBD watershed than the Dalles). Additionally, four smaller watersheds are included: Snake River at King Hill (SKHI) for upper and middle snakes separated by USGS WBD HUC-4. Yakima (YAK) for Yakima separated by USGS WBD HUC-4. Brilliant (BRI) for Kootenay separated by USGS WBD HUC-6. Long Lake (LLK) (located reasonably close to the outlet and closest among all natural flow locations provided by BPA) for Spokane is separated by USGS WBD HUC-6.

Sub-basin Elevation Extraction

Sub-basin elevations were extracted from the *Ban and Lettenmaier* [2022] 1/16th degree elevation dataset aggregated from the GTOPO global 30 Arc Second (~1km) Elevation Data Set [*Gesch et al.*, 1999], with the mask of subbasin shapefile boundaries delineated as described above in "Naturalized Flow Subbasin Delineations."

Data availability

Historical naturalized flow data for CA were obtained from California Data Exchange Center (https://cdec.water.ca.gov/dynamicapp/QueryWY). UCRB natural flows were obtained from the Bureau of Reclamation (https://www.usbr.gov/lc/region/g4000/NaturalFlow/current.html). PNW flow was obtained from Bonneville Power Administration (https://www.bpa.gov/-/media/Aep/power/historical-

streamflow-reports/historic-streamflow-nrni-flows-1929-2008-corrected-04-2017.csv). We also provide the sub-basin delineated shapefiles for the three major river basins (PNW, UCRB, and CA), UCRB historical VIC simulation outputs driven by H&L forcing, and sub-basin averaged GCM-VIC outputs, as source data provided with this paper, available in figshare.

Acknowledgements

We thank Park Williams, Daniel Cayan, Yongkang Xue, Yongwei Sheng, Steve Margulis, and Brad Udall for their helpful comments. We thank James R. Prairie and Brad Udall for their help in providing the Colorado River Basin natural flow polygons. We thank Yiwen Fang for her helpful discussion of California's natural basin polygon selection. This work was partially supported by the Center for Western Weather and Water Extremes 370 (CW3E) at the Scripps Institution of Oceanography via AR Program Phase 3, Grant 3714600014294, sponsored by the California Department of Water Resources.

Author information

Authors and Affiliations

Department of Geography, University of California, Los Angeles

Zhaoxin Ban & Dennis P. Lettenmaier

Contributions

ZB conceived the study, analyzed the data, performed the modeling, interpreted the results, and wrote the manuscript. DPL supervised the progress and participated in the interpretation. All authors discussed the results and commented on the manuscript.

Corresponding Author

Correspondence to Dennis P. Lettenmaier

Competing interests

The authors declare no competing interests.

Additional Information

Supplementary Information is available for this paper.

Correspondence and requests for materials should be addressed to dlettenm@ucla.edu.

References

Ashfaq, M., D. Rastogi, J. Kitson, M. A. Abid, and S. C. Kao (2022), Evaluation of CMIP6 GCMs over the CONUS for downscaling studies, *Journal of Geophysical Research: Atmospheres*, *127*(21), e2022JD036659.

Ban, Z., and D. P. Lettenmaier (2022), Asymmetry of Western US river basin sensitivity to seasonally varying climate warming, *Water Resources Research*, *58*(2), e2021WR030367.

Ban, Z., C. Xin, Y. Fang, X. Ma, D. Li, and D. P. Lettenmaier (2023), Snowmelt-radiation feedback impact on Western U.S. streamflow, *Geophysical Research Letters*.

Bass, B., S. Rahimi, N. Goldenson, A. Hall, J. Norris, and Z. J. Lebow (2023), Achieving Realistic Runoff in the Western United States with a Land Surface Model Forced by Dynamically Downscaled Meteorology, *Journal of Hydrometeorology*, *24*(2), 269-283.

Bohn, T. J., B. Livneh, J. W. Oyler, S. W. Running, B. Nijssen, and D. P. Lettenmaier (2013), Global evaluation of MTCLIM and related algorithms for forcing of ecological and hydrological models, *Agricultural and forest meteorology*, *176*, 38-49.

Daly, C., R. P. Neilson, and D. L. Phillips (1994), A statistical-topographic model for mapping climatological precipitation over mountainous terrain, *Journal of Applied Meteorology and Climatology*, *33*(2), 140-158.

Gesch, D. B., K. L. Verdin, and S. K. Greenlee (1999), New land surface digital elevation model covers the Earth, *Eos, Transactions American Geophysical Union*, *80*(6), 69-70.

Hamlet, A. F., and D. P. Lettenmaier (2005), Production of temporally consistent gridded precipitation and temperature fields for the continental United States, *Journal of Hydrometeorology*, *6*(3), 330-336.

Hamlet, A. F., D. Huppert, and D. P. Lettenmaier (2002), Economic value of long-lead streamflow forecasts for Columbia River hydropower, *Journal of Water Resources Planning and Management*, *128*(2), 91-101.

Johnson, T., J. Butcher, D. Deb, M. Faizullabhoy, P. Hummel, J. Kittle, S. McGinnis, L. Mearns, D. Nover, and A. Parker (2015), Modeling streamflow and water quality sensitivity to climate change and urban development in 20 US watersheds, *JAWRA Journal of the American Water Resources Association*, *51*(5), 1321-1341.

Jones, K. A., L. S. Niknami, S. G. Buto, and D. Decker (2022), Federal Standards and Procedures for the National Watershed Boundary Dataset (WBD): Chapter 3 of Section A, Federal Standards, Book 11, Collection and Delineation of Spatial Data*Rep. 2328-7055*, US Geological Survey.

Krantz, W., D. Pierce, N. Goldenson, and D. Cayan (2021), Memorandum on Evaluating Global Climate Models for Studying Regional Climate Change in California.

Liang, X., D. P. Lettenmaier, E. F. Wood, and S. J. Burges (1994), A simple hydrologically based model of land surface water and energy fluxes for general circulation models, *Journal of Geophysical Research: Atmospheres*, *99*(D7), 14415-14428.

Livneh, B., E. A. Rosenberg, C. Lin, B. Nijssen, V. Mishra, K. M. Andreadis, E. P. Maurer, and D. P. Lettenmaier (2013), A long-term hydrologically based dataset of land surface fluxes and states for the conterminous United States: Update and extensions, *Journal of Climate*, *26*(23), 9384-9392.

Livneh, B., T. J. Bohn, D. W. Pierce, F. Munoz-Arriola, B. Nijssen, R. Vose, D. R. Cayan, and L. Brekke (2015), A spatially comprehensive, hydrometeorological data set for Mexico, the US, and Southern Canada 1950–2013, *Scientific data*, *2*(1), 1-12.

Margulis, S. A., G. Cortés, M. Girotto, and M. Durand (2016), A Landsat-era Sierra Nevada snow reanalysis (1985–2015), *Journal of Hydrometeorology*, *17*(4), 1203-1221.

Milly, P. C., and K. A. Dunne (2020), Colorado River flow dwindles as warming-driven loss of reflective snow energizes evaporation, *Science*, *367*(6483), 1252-1255.

Musselman, K. N., M. P. Clark, C. Liu, K. Ikeda, and R. Rasmussen (2017), Slower snowmelt in a warmer world, *Nature Climate Change*, *7*(3), 214-219.

Neto, A. A. M., G.-Y. Niu, T. Roy, S. Tyler, and P. A. Troch (2020), Interactions between snow cover and evaporation lead to higher sensitivity of streamfiow to temperature, *Communications Earth & Environment*, *1*(1), 1-7.

Niu, G. Y., Z. L. Yang, K. E. Mitchell, F. Chen, M. B. Ek, M. Barlage, A. Kumar, K. Manning, D. Niyogi, and E. Rosero (2011), The community Noah land surface model with multiparameterization options (Noah-MP): 1. Model description and evaluation with local-scale measurements, *Journal of Geophysical Research: Atmospheres*, *116*(D12).

Payne, J. T., A. W. Wood, A. F. Hamlet, R. N. Palmer, and D. P. Lettenmaier (2004), Mitigating the effects of climate change on the water resources of the Columbia River basin, *Climatic change*, *62*, 233-256.

Pierce, D., and D. Cayan (2016), Downscaling humidity with localized constructed analogs (LOCA) over the conterminous United States, *Climate dynamics*, *47*, 411-431.

Pierce, D. W., D. R. Cayan, and B. L. Thrasher (2014), Statistical downscaling using localized constructed analogs (LOCA), *Journal of hydrometeorology*, *15*(6), 2558-2585.

Pierce, D. W., D. R. Cayan, D. R. Feldman, and M. D. Risser (2023), Future Increases in North American Extreme Precipitation in CMIP6 Downscaled with LOCA, *Journal of Hydrometeorology*, *24*(5), 951-975.

Pierce, D. W., D. R. Cayan, E. P. Maurer, J. T. Abatzoglou, and K. C. Hegewisch (2015), Improved bias correction techniques for hydrological simulations of climate change, *Journal of Hydrometeorology*, *16*(6), 2421-2442.

Pierce, D. W., D. R. Cayan, J. Goodrich, T. Das, and A. Munévar (2022), Evaluating global climate models for hydrological studies of the upper Colorado River Basin, *JAWRA Journal of the American Water Resources Association*, *58*(5), 709-734.

Su, L., Q. Cao, M. Xiao, D. M. Mocko, M. Barlage, D. Li, C. D. Peters-Lidard, and D. P. Lettenmaier (2021), Drought variability over the conterminous United States for the past century, *Journal of Hydrometeorology*, *22*(5), 1153-1168.

VanRheenen, N. T., A. W. Wood, R. N. Palmer, and D. P. Lettenmaier (2004), Potential implications of PCM climate change scenarios for Sacramento–San Joaquin River Basin hydrology and water resources, *Climatic change*, *62*, 257-281.

Yamazaki, D., D. Ikeshima, J. Sosa, P. D. Bates, G. H. Allen, and T. M. Pavelsky (2019), MERIT Hydro: A high-resolution global hydrography map based on latest topography dataset, *Water Resources Research*, *55*(6), 5053-5073.

Yang, Z. L., G. Y. Niu, K. E. Mitchell, F. Chen, M. B. Ek, M. Barlage, L. Longuevergne, K. Manning, D. Niyogi, and M. Tewari (2011), The community Noah land surface model with multiparameterization options (Noah-MP): 2. Evaluation over global river basins, *Journal of Geophysical Research: Atmospheres*, *116*(D12).

Chapter 5 Conclusions

This dissertation aims to provide a better understanding of the likely evolution of streamflow in the snow-affected regions of the western U.S. (WUS), as the climate warms. My analyses are based on a combination of observations and land surface models. At the outset, I posed three scientific questions that guided my research:

1) How does seasonal warming affect annual streamflow in different watersheds, and why?

2) What composes runoff during water-scarce seasons, and how does the composition change under warming?

3) What mechanism dominates annual runoff decline under warming in snow-affected areas, and how do its dynamics affect the evolution of runoff?

To address these questions, I conducted controlled warming experiments using land surface models applied over the WUS. I developed customized algorithms to extract, from hydrologic models, information about snowmelt, infiltration, evapotranspiration, and streamflow generation. I also assembled observations of streamflow from multiple sources and projections of future climate change using CMIP6 downscaled climate dataset over the WUS [*Ashfaq et al.*, 2022; *Krantz et al.*, 2021; *D W Pierce et al.*, 2022], all of which were used in my assessments of hydrologic process change under climate warming.

In **Chapter 2,** I examined the spatial patterns of the relative response of annual streamflow to warm vs. cool season warming across the WUS. I found that the relative responses to seasonal warming (asymmetry) are similar for large and HUC-8 basins. My observation-based investigation suggests a smaller asymmetrical response pattern but a similar direction to model results.

I also evaluated a) observation-based support for model-based sensitivity estimates; b) the impacts of different basin surface characteristics on the patterns of annual streamflow relative

response to seasonal warming; and c) the processes that contribute most to the annual streamflow response asymmetry across the 616 HUC-8 basins. I found that cooler inland basins are more sensitive to warm-season warming, and warmer coastal regions are more sensitive to cool-season warming. Considering the background of the projected warm season warming signal is stronger than cool season warming, this pattern implies that the cooler inland basins will experience stronger annual streamflow declines under projected warming. Furthermore, I showed that increased vegetation can enhance the asymmetrical response pattern between warmer and cooler basins.

Finally, I conducted an attribution analysis and identified different warming-associated processes that dominate the asymmetry of annual streamflow response to seasonal warming across the WUS. In extremely cold basins, available radiation changes with reduced snow cover dominate the streamflow response asymmetry. In basins with intermediate temperatures, vapor pressure deficit changes dominate, and in basins with the warmest temperatures, surface resistance increases under warmer temperatures dominate.

In **Chapter 3**, I explicitly quantified the contributions from cool-season rainfall, warm-season rainfall, and snowmelt to summer streamflow using a customized-period water tracking algorithm (details provided in Appendix B) that is an extension of a less flexible algorithm developed by *Li et al.* [2017]. I found that seasonal rainfall provides important volumetric contributions to summer streamflow for many streams in the WUS. Cool-season rainfall contributes the most in low-elevation coastal streams, while warm-season rainfall dominates in the southern interior of our WUS domain. As the climate continues to warm and snowmelt declines, seasonal rainfall's contribution to summer streamflow will increase. This increase will be mostly from warm-season rainfall, offsetting about two-thirds of the reduction in snowmelt contribution.

The other one-third will be offset by cool-season rainfall. The contribution increase from cool-season rainfall is especially large in years with warm snow droughts and abnormally dry summers.

I also found that seasonal rainfall dominates summer streamflow variability across about 70% of the WUS. By incorporating cool-season and Apr-Jun rainfall as predictors, the loss of summer streamflow predictability due to reduced snowmelt contribution can be substantially mitigated. My findings in this chapter highlight the importance of alternative (to snowmelt) contributions to summer streamflow, which are especially important as snowpacks decline.

In **Chapter 4**, I used a combination of naturalized streamflow records, LSM-based 1°C/2°C warming experiments, and elevation-wise analysis of LSM-GCM output to study the evolving sensitivity of SWE loss, ET increase and runoff loss per unit (one degree C) warming as the reference climate warms. I discovered a hint of decelerated runoff decline rates in the historical record for UCRB. Furthermore, my analysis of LSM control warming experiments demonstrates a reduced sensitivity of snow and subsequent runoff changes per degree of warming as the climate warms when precipitation is fixed. In GCM-LSM results, despite the non-constant warming rate and changing precipitation obscuring the evolving runoff sensitivity, I detected a generally slower snow loss in sub-basins with lower elevations and/or less snow, which are analogs to a warmer future condition. Under near-linear (with time) warming (e.g., IPCC emissions scenario SSP245), there is also a hint of deceleration in runoff and runoff ratio decline, and the same for the changing rate in snow loss and related net radiation increase. Comparing SSP245 with a more rapid future warming scenario (SSP585), I found that the runoff evolution turns from increasing under SSP245 to decreasing under SSP585, magnifying, or reversing the effect of differences in precipitation between the two warming scenarios. These findings suggest that the difference in runoff evolution is strongly affected by the different warming rates. If climate warming can be controlled to a stable

rate (like SSP245), there is a potential for decelerating (annual) runoff decline or even runoff increase if precipitation across the WUS were to increase (which is predicted by many IPCC CMIP6 models).

The findings in this dissertation have important implications for understanding and managing the ongoing and future evolution of streamflow across the snow-affected WUS. The findings of all three chapters are consistent to the extent that cooler-inland basins are more sensitive to seasonal warming, and have larger runoff sensitivities to annual warming than warmer coastal basins. Stated otherwise, snow-affected inland mountainous regions will experience the strongest runoff declines in a warmer future. However, my findings in Chapter 4 also offer some optimism for WUS water supplies in that with less snowpack and increased precipitation (as predicted by many CMIP6 models (see Chapter 4 Fig. 3), reduced warming-sensitivity of runoff as the climate warms could result in streamflow increases in the WUS, leaving more time for human beings in the WUS to safely adapt to the future more rain-dominated runoff.

The findings of my dissertation work should motivate continued research into the future evolution of water resources as WUS snowpacks further shrink. Further efforts related to this direction could involve further evaluation of mechanisms related to the decreasing sensitivity of snow loss and runoff to warming. Some examples of mechanisms include: i) The rate of snowline elevation increases with warming decrease at higher elevations. Under a warmer reference climate, snowlines are higher, leading to a slower snow loss per unit of temperature warming; ii) Earlier shift of the snowmelt season to a period with lower available energy could reduce the overall efficiency of energizing evapotranspiration by the snowmelt-radiation feedback; iii) less snow coverage under a warmer reference climate leads to less snow coverage and albedo change during the melt season under a warmer reference climate.

Besides the snowmelt-radiation feedback, the emerging mega-drought over the last two decades may also profoundly impact snowmelt-affected streamflow, which may be even more important than direct effects of warming. Droughts occurring in summer can consume soil moisture that remains to be recharged by snowmelt the following spring and reduce the generation of both cool and warm season streamflow. This could potentially lead to overestimation of streamflow forecasts in the post-drought years based on currently established snow-based relationships. Similar to the snow loss and snowmelt-radiation feedback, there could also be non-stationarity in drought impacts. For example, soil in some parts of Arizona is already almost completely dessicated in the summer and thus becoming immune to drought-driven soil moisture deficits from the previous year (i.e., soil cannot get any drier). Considering the opportunity for soil moisture change in other regions, soil dryness could also be a very important factor affecting the runoff evolution. If the soil becomes drier with more severe drought and increasing temperature in the future, the following-year streamflow may have stronger declines. Still, if soil already becomes as dry as possible, the sensitivity of this soil dryness to temperature will shrink as well. We can envision that with progressively stronger droughts, the soil moisture deficit impact on streamflow may also show strong non-linearity, accompanied by drought-related wildfire and consequent change in vegetation evapotranspiration, the relationship could be further complicated. Possible future work to examine these drought-related ongoing changes (e.g., soil dryness) and its relative magnitude to control the streamflow compared to the evolving snowmelt-radiation feedback and changing precipitation could provide important insight into future streamflow evolution.

Besides the change in soil dryness, the incoming water (i.e., precipitation) can also change. In the future climate, there is a high probability of a shift towards a stronger cold winter contribution to annual precipitation. The other (probably even more certain) result is the

seasonality that event scale precipitation will be more dominated by the heavier precipitation amounts occasionally occurring, e.g., atmospheric rivers become stronger. Changes in precipitation seasonality could further affect the seasonal rainfall contribution to streamflow. Further analysis could use a refined water source tracking algorithm (like the one I used in Chapter 3) focused on the winter season, when precipitation from CMIP6 is emerging to be more concentrated in for the maritime parts of WUS, or even more narrowly focused on the event scale.

In summary, more attention to runoff-climate response factors that have been ignored in past studies are in order. For example, the impact of increasing atmospheric opacity on radiation and thus evapotranspiration and streamflow loss (associated with atmospheric CO_2 and water vapor increase) has been missing in many off-line climate changes studies. As shown in *Ban et al.* [2023b], including this effect can substantially affect estimates of streamflow sensitivity to warming. On the other hand, the quantitative analysis of how the impact of currently-known mechanisms (such as snowmelt-radiation feedback) on streamflow evolves under a warmer climate will enable us to predict the behavior of future streamflow more precisely. Moreover, more attention to vegetation dynamics and discrete events such as wildfire, droughts, and event scale precipitation are needed to better understand their aggregate effect on water resources [*Williams et al.*, 2022]. Finally, higher resolution Earth System Models aided with the progress in data science, and better incorporation of satellite data could also help to understand the effects of the coupled atmosphere-land surface system at spatial scales relevant to hydrologic response. Through aforementioned explorations and collective effort to mitigate climate warming, human beings would be better equipped to handle future water crisis.

References

Ashfaq, M., D. Rastogi, J. Kitson, M. A. Abid, and S. C. Kao (2022), Evaluation of CMIP6 GCMs over the CONUS for downscaling studies, *Journal of Geophysical Research: Atmospheres*, *127*(21), e2022JD036659.

Ban, Z., C. Xin, Y. Fang, X. Ma, D. Li, and D. P. Lettenmaier (2023), Snowmelt-radiation feedback impact on Western U.S. streamflow, *Geophysical Research Letters*.

Krantz, W., D. Pierce, N. Goldenson, and D. Cayan (2021), Memorandum on Evaluating Global Climate Models for Studying Regional Climate Change in California.

Li, D., M. L. Wrzesien, M. Durand, J. Adam, and D. P. Lettenmaier (2017), How much runoff originates as snow in the western United States, and how will that change in the future?, *Geophysical Research Letters*, *44*(12), 6163-6172.

Pierce, D. W., D. R. Cayan, J. Goodrich, T. Das, and A. Munévar (2022), Evaluating global climate models for hydrological studies of the upper Colorado River Basin, *JAWRA Journal of the American Water Resources Association*, *58*(5), 709-734.

Williams, A. P., B. Livneh, K. A. McKinnon, W. D. Hansen, J. S. Mankin, B. I. Cook, J. E. Smerdon, A. M. Varuolo-Clarke, N. R. Bjarke, and C. S. Juang (2022), Growing impact of wildfire on western US water supply, *Proceedings of the National Academy of Sciences*, *119*(10), e2114069119.

Appendix A

A.1 A possible alternative index to define asymmetry in Chapter 2

In the published version of Chapter 2, $Pref_Q$ is defined as a ratio with theoretical range (-∞, +∞). This appendix discusses a possible alternative way to design the asymmetry-summarizing metric to better confine the range. Drawing on the history of the development of the Normalized Difference Vegetation Index (NDVI) in remote sensing, a normalized index of the original $Pref_Q$ can be defined in Eq. A1:

$$\text{new index} = \frac{a-b}{a+b} \tag{A1}$$

where $a = \overline{Q_{a,w1d}} - \overline{Q_{a,b}}$ is the annual streamflow change in response to warm season-only warming, and $b = \overline{Q_{a,c1d}} - \overline{Q_{a,b}}$ is the annual streamflow change in response to cool season-only warming. In a and b, Q refers to streamflow, and subscripts follow the definition used in Chapter 2 Eq. 1. As a comparison, the original $Pref_Q$ is a/b.

The new index maps the infinite range to (-1, 1) for basins with a and b of the same sign (i.e., with a positive $Pref_Q$). The effect is illustrated in Figure A1, where only basins with positive $Pref_Q$ are plotted. In Figure A1a, the original $Pref_Q$ is saturated when $Pref_Q$ is larger than 2. In contrast, in Figure A1b, the new index can smoothly stretch the value of asymmetry with better spatial details and spatial variation consistent with Figure A1a.

For basins with positive $Pref_Q$, the new index also maintains the relative order of $Pref_Q$, as shown in Figures A2c-A2d: the new index is negative when $Pref_Q$ is less than one (Figure A2c), corresponds to a stronger annual streamflow response under cool season-only warming; the index becomes positive where $Pref_Q$ is larger than one (Figure A2d), corresponds to a stronger annual streamflow response under warm season-only warming.

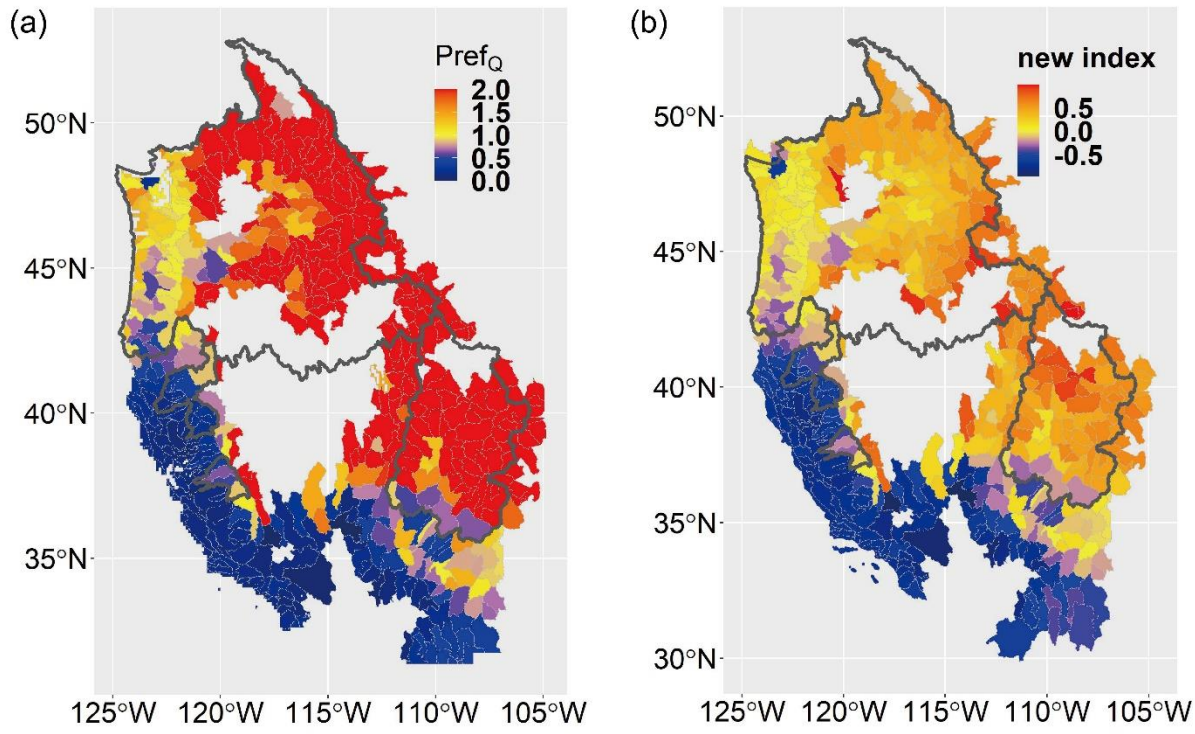

Figure A1. Comparison of spatial maps between $Pref_Q$ (a) and the new index (b). Only basins with positive $Pref_Q$ are plotted. Values for basins with negative $Pref_Q$ are not plotted because the new index does not map the value boundary to a finite range for such cases. Please refer to Figure A2a-A2b and the following paragraph for details.

The new index's value range becomes infinite for basins with a and b of opposite signs. This limitation comes from the mathematical form of the new index, which is equivalent to (a/b-1)/(a/b+1) and is only within a finite range when $a/b > 0$. As shown by Figures A2a-A2b, when $Pref_Q$ is less than zero (i.e., $a/b < 0$), the value range of the new index becomes $(-\infty, +\infty)$ again. Therefore, this new index is only useful for positive $Pref_Q$, the most frequent case for streamflow response in the WUS but cannot maintain the idealized finite range in other basins.

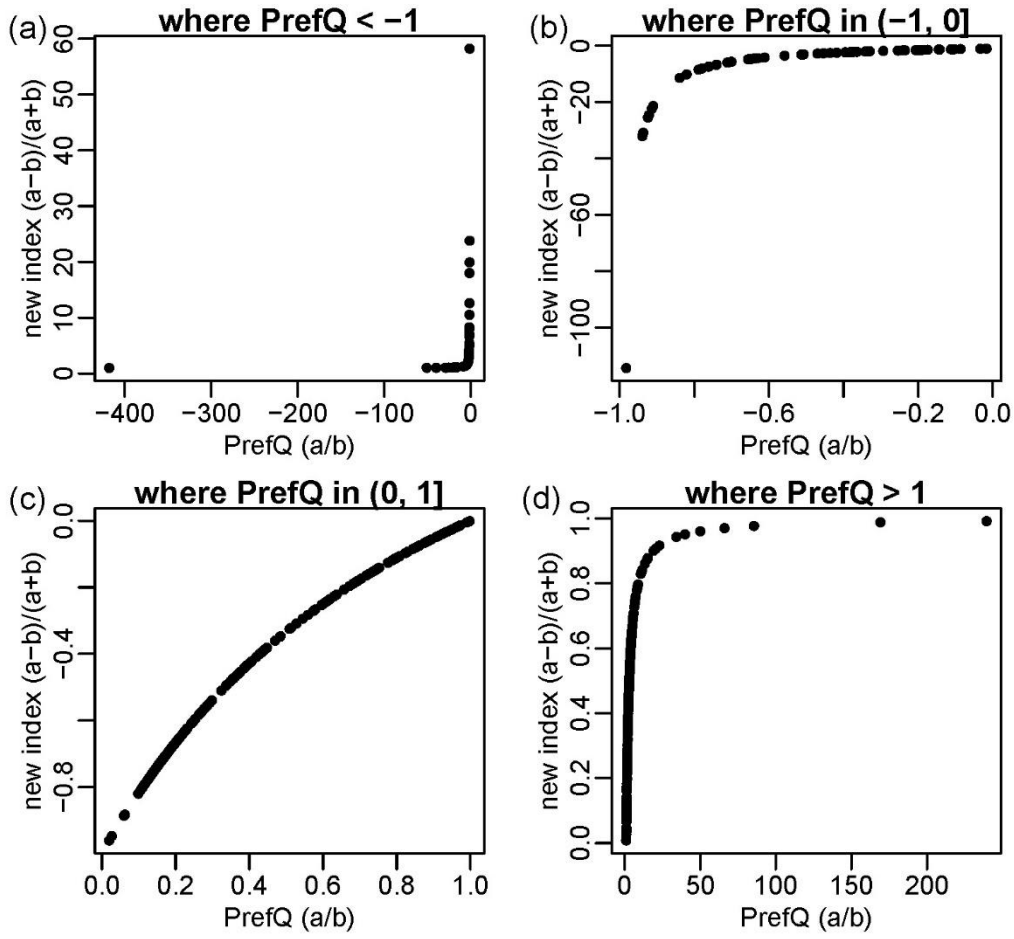

Figure A2. Comparison of the original $Pref_Q$ (x-axis) and the new index across all four different value ranges of $Pref_Q$.

Appendix B

B.1 Details of the custom-period water tracking algorithm in Chapter 3

I refined the snowmelt-tracking algorithm of *Li et al.* [2017] so as to allow tracking of the sources of a custom period's runoff (summer in our case) from specified sources (e.g., snowmelt, winter rainfall, and summer rainfall). The original algorithm had as its target total annual runoff, and the sole source was annual snowmelt and rainfall. The custom tracking separates the contributions from cool and warm season rainfall (in addition to snowmelt) to soil moisture temporally by the time the rainfall occurs. This separation can be specified for temporal periods such as seasonal, monthly, or other finer periods larger than the input data step. This modification does not affect the partitioning of snowmelt from rainfall, which is the same as the original algorithm in *Li et al.* [2017], for which the snowmelt contribution showed good agreement with isotope measurements. The algorithm requires the following land surface model outputs as input: Snowfall (snow), Rainfall (rain), Evapotranspiration (ET), soil moisture (W), snow water equivalent (SWE), snowmelt (M), runoff (R), and baseflow (B) at every model output step. All variables' units are in mm. Hereafter, the same notation is used in Eqs. B1-B20 below. With these variables available, the algorithm should be applicable to any land surface hydrology model.

For the application in Chapter 3, I use three variables: $f_{W,rainw,t}$, $f_{W,rainc,t}$, and $f_{W,snow,t}$, which represent the fractions of soil moisture at every time step coming from the warm season rainfall, cool season rainfall, and snowmelt, respectively. The corresponding terms in the main text (F_rainc, F_rainw, and F_snow) are in Eqs. B18-B20. The algorithm is summarized as follows:

When t=0, initialization:

$$f_{W,rainw,t} = f_{W,rainc,t} = f_{W,snow,t} = 0 \tag{B1}$$

After spin-up:

$$f_{W,rainw,t} + f_{W,rainc,t} + f_{W,snowc,t} = 1 \quad \text{(B2)}$$

The following subsections include details of the algorithm. In all the following equations, subscript t means current timestep, $t-1$ means the previous time step, Δt is the length of the timestep.

B1.1 Calculate infiltration i

$$i_t = rain_t + M_t - R_t \quad \text{(B3)}$$

where $rain_t$, M_t, and R_t are the t-th time step rainfall, snowmelt, and runoff which comes from model (VIC or Noah-MP in our case) output.

B1.2 Full mixing assumption

I use the assumption that snowmelt and rainfall are fully mixed (as in the original paper by *Li et al.* [2017]) to calculate the fraction of infiltration coming from snowmelt and rainfall:

$$i_{snow,t} = \frac{M_t}{M_t + rain_t} i_t \quad \text{(B4)}$$

$$i_{rain,t} = \frac{rain_t}{M_t + rain_t} i_t \quad \text{(B5)}$$

B1.3 Runoff calculation

The runoff generated by snow ($R_{snow,t}$) and rain ($R_{rain,t}$) is separately calculated by subtracting the snow-driven infiltration ($i_{snow,t}$, calculated from Eq. B4) and rain-driven infiltration ($i_{rain,t}$, calculated from Eq. B5) from model output snowmelt (M_t) and rainfall ($rain_t$):

$$R_{snow,t} = M_t - i_{snow,t} \quad \text{(B6)}$$

$$R_{rain,t} = rain_t - i_{rain,t} \quad \text{(B7)}$$

B1.4 Sublimation calculation

The sublimation at each time step can be backed out from the model output snowfall ($snow_t$), model output snowmelt (M_t), and change of model output SWE ($SWE_{t-1} - SWE_t$):

$$sub_t = SWE_{t-1} + snow_t - M_t - SWE_t \quad \text{(B8)}$$

B1.5 Baseflow, ET, and sublimation partitioning

I use the assumption of *Li et al.* [2017] that the fraction of baseflow derived from snow equals the fraction of soil moisture that originated from snow ($f_{W,snow,t}$); the fraction of baseflow derived from cool-season rainfall equals the fraction of soil moisture that originated from cool-season rainfall ($f_{W,rainc,t}$); the fraction of baseflow derived from warm-season rainfall equals the fraction of soil moisture that originated from warm-season rainfall ($f_{W,rainw,t}$):

$$B_{snow,t} = f_{W,snow,t} B_t \quad \text{(B9)}$$

$$B_{rainc,t} = f_{W,rainc,t} B_t \quad \text{(B10)}$$

$$B_{rainw,t} = f_{W,rainw,t} B_t \quad \text{(B11)}$$

Similar to baseflow, the ET and sublimation calculation follows the same fractional scaling using $f_{W,snow,t}$, $f_{W,rainc,t}$, and $f_{W,rainw,t}$, see Eqs. B13-B17 for details. Baseflow, soil moisture, and ET all come from model output, and sublimation is backed out from model outputs according to Eq. B8. Since in Eq. B2, the sum of $f_{W,snow,t}$, $f_{W,rainc,t}$, and $f_{W,rainw,t}$ equals one, the sum of the partitioned three sources' baseflow (or ET, or sublimation) equals the original model output baseflow (or ET, or sublimation).

B1.6 Soil water mass balance and time propagation

According to soil water mass balance, the soil moisture storage change is a result of water gain/loss from infiltration, sublimation, evapotranspiration, and baseflow:

$$W_t = W_{t-1} + i_t \Delta t - (ET_t - sub_t)\Delta t - B_t \Delta t \quad \text{(B12)}$$

Taking the assumption used in S1.5, only the snowmelt-related part of evapotranspiration, infiltration, sublimation, and baseflow affect the part of soil moisture coming from snowmelt. Similarly, only the warm-season rainfall (cool-season rainfall) related parts of evapotranspiration, infiltration, sublimation, and baseflow can affect the part of the soil moisture coming from warm-season rainfall (cool-season rainfall). As a result, Eq. B12 can be split into Eqs. B13-B17 for the separation of snowmelt, cool-season rainfall, and warm-season rainfall.

In the warm season, the tracking process for warm and cool-season rainfall is:

$$f_{W,rainw,t} W_t = f_{W,rainw,t-1} W_{t-1} + \frac{rain_t}{M_t + rain_t} i_t \Delta t - f_{W,rainw,t-1}(ET_t - Sub_t)\Delta t - f_{W,rainw,t-1} B_t \Delta t \quad \text{(B13)}$$

$$f_{W,rainc,t} W_t = f_{W,rainc,t-1} W_{t-1} - f_{W,rainc,t-1}(ET_t - Sub_t)\Delta t - f_{W,rainc,t-1} B_t \Delta t \quad \text{(B14)}$$

In the cool season, the tracking process is:

$$f_{W,rainw,t} W_t = f_{W,rainw,t-1} W_{t-1} - f_{W,rainw,t-1}(ET_t - Sub_t)\Delta t - f_{W,rainw,t-1} B_t \Delta t \quad \text{(B15)}$$

$$f_{W,rainc,t} W_t = f_{W,rainc,t-1} W_{t-1} + \frac{rain_t}{M_t + rain_t} i_t \Delta t - f_{W,rainc,t-1}(ET_t - Sub_t)\Delta t - f_{W,rainc,t-1} B_t \Delta t \text{(B16)}$$

In both seasons, the snowmelt tracking process is:

$$f_{W,snow,t} W_t = f_{W,snow,t-1} W_{t-1} + \frac{M_t}{M_t + rain_t} i_t \Delta t - f_{W,snow,t-1}(ET_t - Sub_t)\Delta t - f_{W,snow,t-1} B_t \Delta t \quad \text{(B17)}$$

B1.7 Calculation of contribution to summer streamflow

The contribution to summer streamflow (Q) from the three sources (cool season rainfall, warm season rainfall, and snowmelt) is calculated as follows:

$$F\_rainc = \left[\sum_{t=Jul1st}^{t=Sep30th} (B_{rainc,t})\right] / \left[\sum_{t=Jul1st}^{t=Sep30th} Q_t\right] \quad \text{(B18)}$$

$$F\_rainw = \left[\sum_{t=Jul1st}^{t=Sep30th} (B_{rainw,t} + R_{rain,t})\right] / \left[\sum_{t=Jul1st}^{t=Sep30th} Q_t\right] \quad \text{(B19)}$$

$$F\_snow = \left[\sum_{t=Jul1st}^{t=Sep30th} (B_{snow,t} + R_{snow,t})\right] / \left[\sum_{t=Jul1st}^{t=Sep30th} Q_t\right] \quad \text{(B20)}$$

References

Li, D., M. L. Wrzesien, M. Durand, J. Adam, and D. P. Lettenmaier (2017), How much runoff originates as snow in the western United States, and how will that change in the future?, Geophysical Research Letters, 44(12), 6163-6172.

Appendix C

C.1 Tables

Table C1. Three major river basins and corresponding station IDs for flows.

Domain	Station_ID
PNW	SKHI (Snake River at King Hill) HCD (Snake River at Hells Canyon Dam Id-Or State Line) BON (Columbia River below Bonneville Dam) IHR (Snake River below Ice Harbor Dam) PRD (Columbia River Below Priest Rapids Dam) YAK (Yakima River at KIONA) LLK (Spokane River at Long Lake) BRI (Brilliant, right downstream of Kootenay River near. Glade) WAT (Waneta)
CA	SRS (Salmon R at Somes Bar) SIS (Sacto Inflow-Shasta) TNL (Trinity River at Lewiston) SBB (Sacramento River above Bend Bridge) FTO (Feather River at Oroville) YRS (Yuba River near Smartville) TRF (Truckee River at Farad) WFC (West Fork Carson River at Woodfords) AMF (American River at Folsom) RRH (Russian River near Healdsberg) CSN (Cosumnes River at Michigan Bar) NPH (Napa River near St Helena) EFC (East Fork Carson River near Gardnerville) MKM (Mokelumne-Mokelumne Hill) WWR (West Walker River near Coleville) EWR (East Walker River near Bridgeport) SNS (Stanislaus River-Goodwin) TLG (Tuolumne River-La Grange Dam) MRC (Merced River near Merced Falls) OWL (Owens River-Long Valley) SJF (San Joaquin River below Friant) KGF (Kings River-Pine Flat Dam) KWT (Kaweah River-Terminus Dam) ASS (Arroyo Seco near Soledad) SCC (Tule River-Success Dam) NCD (Nacimiento River below Dam) KRI (Kern River-Below Isabella) KRB (Kern River-Bakersfield) SSP (Sespe Creek near Fillmore) ANM (Santa Ana River near Mentone)

	ERS (Eel River at Scotia)
UCRB	09072500 (Colorado River at Glenwood Springs, CO) 09095500 (Colorado River near Cameo, CO) 09109000 (Taylor River below Taylor Park Reservoir, CO) 09124700 (Gunnison River above Blue Mesa Reservoir, CO) 09127800 (Gunnison River at Crystal Reservoir, CO) 09152500 (Gunnison River near Grand Junction, CO) 09180000 (Dolores River near Cisco, UT) 09180500 (Colorado River near Cisco UT) 09211200 (Green River below Fontenelle Reservoir, WY) 09217000 (Green River near Green River, WY) 09234500 (Green River near Greendale, UT) 09251000 (Yampa River near Maybell, CO) 09260000 (Little Snake River near Lily, CO) 09302000 (Duchesne River near Randlett, UT) 09306500 (White River near Watson, UT) 09315000 (Green River at Green River, UT) 09328500 (San Rafael River near Green River, UT) 09355500 (San Juan River near Archuleta, NM) 09379500 (San Juan River near Bluff, UT) 09380000 (Colorado River at Lees Ferry, AZ)

C.2 Figures

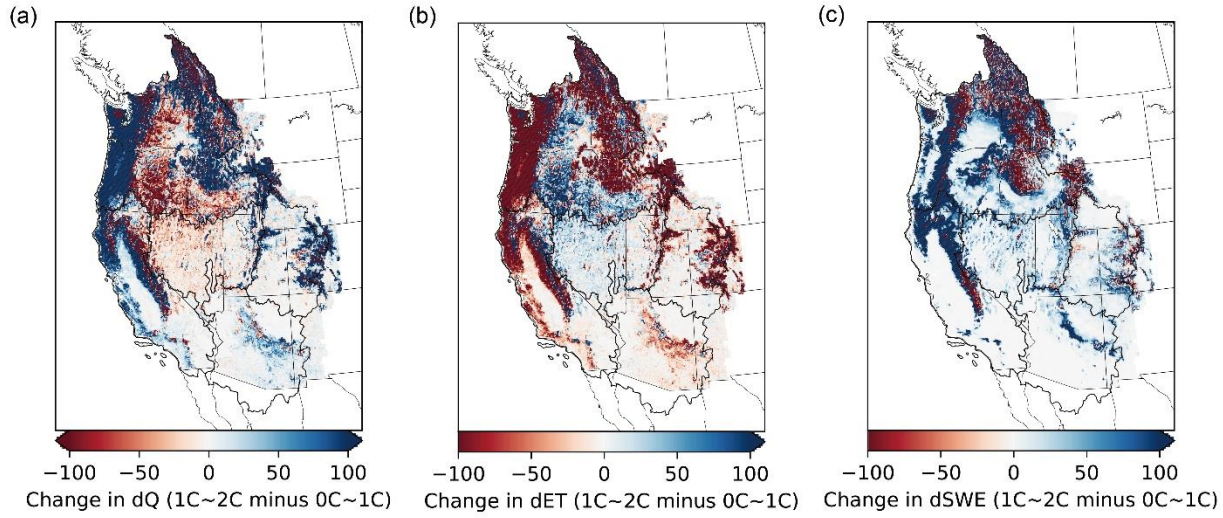

Figure C1. (a) Maps of ΔQ (mm/yr) from 1°C to 2°C warming experiment minus ΔQ (mm/yr) from 0°C to 1°C warming experiment. Similarly, (b) for ΔET (mm/yr), and (c) for ΔSWE (mm/yr). In (a), grid cells with a positive value have a smaller Q decrease under 1~2°C warming than 0~1°C warming. In (b), grid cells with a negative value have a smaller ET increase under 1~2°C warming. In (c), grid cells with a positive value have a smaller SWE decrease under 1~2°C warming. All values are averaged over the historical period (water years 1951-2018). The basin average values for PNW, UCRB, and CA correspond to the basins' 1~2°C column minus 0~1°C column in Chapter 4 Table 1.

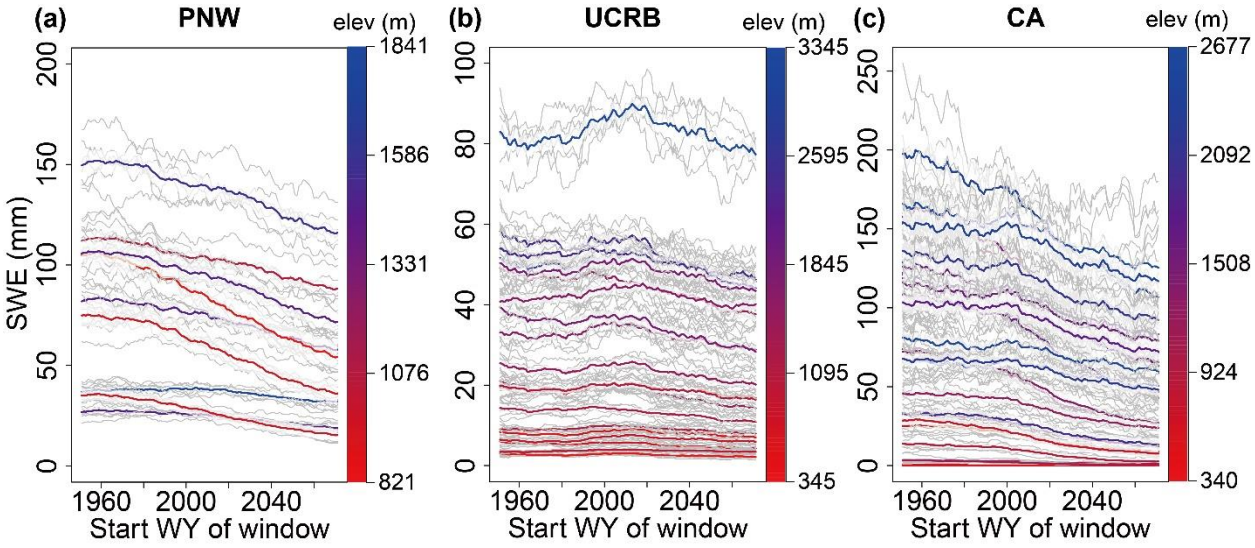

Figure C2. Time series of SSP245-driven VIC output SWE in sub-basins with naturalized flow records, averaged by a 30-year moving window over water years 1951 to 2100 in (a) PNW, (b) UCRB, and (c) CA. Colors indicate the elevation, with blue indicating higher elevation and red indicating lower elevation.

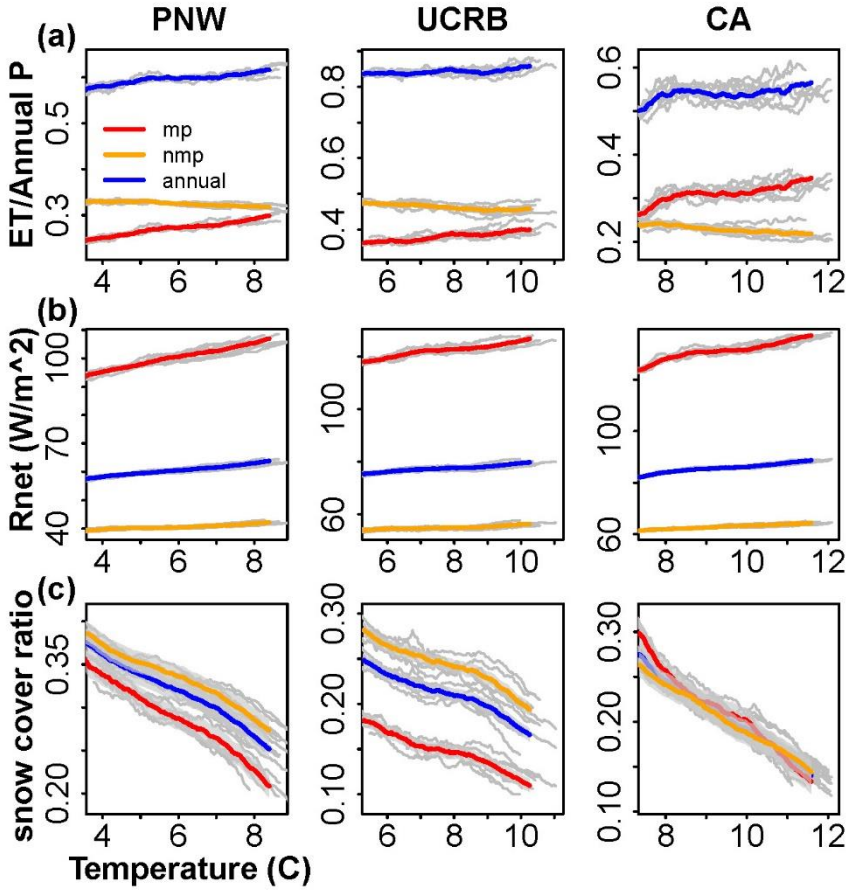

Figure C3. (a) Ratios of annual ET, melt-period (mp, Mar-May) ET, and non-melt-period (nmp, Jun-Feb) to annual precipitation (P) as a function of temperature, derived from the pooled GCM-driven VIC outputs for water years 1951 to 2100; (b) same as (a), but for net radiation averaged over annual period, melt-period, and non-melt-period; (c) same as (b), but for snow cover ratio (fraction of area covered by snow). Note that our definition of melt period (Mar-May) did not consider the timing shift caused by earlier snowmelt. Results are for SSP245 scenario. Corresponding SSP585 results are in Chapter 4 Figure 5.